



UNIVERSITEIT•STELLENBOSCH•UNIVERSITY
jou kennisvennoot • your knowledge partner

Heliostat cost reduction methods applied to a small heliostat

BY

James Nicholas Larmuth

Assignment presented in partial fulfilment of the requirements for the degree of Master of Engineering (Mechanical) in the Faculty of Engineering at Stellenbosch University

Supervisor: Paul Gauché

December 2015



Departement Meganiese en Megatroniese Ingenieurswese
Department of Mechanical and Mechatronic Engineering



DECLARATION

By submitting this assignment electronically, I declare that the entirety of the work contained therein is my own, original work, that I am the sole author thereof (save to the extent explicitly otherwise stated), that reproduction and publication thereof by Stellenbosch University will not infringe any third party rights and that I have not previously in its entirety or in part submitted it for obtaining any qualification.

Date:

Copyright © 2015 University of Stellenbosch

All rights reserved

Abstract

Heliostat cost accounts for 40% of the total capital expenditure of a typical central receiver system. There is currently no consensus as to what constitutes a cost optimum heliostat within the state of the art. Improved heliostat performance can lead to improved levelized cost of electricity (LCOE). However, improved heliostat performance may also increase heliostat cost, resulting in a net loss in LCOE. This study aims to better understand heliostat cost at the heliostat sub-component level by developing methods for exploring cost reduction.

An existing research heliostat, named Heliopod, was used as a case study and represents a physical dataset against which heliostat cost was explored. A cost model was developed to allow for the cost and performance comparison of heliostat sub-components without the need for a system performance model. The cost model was built from invoiced data for the Heliopod system and correlated with a component based error model for heliostat pointing error. Four discrete auxiliary methods were then used to further explore the sensitivities and effects of design changes on heliostat cost as applied to the Heliopod case study. These auxiliary methods include a Pareto analysis, uncertainty analysis, a size analysis and the use of an influence matrix to explore inter-component effects.

This study indicates that drives hold 40% of the Heliopod total cost and proposes the use of dual linear drives and a fixed horizontal tracking mechanism to provide a 38% cost reduction along with a 56% improvement in pointing accuracy.

Heliostat size was also shown to be an important factor in cost reduction, and this study estimated the optimum heliostat size for the Heliopod system to be less than 2m² as a result of its low controller costs. The size analysis highlighted the leveraging effects of fixed costs on heliostat size as smaller heliostats allow for reduced wind loads. Additionally, reducing heliostat size for increased production volume was also shown to provide further cost benefits without compromising component performance.

The multiple methods used in this study allow for the identification of cost sensitivities and are able to indicate potential design changes for cost reduction with a performance allocation.

Opsomming

Die koste van heliostate beloop 40% van die totale kapitaalbesteding vir 'n tipiese sentrale ontvangersisteen. Tans is daar nie konsensus aangaande wat 'n optimale heliostaat uitmaak nie. Verbeterde heliostaatverrigting kan lei tot 'n verbetering in terme van Gelykmakende Elektrisiteitskoste (GE), maar hierdie verbeterde verrigting kan egter ook lei tot 'n toename in heliostaatskoste wat 'n nettoverlies in GE tot gevolg kan hê. Dié studie poog om heliostaatskoste beter te verstaan deur dit te beskou op die vlak van die heliostaat se subkomponente en metodes te ontwikkel ten einde kostes te verminder.

'n Bestaande navorsingsheliostaat genaamd Heliopod dien as 'n gevallestudie en verteenwoordig 'n werklike datastel waarmee heliostaatskoste ondersoek word. 'n Kostemodel word ontwikkel wat dit moontlik maak om die koste en verrigting van die heliostaat subkomponente te vergelyk sonder dat 'n sisteemverrigtingsmodel nodig is. Die kostemodel word gebou deur gebruik te maak van data van die Heliopodsisteen en word dan gekorreleer met 'n komponentgebaseerde foutmodel vir heliostaat mikfoute. Vier diskrete hulpmetodes word dan gebruik om die sensitiwiteite en effekte van ontwerpveranderinge op heliostaatskoste te ondersoek, soos toegepas op die Heliopod gevallestudie. Hier hulpmetodes sluit 'n Pareto-analise, onsekerheidsanalise, 'n grootte analise en die gebruik van 'n invloedsmatriks om interkomponenteffekte te ondersoek in.

Dié studie dui aan dat aandrywers 40% van die totale Heliopod se totale koste moet uitmaak en stel die gebruik van dubbele lineêre aandrywers en 'n vaste horisontale navolgingsmeganisme voor om 'n kostevermindering van 38% en 'n 56% verbetering in mikakkuraatheid te bied.

Die grootte van die heliostaat is ook 'n belangrike faktor met betrekking tot kostevermindering en die betrokke studie beraam 'n optimale heliostaatgrootte vir die Heliopodsisteen van minder as 2m^2 weens die laer beheerderkoste wat dit tot gevolg sal hê. Die grootte analise beklemtoon die hefboomeffekte van vaste koste vir heliostaatgrootte aangesien kleiner heliostate laer windlaste beteken. Hiermee saam lei 'n kleiner heliostaat vir groter produksievolume ook tot verdere kostevoordele sonder om komponentverrigting in te boet.

Die veelvoudige metodes wat in dié studie gebruik word maak voorsiening vir die identifisering van kostesensitiwiteite en dui potensiële ontwerpveranderinge aan vir kostevermindering met 'n verrigtingsaanduiding.

Table of contents

Table of figures	vi
List of tables.....	viii
Nomenclature.....	ix
Abbreviations.....	xi
1. Introduction.....	1
1.1 Background.....	1
1.2 Central receiver cost improvement goals	2
1.3 The Heliopod.....	3
1.4 Motivation	4
1.5 Research objective	5
1.6 Methodology.....	5
1.7 Research limitations	6
1.8 Study outline	7
2. Literature review	8
2.1 Heliostat anatomy.....	8
2.2 Heliostat tracking mechanisms.....	9
2.3 Traditional heliostats.....	11
2.4 Current commercial heliostats	12
2.5 Heliostat size	15
2.6 Heliostat cost measures.....	16
2.7 Benchmark heliostat costs.....	17
2.8 Heliostat production and manufacture	18
2.9 Conclusion.....	19
3. Method.....	20
3.1 Overview.....	20
3.2 Cost models.....	21
3.3 Error model	23
3.4 Conclusion.....	25
4. The Heliopod.....	26

4.1	Heliopod general description.....	26
4.2	Heliopod cost model	29
4.3	Heliopod error model.....	32
4.4	Heliopod total error	36
4.5	Conclusion.....	38
5.	Analysis	39
5.1	Heliopod Pareto analysis	39
5.2	Uncertainty in component cost reduction	44
5.3	Parametric analysis for Heliopod size	46
5.4	Heliopod component influence	50
5.5	Discussion.....	52
5.6	Analysis adopted	54
5.7	Embodiment.....	54
5.8	Cost and error comparison	56
5.9	Conclusion.....	57
6.	Conclusion.....	58
6.1	Summary of findings.....	58
6.2	Conclusions.....	59
6.3	Summary of contributions.....	60
6.4	Recommendation for future work.....	60
7.	Bibliography.....	61
	Appendices	69
A.	Heliopod general dimensions	70
B.	Heliopod cost breakdown.....	74
C.	Component tests.....	76
D.	Component quotations	78

Table of figures

Figure 1.1: Terrasol Energy 19.9MW Gemasolar plant in Seville Spain	2
Figure 1.2: Left: Total installed cost for a central receiver CSP plant in South Africa; Right: LCOE breakdown for a central receiver CSP plant in South Africa.....	3
Figure 1.3: CAD Render of the solar roof laboratory and the Helio40 installation	3
Figure 1.4: The second generation Heliopod prototype with the Helio18 prototype on the right	4
Figure 2.1: Heliostat components and composition.....	8
Figure 2.2: Azimuth elevation clearance requirement.....	10
Figure 2.3: Fixed horizontal tracking mechanism	10
Figure 2.4: Target aligned/ spinning elevation.....	11
Figure 2.5: From left to right - Traditional glass metal heliostat and stretched membrane heliostats.....	12
Figure 2.6: LEFT: Abengoa' s 140 m ² heliostat installed at Khi Solar One.....	13
Figure 2.7: BrightSource Energy heliostat development.....	13
Figure 2.8: Frist generation eSolar heliostats.....	14
Figure 2.9: Heliostat size trends 1970 to 2010.....	15
Figure 2.10: Costs included in LCOE.....	17
Figure 3.1: Method overview	20
Figure 3.2: Combined effect of sub-component normal vector pointing errors	24
Figure 3.3: Classification of beam error and normal errors	24
Figure 4.1: Individual heliostat description	27
Figure 4.2: Heliostat co-ordinate system and load designations.....	28
Figure 4.3: Invoiced Heliopod component cost in a Pareto chart	30
Figure 4.4: Volume adjusted component cost data for 20 000 units	31
Figure 4.5: Heliopod elevation assembly showing actuator connections.....	33
Figure 4.6: Heliopod elevation geometry modified from Guo et al.....	34
Figure 4.7: Simplified cross-section of the headstock.....	35
Figure 4.8: Facet image at focal length and time (16h00 at 47.5 m).....	36

Figure 4.9: Total heliostat optical error (NVE)	37
Figure 4.10: Tracking error stack and total (NVE)	37
Figure 5.1: Combined cost and error of tracking mechanism components	39
Figure 5.2: Component proportions of total cost (high volume)	40
Figure 5.3: Slew drive manufacturer comparison for 3 inch slew drives	41
Figure 5.4: Actuator manufacturer comparison	42
Figure 5.5: Left: Heliopod elevation assembly errors.	43
Figure 5.6: Generic component cost to area relationships	48
Figure 5.7: Heliostat cost vs. area for the Heliopod system	49
Figure 5.8: Heliostat production volumes for alternate unit sizes	50
Figure 5.9: Heliopod influence matrix	51
Figure: 5.10 The effect of connection interfaces on heliostat drives	52
Figure 5.11: Linear changes to the heliostat tracking unit	54
Figure 5.12: Fixed horizontal tracking mechanism	55
Figure 5.13: Fixed horizontals proposed error stack	56
Figure 5.14: Heliopod departure point	56
Figure 5.15: Component cost and tracking error for the fixed horizontal solution	57

List of tables

Table 2.1: Heliostat cost comparisons	18
Table 4.1: Heliopod design requirements	27
Table 4.2: Peak wind loads for an aspect ratio of 1.5 at 20 km/h	28
Table 4.3: Peak wind loads for an Aspect Ratio of 1.5 at 50 km/h.....	29
Table 4.4: Peak wind loads for an aspect ratio of 1.5 at 135 km/h.....	29
Table 5.1: Triangular distribution for component cost reduction probability.....	45

Nomenclature

Variables

A_f	Solar field reflective area	[m ²]
A_H	Heliostat reflective area	[m ²]
C_{cat-1}	Linear costs of heliostat components	[\$]
C_T	Total cost per unit area	[\$/m ²]
f	Fixed costs	[\$]
k	Aggregated cost of load bearing components	[\$]
N	Number of heliostats	[-]
T	Tolerance clearance	[m]
X	Actuator stroke	[m]
X_0	Actuator body length	[m]
α	Elevation angle	[rad]
β	Azimuth angle	[rad]
α	Elevation angle	[rad]
θ_x	Pylon elevation deflection	[rad]
θ_z	Pylon azimuth deflection	[rad]
σ_{Aberr}	Off-axis reflection error	[rad]
σ_{Axis1}	Tracking error at axis 1	[rad]
σ_{Axis2}	Tracking error at axis 2	[rad]
$\sigma_{Gravity}$	Beam quality error due to gravity	[rad]
σ_{Sun}	Sun-shape error	[rad]
σ_{Tot}	Total optical error	[rad]
σ_{Track}	Tacking error	[rad]
σ_{BQ}	Beam quality error	[rad]
$\sigma_{Specularity}$	Specularity error	[rad]
σ_{Wind}	Beam quality error due to wind	[rad]
R	South African rand	[ZAR]
\$	United States dollar	[USD]
€	euro	[EUR]

Exchange rates

1 USD = 10.31 ZAR

1 USD = 1.3 EUR

Abbreviations

AE	Azimuth Elevation (Tracking System)
BSE	BrightSource Energy
CET	Cost Estimation Techniques
CR	Central Receivers
CSP	Concentrating Solar Power
DFMA	Design for Manufacture and Assembly
DLR	Deutsches Zentrum für Luft- und Raumfahrt (German Aerospace Centre)
FH	Fixed Horizontal (Tracking System)
IEA	International Energy Association
IRENA	International Renewable Energy Agency
LCOE	Levelized Cost Of Energy
MTBF	Mean Time Before Failure
NVE	Normal Vector Error
SU	Stellenbosch University
STERG	Solar Thermal Energy Research Group
TA	Target Aligned (Tracking System)
US DOE	United States Department of Energy

1. Introduction

In Concentrating Solar Power, heliostat cost contributes ~40% of the total central receiver plant capital expenditure (Kolb, et al., 2011). The high capital expenditure required for central receiver systems forms a barrier to the future implementation of this technology. Heliostats have been identified as having significant cost reduction potential. As a result, there is much to be gained by the cost reduction of heliostat systems.

1.1 Background

The International Energy Agency estimates that finite fossil fuels provide more than 80% of current global energy demands (IEA, 2012). The consumption of fossil fuels in this manner is unsustainable, and alternatives are required as a result. Renewable energy technologies can offer alternatives, but because many of these technologies supply intermittent energy, energy storage is needed.

Concentrating Solar Power (CSP) presents a valuable and useful means to harness this intermittent resource as it has distinctly higher capacity factors compared to other renewable energy technologies (IEA, 2010). These increased capacity factors are primarily due to its ability to incorporate utility-scale thermal storage with efficiencies well above 90%, allowing it to produce dispatchable electricity (Kolb, et al., 2011).

CSP systems incorporate a solar collector that concentrates the solar energy and transmits it to a working fluid via a receiver. The working fluid then drives a heat engine which carries out work (Kishore, 2009). Within CSP technology there are four main plant configurations, namely parabolic trough, linear Fresnel, parabolic dishes and central receiver systems (IEA, 2010).

The primary distinction between these plant formats is the type of focal image generated at the receiver. Line focusing configurations such as parabolic trough and linear Fresnel systems typically concentrate solar radiation to factors between 50 and 100 (Lovegrove & Pye, 2012). Point focus configurations such as parabolic dish and central receiver systems concentrate to factors between five hundred and several thousand (Lovegrove & Pye, 2012).

Central receiver plants operate by using a solar field consisting of large numbers of heliostats that focus solar radiation onto a fixed point (the receiver) located on a

central tower (Figure 1.1). The central receiver then heats a working fluid from which power is generated.



Figure 1.1: Terrasol Energy 19.9MW Gemasolar plant in Seville Spain (Terresol Energy, 2011)

Multiple heliostats collectively make up the solar field of a central receiver system. The primary function of the solar field is to reflect the maximum amount of solar radiation into the receiver aperture with the most even distribution possible (Ulmer, 1998).

A heliostat has two axes of rotation which allow for the reflective surface to follow the sun and provide a continuous reflection of solar irradiance onto the central receiver (Schramek & Mills, 2004).

1.2 Central receiver cost improvement goals

Conventional CSP systems typically have low to no fuel costs but have large capital costs (Lovegrove & Pye, 2012). The levelized cost of energy (LCOE) of a CSP system can be reduced by improving the annual performance of the plant and/or lowering the capital and operational costs (Kolb, et al., 2011).

The high capital investment costs associated with CSP plants reportedly create a barrier for future plant development and technology growth (IEA, 2010). The single largest cost item typically included in this barrier is the solar field (IRENA, 2012; Kolb, et al., 2011). Figure 1.2 shows the proportions of plant LCOE and capital expenditure held by a heliostat field in a typical 50 MW central receiver system. Based on the proportions shown in Figure 1.2, heliostat cost reductions form a

prominent area for reducing the capital cost barrier, as well as lowering the LCOE of central receiver systems.

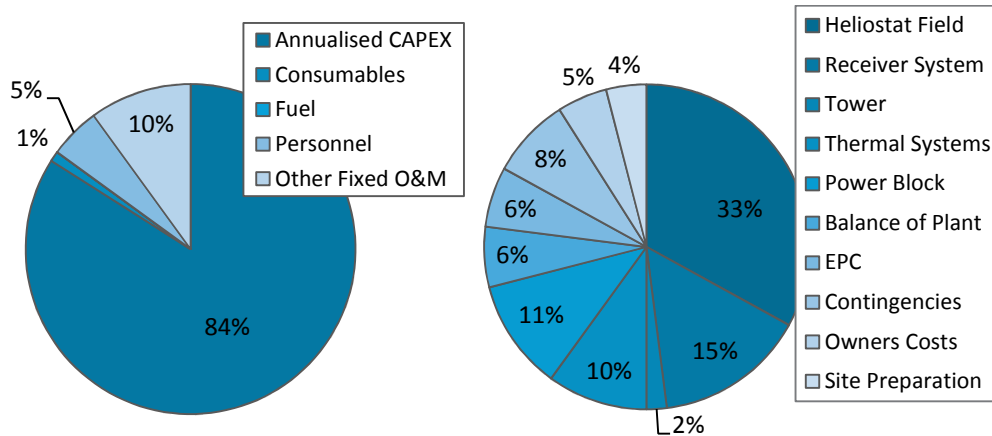


Figure 1.2: Left: Total installed cost for a central receiver CSP plant in South Africa; Right: LCOE breakdown for a central receiver CSP plant in South Africa, adapted from IREANA (2012)

Heliostat costs are measured in cost per unit of reflective area ($\$/\text{m}^2$) (Kolb, et al., 2011). In 2011 the United States Department of Energy (US DOE) updated the SunShot Goal for heliostat cost reduction, setting a cost target of $\$75/\text{m}^2$ to be achieved by 2020. This target corresponds to a benchmark LCOE of $6\text{¢}/\text{kWh}$ (Kolb, et al., 2011). Vant-Hull (2012) considers the SunShot Goal of $\$75/\text{m}^2$ a difficult target to realize. Pfahl (2014) suggests that this goal is unobtainable with traditional heliostat designs and radically different approaches with new innovations are required to achieve this goal.

1.3 The Heliopod

Stellenbosch University has a locally developed heliostat test facility with a field aperture of approximately 40 m^2 . The facility is located in the open air solar roof laboratory at the Department of Mechanical and Mechatronic Engineering. The facility, named Helio40, forms an intermediate scale-up of an existing 1.62 m^2 heliostat array consisting of 18 micro-heliostats (Malan & Gauché, 2013).

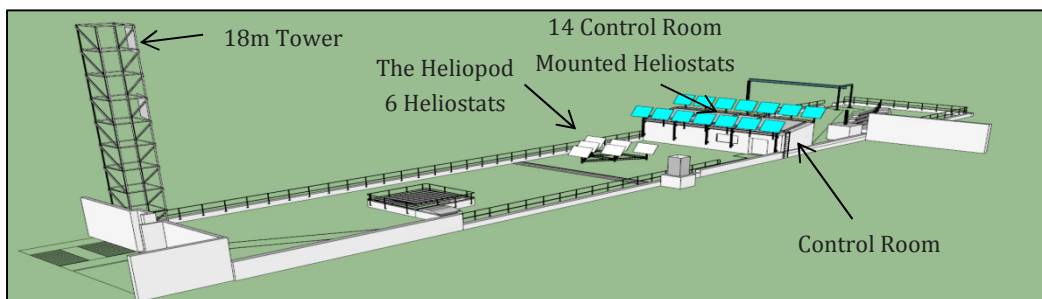


Figure 1.3: CAD Render of the solar roof laboratory and the Helio40 installation (Larmuth, et al., 2014)

The Stellenbosch University solar roof laboratory consists of a 1 300 m² surface with an existing control room and an 18 m tall multipurpose tower. The Helio40 system has been integrated into the Solar Roof laboratory with the total field installation consisting of fourteen heliostats located on the roof of the control room and a further six heliostats fixed to a triangular floor mounted lattice pedestal.

The six lattice pedestal mounted heliostats form an independent prototype called a Heliopod. The Heliopod prototype is a second generation experimental prototype that aims to provide insight into early commercial heliostat development. The Heliopod holds six single faceted tracking mechanisms mounted on a common triangular pedestal.

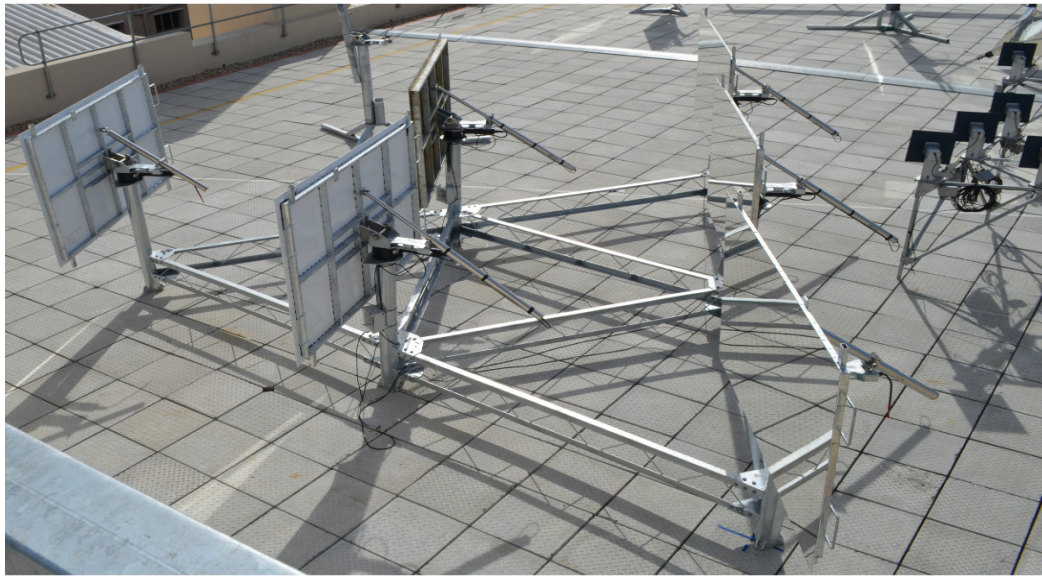


Figure 1.4: The second generation Heliopod prototype with the Helio18 prototype on the right.

In the case of this study, the Heliopod system provides a physical heliostat dataset and benchmark against which alternate costs and higher level design philosophies can be tested. This heliostat was used as a benchmark dataset for this study; further details on its design are discussed in Chapter 4.

1.4 Motivation

Heliostat cost improvement is complex due to an inherent cost duality. Heliostat design affects both plant capital cost and plant efficiency. Improved heliostat performance should lead to higher energy yield at the receiver and improved LCOE. However, an upper limit exists where increasing heliostat cost for increased performance leads ultimately to net losses in LCOE (Blackmon, 2012).

Several system and optical performance models exist, which provide insight into this complexity. A review of these models can be seen by Stine & Geyer (2001) and

Bode & Gauché (2012). However, these system and optical performance models are complex and do not allow for detailed cost analysis at the heliostat sub-component level.

Existing work by Sandia National Laboratories (Kolb, et al., 2007; Kolb, et al., 2011) covers broader aspects of heliostat component cost with emphasis on developing a heliostat cost benchmark and identifying the price reduction potential of various, specific heliostat technology improvement opportunities. Blackmon (2013) presents a method for determining the optimum size of a heliostat based on the cost of the respective heliostat components. Blackmon (2013), Bhargav et al. (2014) and Kolb et al (2007) have explored the effects of heliostat size on cost. Ulmer (1998) shows some positive implications of structural improvements on the beam quality of a specific large area heliostat and concludes with a case specific solution for improved beam quality and cost.

These studies examine component and cost of production but do not directly align these aspects of cost with generic performance sensitivities at a component level. Heliostat sub-components have differing performance metrics depending on their specific function and implementation within the heliostat. Comparing the cost of the respective components relative to their performance can provide insight into higher level design decisions and steer design towards a low cost heliostat.

1.5 Research objective

This report aims to understand heliostat cost at the heliostat component level, allowing for recommendations of heliostat cost improvements. The study presented herein builds on the existing work done by Blackmon (2013), Brandt & Chang (1981) and Kolb et al (2007) and presents a method for strategic heliostat cost vs. performance comparison at the heliostat component level.

The primary objective pursued in this study, therefore, is to develop a method for heliostat cost and performance comparison. The method will then be tested with a case study, which in this case relates to the Heliopod system.

1.6 Methodology

Following the objective set out in section 1.5, a techno-economic study is completed. A model is built and applied to a specific case study. The research methodology used in this study is summarised by the following:

- Present literature review of the state of art in heliostats and heliostat cost analysis methods.
- Review general costing methods applicable to heliostats.

- Develop cost and performance evaluation methods by the selection and/or adaption of existing and new methods.
- Test the method by application on the SU Heliopod case study.
- Use the method to recommend strategic improvements to the SU Heliopod case study.

1.7 Research limitations

Cost analysis is a broad topic that encompasses every aspect the heliostat system. In order to confine this research to a tangible scope, the following research limitations are implemented.

Modelling both heliostat component cost and performance as a function of LCOE ultimately involves a systems performance study. Since heliostat cost research is in its infancy, the work presented here focused on gaining greater resolution on cost at the heliostat component level. As a result, this study does not account for plant performance and LCOE but rather identifies heliostat component cost and performance sensitivities that can later be built into a new or existing system performance model.

In the case of the cost model, only direct material and direct labour costs are considered for the respective heliostat components as these values typically embody costs incurred at the factory gate and can be used to estimate costs at volume. Secondary costs such as supply chain, logistics, O&M, product lifetime and ground preparation are excluded to maintain focus on heliostat component costs.

Heliostat total optical performance includes several performance sub-measures, of which a primary measure is beam quality. This study was concerned with the heliostat tracking mechanism, structure and the respective tracking components, and therefore it is focused on the cost implications of pointing error within an operational wind speed range. The remainder of optical performance concerned with surface slope errors, sun shape, optical aberration and specularities are aspects of facet profile, tracking axes and canting performance, which were not directly included herein. STERG has an existing research endeavour that covers some of these optical performance measures of heliostat reflector profiles (Landman, 2013).

The author conducted this study while under the employment of a Stellenbosch University heliostat development project. Some areas of this study were guided by the efforts of the larger heliostat development project, and work done by other project members is clearly indicated within this study.

1.8 Study outline

Chapter 2 presents a literature survey on the state of the art in heliostats as well as existing heliostat cost related publications.

Chapter 3 describes the methodology used to investigate cost sensitivities and outlines the cost and error model used to measure heliostat performance and cost in the subsequent chapters.

Chapter 4 applies the cost and error model to the Heliopod system and creates a benchmark for further analysis.

Chapter 5 forms the primary body of analysis where cost and performance were evaluated and an improvement is suggested.

Chapter 6 applies this improvement and compares it to the original benchmark set out in Chapter 4.

Chapter 7 concludes this assignment with a summary of findings and list contributions and provides recommendations for further work.

2. Literature review

In this chapter, heliostats will be discussed in more detail. Emphasis is placed on understanding the state of the art in their anatomy and operation by using conventional examples from literature and industry. Comment on traditional and commercial heliostats is also provided with a review on existing literature relating to heliostat costs.

2.1 Heliostat anatomy

Heliostats typically consist of a composition of several essential components as described in Figure 2.1 below.

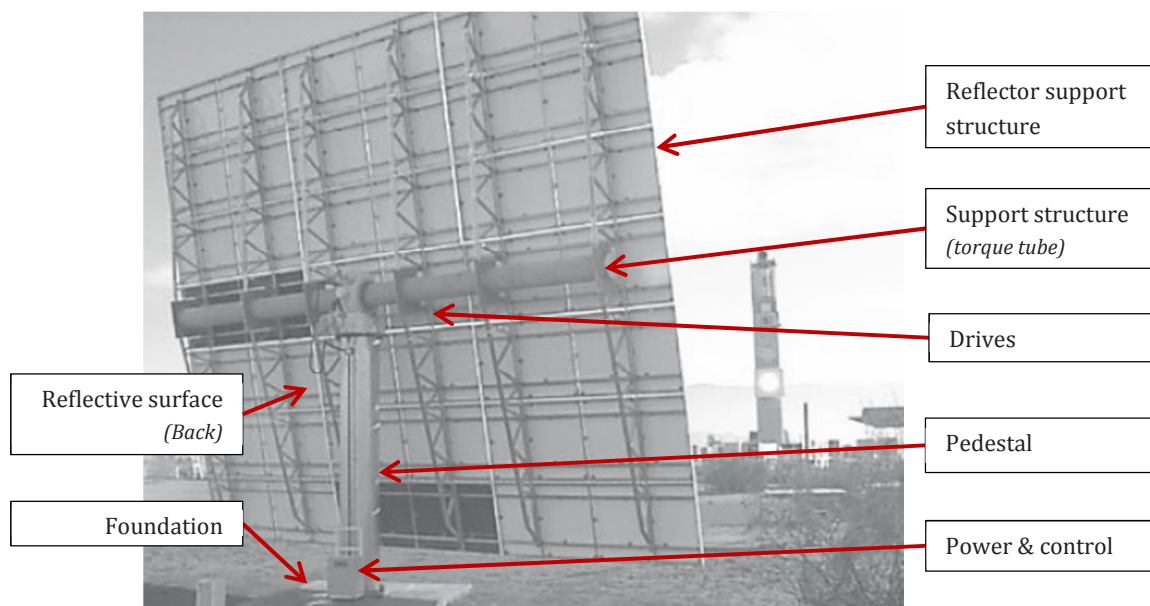


Figure 2.1: Heliostat components and composition (Mancini, 2000)

The reflective surface is made up of one or more facets mounted to a supporting structure. Collectively, the facets make up the total heliostat aperture. The reflective surface is either concave or flat, depending on the desired concentration ratio (Lovegrove & Pye, 2012). In multifaceted designs, canting strategies are typically incorporated to allow for the rays of each independent facet to merge and form a single image with a higher concentration ratio (Landman, 2013).

The support structure carries the weight of itself and the adjoining heliostat components. Primarily, the structure transfers wind and gravitational loads through the drives, pedestal and foundation into the ground and should provide ridged reflector support during operational windspeed (Mancini, 2000).

The heliostat drives are responsible for the heliostats tracking movement as they provide the positive force required to move the reflective surface and support structure about the heliostats two rotational axes (Mancini, 2000).

The heliostat control system holds the electronics, sensors and software required to allow the heliostat to continuously reflect the solar energy toward the receiver (Falcone, 1986).

In traditional heliostat designs, the pedestal manifests in the form of a steel pylon, which has a poured in place concrete foundation (Mancini, 2000). The pedestal, however, also can have alternate designs that exclude the foundation due to ganged pylons, pile driven pylons or wider lattice structures that form the pedestal (Coventry & Pye, 2013).

2.2 Heliostat tracking mechanisms

The two rotational axes are required for solar tracking and can be arranged in many different configurations, each with their own practical benefits and disadvantages (Schramek & Mills, 2004). Three common arrangements, referred to as tracking mechanisms, are discussed here; these are azimuth elevation (AE), fixed horizontal (FH) and target aligned (TA).

In a tracking mechanism, one of the two rotational axes is in a fixed position and is ultimately constrained by the ground. For the following study, this axis is referred to as the primary axis. The subsequent axis moves relative to the primary axis and is attached to the reflector. This axis is referred to as the secondary axis.

2.2.1 Azimuth elevation tracking

The most common tracking mechanism used in commercial systems today is the AE configuration (Schramek & Mills, 2004). In an AE mechanism, the primary axis rotates around the zenith and, therefore, moves the heliostat in azimuth. The secondary axis rotates around the horizontal and creates the elevation movement (See Figure 2.2)

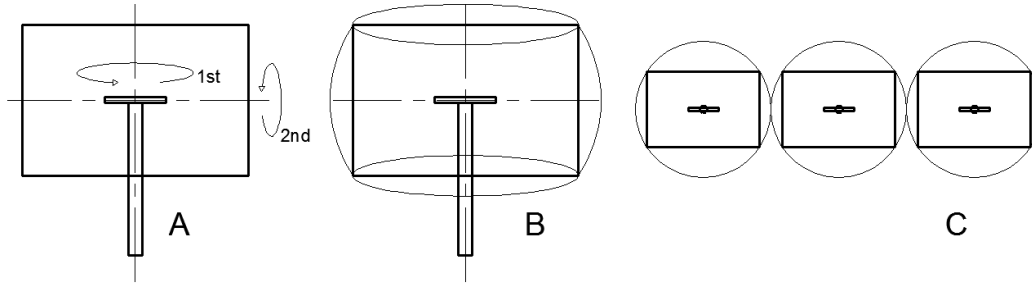


Figure 2.2: Azimuth elevation clearance requirements adapted from Schramek & Mills (2004)

This arrangement typically operates with two orthogonal rotary drives or a combination of an azimuth rotary drive and a linear actuator. The use of an azimuth rotary drive in this configuration has the advantage of a 360° azimuth displacement, allowing for non-specific installation. A disadvantage of the AE configuration is that its three dimensional rotation (Figure 2.2 B) requires larger heliostat centre-to-centre distances in order to avoid heliostat corner collision (Schramek & Mills, 2004; Cordes, et al., 2012). The arrangement therefore experiences lower field packing ratios (Figure 2.3, Figure 2.2C). Despite this drawback, advanced control software has been incorporated at the BrightSource Ivanpah plant to avoid AE heliostat collisions in fields with high packing ratios (Koretz, 2014).

2.2.2 Fixed horizontal tracking

In the FH configuration, the primary axis rotates around the horizontal while the secondary axis moves with a limited range of motion ($<360^\circ$) about the vertical (Figure 2.3).

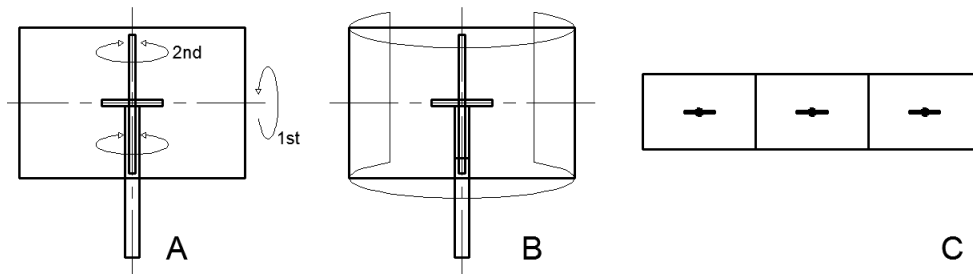


Figure 2.3: Fixed horizontal tracking mechanism adapted from Cordes et al. (2012)

This tracking mechanism allows for easy integration with linear drives as well as reduced collision and improved packing ratios without the need for collision prevention software (Cordes, et al., 2012).

2.2.3 Target aligned tracking

The TA tracking mechanism operates by permanently aligning the primary axis with the receiver and allowing the secondary axis to rotate about the aligned axis. Conventional tracking mechanisms such as AZ and FH mechanisms suffer from

optical losses due to astigmatism caused by non-normal incidence (Zaibel, et al., 1995).

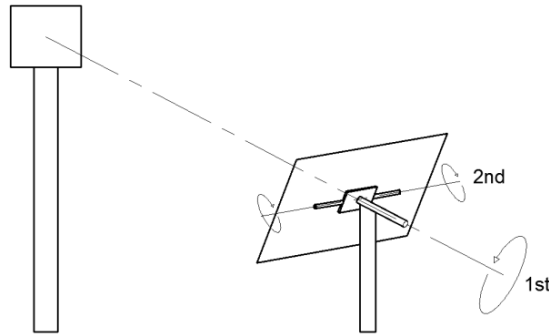


Figure 2.4: Target aligned/ spinning elevation modified from Zaibel et al. (1995)

Chen et al. (2004) compare in detail the effects of the TA tracking mechanism to the azimuth elevation. Amongst other benefits, they find it to provide smaller disparity in image spread as well as more uniform flux spread.

2.3 Traditional heliostats

Despite a large variety of heliostat designs, Kolb et al (2007) describe two primary classifications of heliostat, namely stretched membrane heliostats and glass metal heliostats.

Stretched membrane technology incorporates facet(s) with a flexible membrane attached to a steel rim (Kolb, et al., 2007). Murphy et al. (1985; 1984) show that the primary benefits gained from using a stretched membrane heliostat is the high tension reflective surface, which allows for significant weight reduction in structural components as well as high reflectivity and low slope error. A substantial amount of research has been published with regards to stretched membrane heliostats (Alpert et al. 1990; Anderson et al. 1985; Kolb et al 2007; Murphy 1984; Murphy et al. 1985). The primary disadvantages to streched membrane technology are the degradation in the polymer mirror and the need to incorporate vacume pumps into the facet (Pfahl, 2014).

Glass metal heliostats consist of a concentrator made up of single or multiple silvered float glass facets mounted to a steel backing. This class of heliostat is common in all commercial systems to date and has been developed for central receiver systems since the mid 1970's (Kolb, et al., 2007; Ulmer, 1998). The first generation development of early glass metal heliostats in the USA resulted in the selection of the 40m² McDonnell Douglas pedestal mounted heliostat for use in the Solar One pilot plant in 1982 (Kolb, et al., 2007). McDonnell Douglas furthered this design by increasing its size to 100 m². The increased size showed cost reductions of

up to 20% due to economies of scale associated with field wiring and control costs (Kolb, et al., 2007).

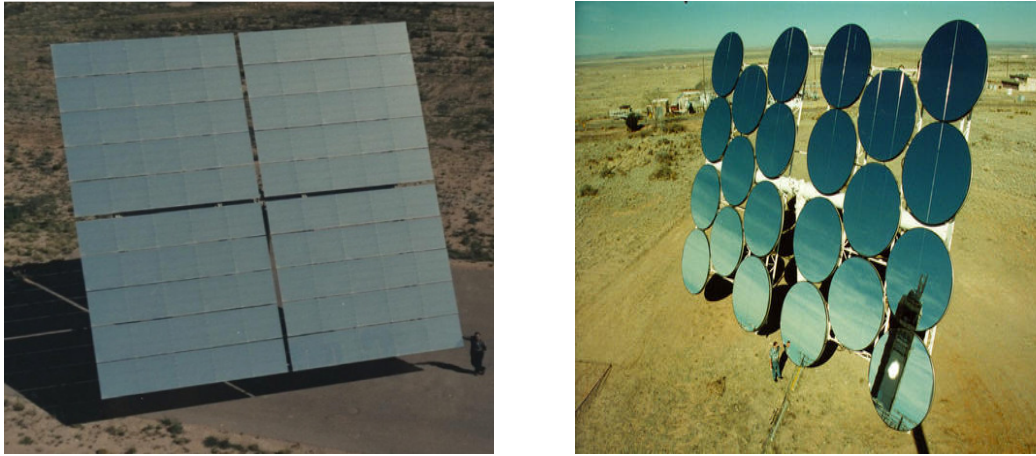


Figure 2.5: From left to right - Traditional glass metal heliostat (ATS150) (Kolb, et al., 2007) and stretched membrane heliostats (SAICE 175) (Kolb, et al., 2007)

Following the McDonnell Douglas heliostat, Sandia proposed larger heliostats for further cost reduction. The development of the Advanced Thermal Systems (ATS) heliostat formed a 148 m² prototype that operated for 20 years at Sandia's test facilities in Albuquerque, New Mexico. The ATS heliostat is currently the basis for the benchmark cost point established for heliostat design (Kolb, et al., 2011).

2.4 Current commercial heliostats

The recent resurgence of activity in the CSP market has resulted in several new full scale central receiver systems as along with several smaller demonstration plants. Some of these designs represent linear developments from traditional designs while others offer more radical design alternatives. Three prominent developers of commercial heliostats are discussed below.

2.4.1 Abengoa Solar

The heliostats installed at Abengoa's PS10 and PS20 plants are 120 m² glass metal torque tube designs very similar to that of the ATS 150 (Abengoa, 2009). Abengoa's most recent commercial heliostat, installed at Khi Solar One in South Africa, is a 140 m² multifaceted glass metal design as shown by Figure 2.6a. The heliostat structure is a conventional torque tube design driven by hydraulic actuators and mounted on a spiral wound steel tube pedestal and concrete pier.

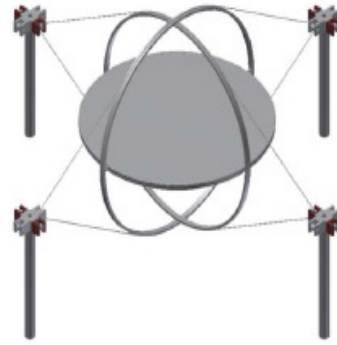


Figure 2.6: LEFT: Abengoa's 140 m² heliostat installed at Khi Solar One.
RIGHT: Conceptual design of a stretched membrane heliostat

Realising the need for further solar field cost reduction Abengoa have pursued more radical heliostat designs under the US DOE SunShot program. Figure 2.6b shows one of 40 early concepts developed by Abengoa under the SunShot program (Tilley, 2013). As a result of the SunShot program Abengoa are now developing an 18 m² ballast mounted heliostat with claims of achieving less than \$120/m² (Tilley, 2013).

2.4.2 BrightSource Energy

BrightSource Energy's (BSE) first generation heliostat was a 7 m² single faceted heliostat design, that incorporated a custom stepper motor slew drive system, which housed integrated connection interface for a linear actuator (Franck, et al., 2009; Silberstein, et al., 2009). Motivation for the small size was smaller drives, reduced steel costs, shorter pylons (to reduce installation costs and wind loading) and a single facet, which reduced canting costs and improved beam quality (Franck, et al., 2009).

Later versions (Figure 2.7b) installed at their Negev test facility show a refined slew drive casting and the use of a spring pre-load mechanism to reduce backlash effects in the azimuth direction (Pfahl, 2014). A pile driven 6" steel pylon was used for the pedestal, which removed the need for ground preparation and concrete foundation (Silberstein, et al., 2009).



Figure 2.7: BrightSource Energy heliostat development. (a) First generation heliostat (Franck, et al., 2009). (b) The LH1 Negev heliostat (Silberstein, et al., 2009). (c) Ivanpah heliostat (BSE, 2014)

The current design installed at Ivanpah is significantly larger (15.2 m²) and fitted with a dual facet and torque tube (Figure 2.7c). A similar pile driven pylon is used here as along with an evolutionary integrated steel drive casting connected to the reflectors centre of gravity (Pfahl, 2014). More recently, however, BrightSource has increased the size of their heliostat to 19 m² to compensate for an earlier conservative drive selection (Koretz, 2014) (Coventry & Pye, 2013).

Although increasing in size, BrightSource still maintains that smaller heliostats are more easily incorporated into automated production and assembly systems (Toister & Koretz, 2013). Their smaller size allows for reduced manufacture overhead due to smaller assembly buildings, material handling systems as well as easier transportation (Toister & Koretz, 2013) (Coventry & Pye, 2013).

2.4.3 eSolar

First generation eSolar heliostat designs (Figure 2.8a) incorporated a small heliostat (1.14 m²) that has the benefit of increasing production volume and allowing a large portion of manufacture and assembly to be completed in an offsite production facility (Schell, 2009). Further advantages to the small heliostat size are gained by the reduction in weight and short height above ground, thereby reducing wind loads (Schell, 2009). Similar to BSE, eSolar has also moved away from conventional concrete foundations and has developed a frame and ballast system that interlinks the heliostats and allows for cleaning by an autonomous robot (Schell, 2009).



Figure 2.8: (a) First generation eSolar heliostat (Schell, 2009). (b) 2nd generation plastic drive (Ricklin, et al., 2013b) (c) 2nd generation heliostat system (Ricklin, et al., 2013a)

eSolar's more recent design (Figure 2.8c) includes a larger facet size (2.2 m²) and the use of a plastic drive train (Ricklin, et al., 2013a). A further change is the move from the ballasted lattice frame to that of a modular, triangular pedestal that houses three heliostats and can be placed in any terrain (Ricklin, et al., 2013b).

2.4.4 Novel and conventional heliostat concepts

In addition to the previously mentioned commercial designs, many other developments are currently underway and are listed in Pfahl (2013). Several

concepts are worth noting here. The DLR is currently developing an 8 m² autonomous heliostat with rim drives, which is expected to have significant cost savings (Pfahl, et al., 2013) (Buck, 2014). This heliostat is discussed further in Sections 2.7 and 0. CSIRO has developed a 4.5 m² heliostat that incorporates dual linear actuators in a fixed horizontal tracking mechanism (Pfahl, 2014) (Blackmon, 2012). HelioTower has proposed the development of hexagonal fixed horizontal heliostats in the region of 40 m² (Cordes, et al., 2012; Bhargav, et al., 2014), and Google have pursued a novel cable driven heliostat that requires no foundation or ground preparation (Google, 2013).

Pfahl (2014) presents a comprehensive survey of heliostat concepts for cost reduction, of which positive and negative aspect of individual design concepts are highlighted. Pfahl argues that in order to reduce cost, significant innovation and deviation from the traditional design philosophy is required.

2.5 Heliostat size

Early heliostat developments range from Martin Marietta's 40 m² heliostat to the proposal of a 320 m² heliostat by Amonix (Blackmon, 2012) (Kolb, et al., 2007). A collection of heliostat sizes from 1960 to 2014 is shown in Figure 2.9.

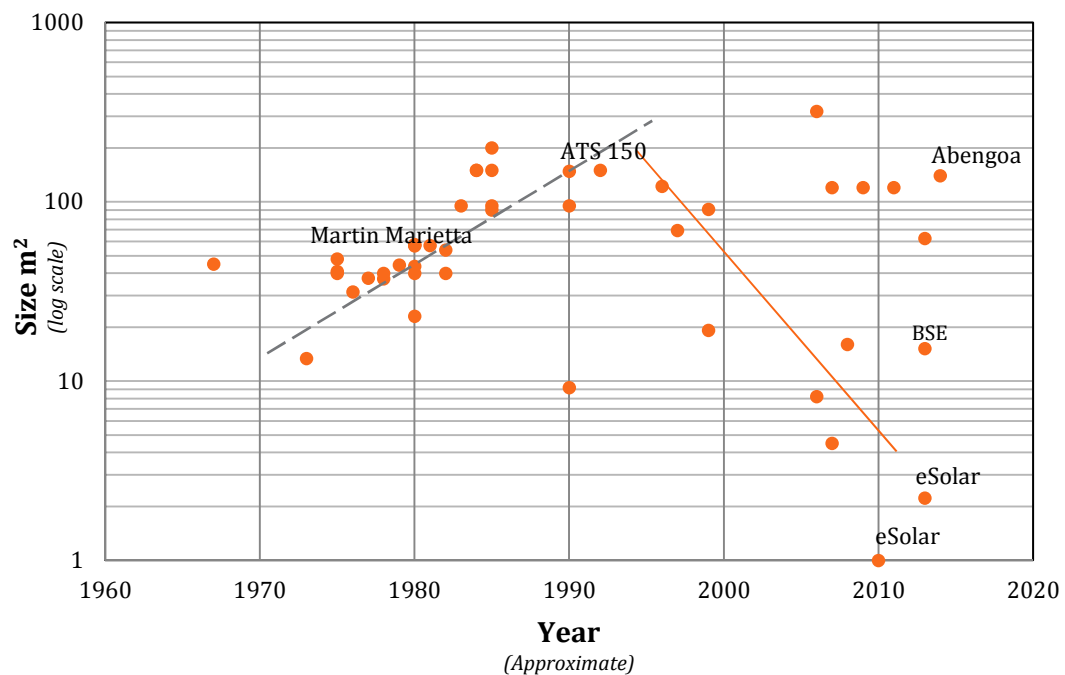


Figure 2.9: Heliostat size trends 1970 to 2010 adapted from Blackmon (2012) with added data from Kolb, et al (2007) NREL (1998) Winter, et al. (1991) and Coventry & Pye, (2013)

No clear indication of optimum heliostat size is provided by industry since commercial heliostat developers are currently developing a range of heliostat size

solutions. An illustrative trend to increase heliostat size can be seen from the early stages of central receiver development. However with the onset of innovative designs (solid trend), smaller heliostats have also been developed.

Since larger heliostats are less affected by the high cost of control electronics and field wiring the original intention for developing larger heliostats was to reduce costs based on economies of scale (Kolb, et al., 2011). Other more recent studies show that reducing size can provide significant cost benefit due to reduced wind loading on smaller heliostats, provided low controller costs can be achieved (Blackmon, 2013; Blackmon, 2012).

Cordes et al. (2012) suggest that an optimum size does not exist, and that it is rather a function of the specific heliostat component supply chain. Only independent case specific analysis will yield a size optimum heliostat (Cordes, et al., 2012); this is later emphasised by (Bhargav, et al., 2014).

Coventry and Pye (2013) highlight some important cost benefits pertaining to the use of smaller heliostats:

- Increased heliostat unit quantities for the same field size, therefore, higher production volumes for components.
- Increased availability of industry standard off-the-shelf parts due to component similarity with other high volume components.
- Smaller components are open to a wider range of low-cost manufacturing processes such as casting, stamping and forming.
- Smaller components are better suited to automated assembly lines and result in reduced savings on assembly infrastructure.
- Simplified transport and off-site manufacturing.

2.6 Heliostat cost measures

Heliostats are typically measured by cost per meter squared (Kolb, et al., 2007). This metric is a measure of the total sum of all the heliostat component costs divided by the reflective area. Comparing the cost of individual heliostat components in this metric can be misleading since it doesn't allow for a fair comparison of component costs, which are independent of area (Blackmon, 2013). Blackmon states that to better understand the cost implications of design choices, a systems level approach is ultimately required, which allows for the inclusion of heliostat optical performance as well as secondary cost effects such as transport, site preparation, cost of finance and O&M (2012, p. 545).

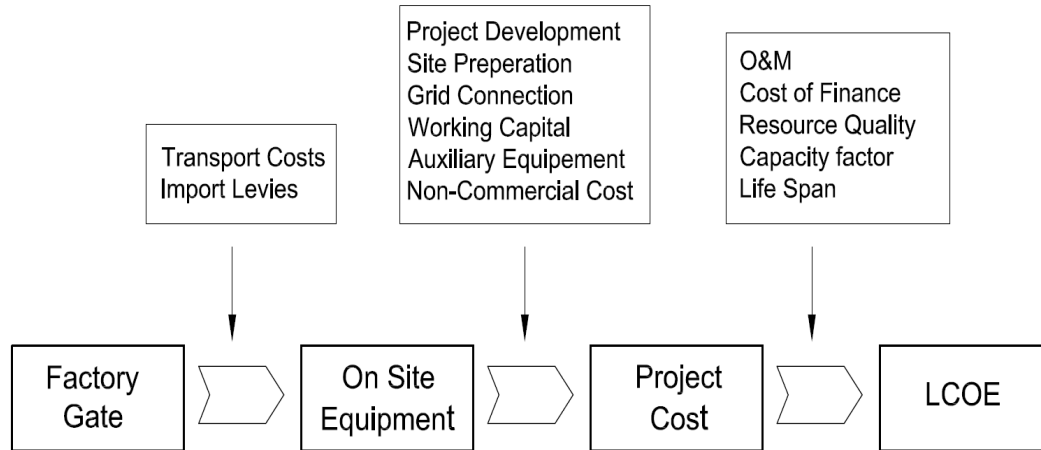


Figure 2.10: Costs included in LCOE modified from IRENA (2012)

Brandt and Chang (1981) establish a heliostat cost analysis tool (HELCAAT) that is inclusive of all production and overhead costs at the factory gate. This cost analysis tool was developed to provide a structure for heliostat costs as well as establish cost centres and calculate a representative product price based on the known input costs such as direct labour, direct materials, etc. HELCAAT excludes heliostat performance and system effects and is only able to measure heliostat production costs.

2.7 Benchmark heliostat costs

Currently, limited heliostat component cost data is available in the public domain. The lack of available information is mostly due to commercial secrecy since commercial solar field manufacturers do not typically publish their cost datasheets. Table 2.1 represents some relevant heliostat cost data available to the author. The cost data tabulated here can be seen as representative of the present state of commercial and aspirational heliostat competitors in the CSP market.

To date the most widely published and reviewed heliostat cost data is that of the 148 m² ATS heliostat, which operated at NSTTF in Albuquerque between 1984 and 2000. This heliostat is discussed in detail in the Heliostat Cost Reduction Study (Kolb, et al., 2007) and forms the current international benchmark for heliostat cost (Kolb, et al., 2011). Detailed cost data for a second heliostat was also published in Kolb et al (2007): the 30 m² Heliostat Incorporated (HI) heliostat. The third heliostat dataset shown in Table 2.1 is that of the 170 m² SAIC Phase 2 stretched membrane heliostat, which was evaluated as part of the US DOE's solar manufacturing technology (SolMAT) initiative (NREL, 1998).

Table 2.1: Heliostat cost comparisons¹ (\$/m²,) (Kolb, et al., 2007) (NREL, 1998) (Buck, 2014)

	ATS Heliostat	HI Heliostat	SAIC SM Heliostat	BSE Heliostat	DLR Novel Heliostat
<i>Confidence</i>	<i>Published Data (Unproven)</i>	<i>Published Data (Unproven)</i>	<i>Published Data (Unproven)</i>	<i>DLR Estimate</i>	<i>Aspirational DLR Estimate</i>
<i>Size</i>	<i>148 m²</i>	<i>38 m²</i>	<i>170 m²</i>	<i>15 m²</i>	<i>8 m²</i>
Production Rate	5 000/yr.	1000 units	2000/yr.	-	-
Direct Cost/Area	\$130.22	\$129.72	\$181.83	\$124.37	\$90.12
Mirror Module	\$28.31	\$33.01	\$46.92	\$16.44	\$16.44
Mirror Support Structure	\$24.91	\$7.16	\$83.36	\$39.73	\$28.77
Elevation Assembly	\$0.00	\$0.00	\$0.00	\$6.85	\$13.70
Drive 1 (Azimuth)	\$27.41	\$30.02	\$18.43	\$28.77	\$2.74
Drive 2 (Elevation)	\$27.41	\$30.02	\$18.43	\$8.22	\$2.74
Controls and Cabling †	\$2.23	\$24.68	\$2.62	\$8.84	\$10.21
Pedestal	\$19.94	\$4.83	\$12.06	\$15.53	\$15.53
Direct Heliostat Support	\$0.00	\$0.00	\$0.00	\$0.00	\$0.00
Field Costs	\$18.88	\$26.96	\$32.02	\$57.84	\$57.84
Foundation	\$2.74	\$2.41	\$18.92	\$7.76	\$7.76
Field Wiring	\$8.70	\$15.31	\$7.26	\$14.73	\$14.73
Alignment and Checkout	\$7.45	\$9.23	\$5.85	\$35.35	\$35.35
Total Installed Cost	\$149.10	\$156.68	\$213.85	\$182.21	\$147.96

Cost estimates for BSE's 15 m² heliostat have also been included; these estimates are adapted best guess values as presented by the DLR (Buck, 2014). BSE is currently the largest international commercial heliostat producer and forms the most appropriate high volume commercial benchmark to date. Aspirational costs are also included for a novel rim drive heliostat currently under development at the DLR. This heliostat is an extremely low cost but novel alternative that is yet to be fully tested and evaluated (Buck, 2014).

2.8 Heliostat production and manufacture

Several early studies exist pertaining to heliostat manufacture and production for specific heliostat designs (Drumheller, et al., 1980) (Britt, et al., 1979) (Brandt & Chang, 1981) (Drumheller, et al., 1979).

Britt et al. (1979) show that increasing volume production to 25 000 units per annum (p.a.) on the first generation McDonnell Douglas heliostat, reduces cost between one 33% and 50% of the cost of the heliostat in job shop production. However, significant capital investment cost for tooling and production facilities is

¹ 1.37EUR to USD and 10.37USD to Rand - 2013.

†Control and Cabling costs are fixed costs which are independent of area. These costs are represented as \$/m² and should be multiplied by area for fair comparison between heliostats.

required. Britt et al. (1979) also show that 81% of the factory cost for heliostat manufacture is material cost, thereby highlighting the importance of heliostat material cost reduction. Drumheller et al. (1979) further the need for reduced material cost by showing a 20% cost reduction in the McDonnell Douglas heliostat by increasing production volume from 25 000 units pa to 250 000 units pa.

More recently, Kolb et al (2007, p. 97) state that “heliostat price is strongly dependant on production rate” as price reductions of 38 \$/m² are seen by increasing volume form 5 000 units p.a to 50 000 units p.a. on the ATS 150 heliostat.

These effects of volume production tie in with the fundamental principles of design for manufacture and assembly (DFMA) as shown by (Boothroyd, 2010).

2.9 Conclusion

Heliostat cost analysis is currently in its infancy and is an overarching topic that covers a wide spectrum of design issues. Although some cost sensitivities have been shown in literature, there is still no clear indication of what constitutes a cost optimum heliostat. The wide variety of current commercial heliostat designs and sizes further illustrates this point.

System performance models are presented in literature, but limited publications covering heliostat cost or methods for exploring heliostat cost have been found at the heliostat component level. A means to compare heliostat cost and performance is required at the heliostat sub-component level.

The following chapter provides a method outline for the cost and performance analysis pursued by this study.

3. Method

A method is presented for exploring heliostat cost by deconstructing various tangible features of the heliostat cost problem into discrete models for analysis. In addition to providing an overview of this process, this chapter also gives the generic theoretical foundation to the method applied in the subsequent chapters.

3.1 Overview

Two discrete models are initially presented in Chapter 4 that estimate and evaluate heliostat cost and performance by means of a cost and error model, allowing for the establishment of a cost and performance reference point for further analysis. The subsequent analysis shown in Chapter 5 then uses four auxiliary methods to explore several tangible cost sensitivities associated with generic and specific proponents of heliostat design.

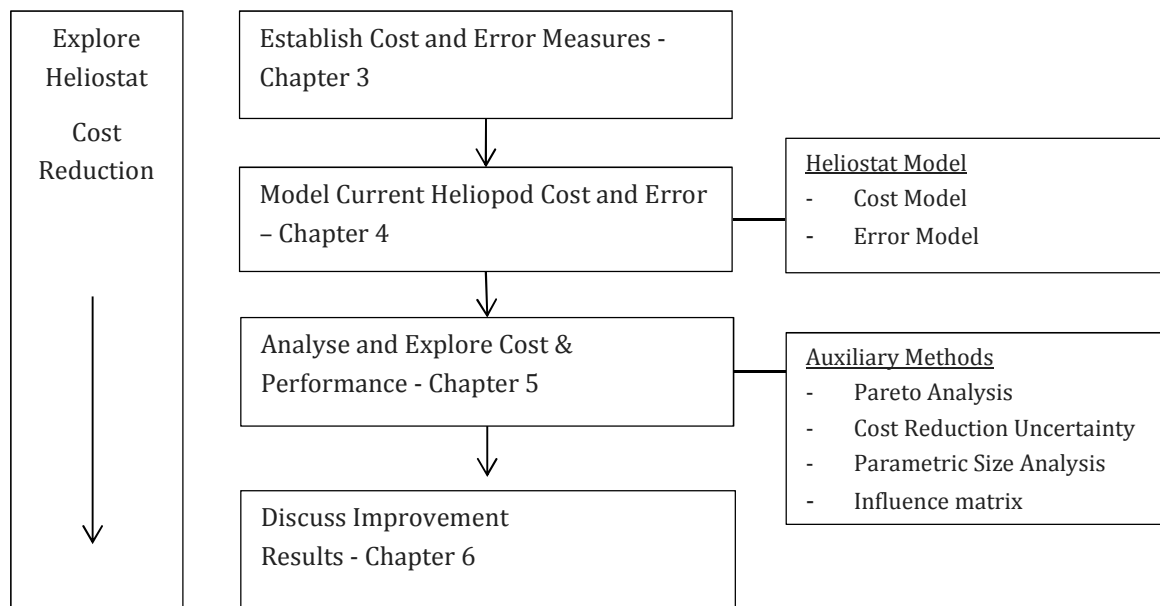


Figure 3.1: Method overview

In Chapter 4, the cost and error models will use geometry and cost data from the existing Heliopod design to form a known dataset. The result of the analysis on this dataset steers third generation design choices towards a lower cost solution.

3.2 Cost models

Allocating a degree of confidence to results produced by a cost model will depend on the class of cost estimation technique incorporated into the model. Three common approaches are discussed below. These approaches are considered as classical cost estimation techniques (Cavalieri, et al., 2004).

3.2.1 Regression based cost models

Regression based models are qualitative and use historical cost data of a similar product to establish a linear relationship between product cost and a certain design variable (Niazi, et al., 2006). This cost to design variable relationship is then typically employed to forecast the cost performance for that variable on the current product being developed. These models can be misleading as the degree of similarity between the historical data and the current product are often difficult to quantify (Cavalieri, et al., 2004). Further, isolating a desired variable from historical data can often be difficult as learning rates and specific context factors, that are inherent to the desired variable, may skew results (Cavalieri, et al., 2004).

3.2.2 Parametric cost models

Parametric models are quantitative in nature as they express cost as an analytical function of product variables (Cavalieri, et al., 2004, p. 168). The variables in question are typically a product's features, geometry, sub-components or performance characteristics. These variables are referred to as the cost drivers while the analytical function linking the cost driver to the final cost is called the Cost Estimation Relationship (CER). Typically, the CER used in a parametric analysis are built through the use of statistical methodologies or logical engineering judgement, which in some cases can be simplified with certain case dependant assumptions. Similar to the regression analogy discussed above, the degree of confidence in the model's accuracy depends on the accuracy of the CER and the assumptions or statistical methodologies used to create it. Often regression methods can be used to validate these CERs (Niazi, et al., 2006).

3.2.3 Analytical cost models

Using an analytical cost model is highly quantitative and is used when a product is already well defined or in the prototype stages. This process typically involves the decomposition of the product into elementary units, operations and activities that represent different resources consumed during the production process (Niazi, et al., 2006).

3.2.4 Auxiliary methods

In addition to the classical methods discussed above, four discrete methods are later used in Chapter 5.

A Pareto chart is used as a means to determine the component or components that hold the most significant scope for cost reduction. The chart is based on Pareto's rule, which states that "20 percent of a set of independent variables is responsible for 80 percent of the result" (Tsai, 1998, p. 752). The Pareto chart arranges the proportion of total costs/m² held by individual heliostat components from largest to smallest, allowing for the qualitative identification of component cost sensitivities and, therefore, the identification of the greatest total cost reduction opportunity. Further analysis allows for the determination of possible courses of action that are likely to lead to the largest cost reduction or performance improvement. This is achieved by estimating the potential benefit of the proposed course of action and ranking the outcome in order of highest to lowest. This ranking allows for the strategic identification of the component contributing to the highest cost or tracking error.

A comparative triangular distribution is also used in conjunction with an analytical cost model. This distribution compares two already known heliostat component benchmark costs with that of the Heliopod case study. If any existing heliostat embodiment with a known corresponding cost has already been achieved or claimed, the probability of realizing lower component costs on the Heliopod can be estimated. A similar study was completed by Kolb et al (2007), which examined the price reduction potential of research proposals in heliostat cost reduction.

An abstracted parametric cost analysis for heliostat size (Blackmon, 2013) is also explored and applied to the Heliopod case study. This parametric model establishes 3 discrete cost categories for heliostat components and employs a unique CER for each category. The CER then allows for the relationship between cost and heliostat size to be explored parametrically.

Lastly, an investigation to further the understanding of the "knock-on effect" of heliostat components on each other, an Influence matrix (IM) (Gauche & Wei, 2002), is proposed. The IM used here qualitatively shows how specified parameters of one component can have a knock-on effect on other components through the heliostat. This allows the net cost effects to be noted and later calculated.

3.3 Error model

The total power intercepted at the receiver is the heliostats primary performance measure (Schwarzbözl, et al., 2009). The degree of optical error has a direct effect on the total useful power reaching the receiver since it defines both the image position as well as the flux distribution (Biggs & Vittitoe, 1979).

Total optical error (σ_{Tot}) is representative of the final reflected image shape and position relative to the ideal central mirror normal. (Biggs & Vittitoe, 1979; Ulmer, 1998). Several factors contribute to the total optical error such as optical aberration, sun shape, beam quality and aim point uncertainty. Assuming statistical independence, these errors can be combined into a circular normal distribution as shown by Schwarzbözl et al. (2009) in Equation 3.4.

$$\sigma_{Tot}^2 = \sigma_{Aberr}^2 + \sigma_{Sun}^2 + \sigma_{BQ}^2 + (2\sigma_{Track})^2 \quad (3.4)$$

The term σ_{Sun} represents the error as a result of sun-shape and is well documented in Schwarzbözl et al. (2009), Biggs and Vittitoe (1979) and Bent et al. (1980). The term σ_{Aberr} signifies the error due to optical aberration caused by off-axis reflection; this can be seen in detail by Schwarzbözl et al. (2009)

The beam quality, represented by σ_{BQ} , is the measure of all imperfections specific to the physical reflecting surface (Schwarzbözl, et al., 2009). These include specularity, slope error and shape error caused by environmental effects such as wind and gravity. Due to the law of refraction (Snell's law), an error resulting from angular displacement in the mirror-normal causes an error of twice the magnitude in the reflected beam (Duffie & Beckman, 2006). Consequently, slope error is typically shown in terms of the divergence half angle (Ulmer, 1998). Again a statistically independent circular normal distribution is assumed and is shown in Equation 3.5 (Ulmer, 1998).

$$\sigma_{BQ}^2 = \sigma_{Specularity}^2 + (2\sigma_{Slope})^2 + \sigma_{Wind}^2 + \sigma_{Gravity}^2 + \sigma_{...}^2 \quad (3.5)$$

Aim point errors, or tracking errors, are of interest to this study. These errors are deviations of the mirror normal from its ideal direction (Schwarzbözl, et al., 2009). Aim point errors are also subject to Snell's law, and as a result the error in the beam is double the normal vector error (as shown by Figure 3.3). Tracking errors are represented by Equation 3.6 (Schwarzbözl, et al., 2009). Here, each of the statistical errors is combined into a circular symmetric distribution.

$$\sigma_{Track} = \sqrt{\sigma_{Axis\ 1} \times \sigma_{Axis\ 2}} \quad (3.6)$$

Errors are stacked for each axis as shown by Figure 3.2. These errors are summed in quadrature for each axis by Equation 3.7

$$\sigma_{Axis} = \sqrt{\sigma_1^2 + \sigma_2^2 + \sigma_3^2 \dots} \quad (3.7)$$

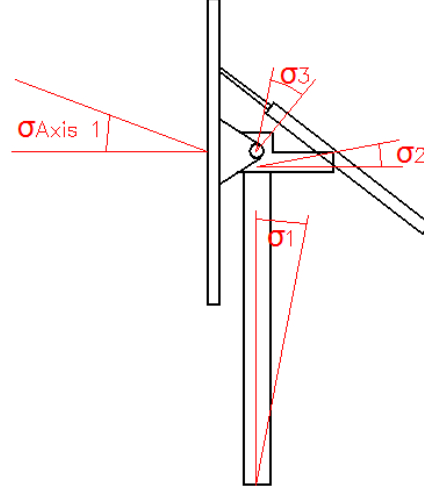


Figure 3.2: Combined effect of sub-component normal vector pointing errors

For the purpose of this study, Normal Vector Error (NVE) will be the reference for error measure. Once NVE errors are established, these values can be doubled to account for the reflected beam error often referred to as on-target error.

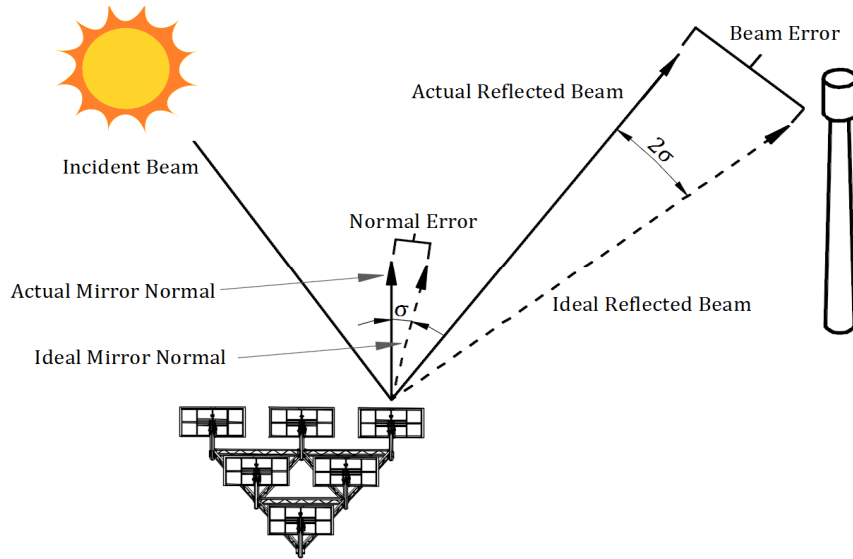


Figure 3.3: Classification of beam error and normal errors for an isolated heliostat. Modified from Zavoico (2001) and Slack et al. (2015)

When evaluating a heliostat optical performance it is important to consider all of the above errors. Zavoico (2001) suggests the creation of an error stack that allows for

the strategic identification of key error contributors within both beam quality and tracking error. This error stack will differ significantly depending on heliostat design as well as the degree of component error resolution required from the analysis.

In this study, a mixture of empirical and analytical methods was used to determine the total heliostat tracking error. In the following chapter, each component's respective tracking error will be determined individually and combined statistically as shown above.

3.4 Conclusion

A cost effective heliostat solution would have to satisfy a variety of performance and secondary cost trade-offs that positively affect LCOE. The sensitivities associated with these performances and secondary costs appear complex, and the effects of design changes to relatively simple heliostat components can have large implications on system costs.

No single method exists for comparing heliostat cost and performance. Due to the complexity of heliostat cost, multiple methods for exploring cost are proposed. The fundamental methods and theoretical foundation of cost and error modelling described in this chapter are used in the proceeding chapter to quantify the cost and performance of the Heliopod system. The multiple auxiliary methods are then used to further explore heliostat cost within the Heliopod system.

4. The Heliopod

The following chapter provides detailed understanding into the current Heliopod design and establishes a departure point for both component cost and tracking error performance. This departure point is used in later chapters as a benchmark against which further improvements can be measured and investigated.

Sections 4.1, 4.2 and 4.3 of this chapter include text from the author's prior work as published in the peer reviewed proceedings from the 2014 South African Solar Energy Conference, Port Elisabeth (Larmuth, et al., 2014).

4.1 Heliopod general description

The Heliopod was developed as a research heliostat. As a result, its design differs from that of commercial field based heliostats. In addition, the design, development and construction process was allocated a 12 month delivery schedule resulting in certain design decisions being constrained by lead times. The location of the Heliopod on the roof of a University building presented a variety of optical safety concerns, leading to design requirements that prioritised design-for-safety before performance, schedule and cost. These design priorities resulted in a high cost heliostat with several design features specific to safe operation in its exact application on the solar roof laboratory.

The Heliopod incorporates six facets with a total reflective area of 13.4 m^2 . Each individual facet has a glass metal construction consisting of a float glass mirror with a reflective area of 2.23 m^2 bonded to a galvanised steel backing frame. The six heliostats have azimuth elevation tracking mechanisms driven by linear actuators in the elevation and a slew drive in the azimuth. The heliostat pedestals are connected by a hot dip galvanised steel lattice truss, which creates a direct heliostat support and removes the need for a traditional heliostat foundation. Structural components are all manufactured from standard off-the-shelf mild steel cross sections and laser cut plate work weldments. Additional Heliopod details are shown in appendix A.

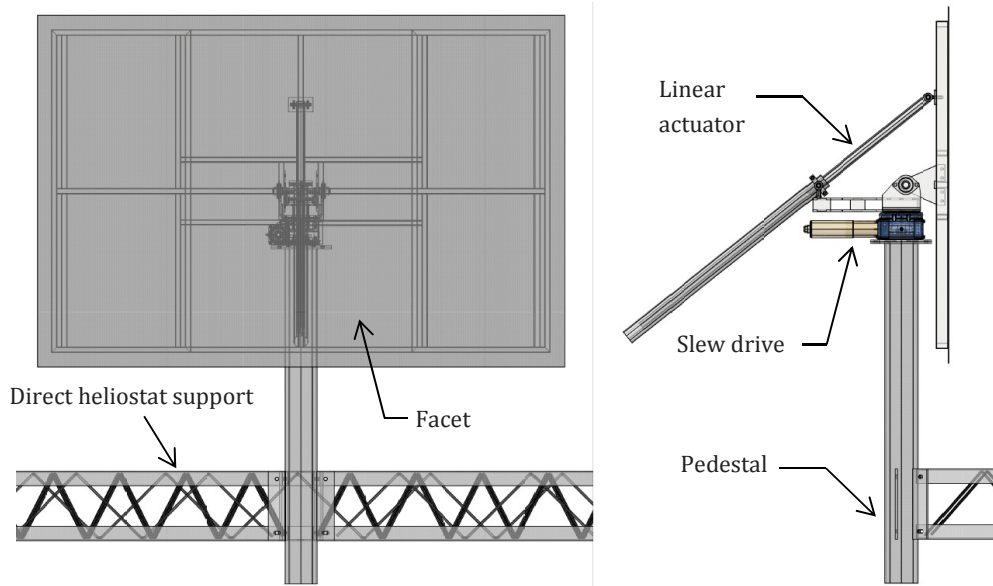


Figure 4.1: Individual heliostat description

4.1.1 Design requirements

Design requirements were set up upon which the research Heliopod design was based.

Table 4.1: Heliopod design requirements

Requirement	Minimum Requirement Value
On-target accuracy	1.875 mrad normal vector error (sum of component Error) 150 mm deviation on target at a 40 m slant range
Component accuracy	0.625 mrad RMS tracking error 0.625 mrad pedestal flex 0.625 mrad mechanism flex
Operational winds	Track up 20 km/h Stow between 20 km/h and 50 km/h Survive stow loads of up to 100 km/h
Reflector Image	Image minimized for 14:00 – 16:00 experiments to have >75% of reflected energy falling within focused image area on target at 20 km/h
Flexibility	Modular Design: swappable heliostat facets, drives and pylons
Foundation	Floor standing steelwork lattice pedestal to meet component accuracy specifications. Control room roof structure to meet pedestal accuracy specifications.
Tracking mechanism	Default pedestal with either azimuth elevation tracking or fixed horizontal

Array layout	2/3 of aperture installed on control room roof and 1/3 of aperture positioned on lab floor
System Life Span	5 Years

4.1.2 Heliopod design loads

Experimental wind tunnel data, published by Peterka and Derickson (1992), allowed for the calculation of worst-case, quasi-Static wind force and moment values about the X, Y and Z heliostat axes (see Figure 4.2). These published force and drag coefficients consider only isolated heliostats with an aspect ratio of 1. The original wind loading data used for the Heliopod design incorporated this method as it only considered square heliostats and used large factors of safety along with conservative wind load coefficients. Revised wind loading data is presented below based on Peterka and Derickson (1992) with corrections for aspect ratio and revised load coefficients as shown by Pfahl et al. (2011) and Pfahl et al. (2011).

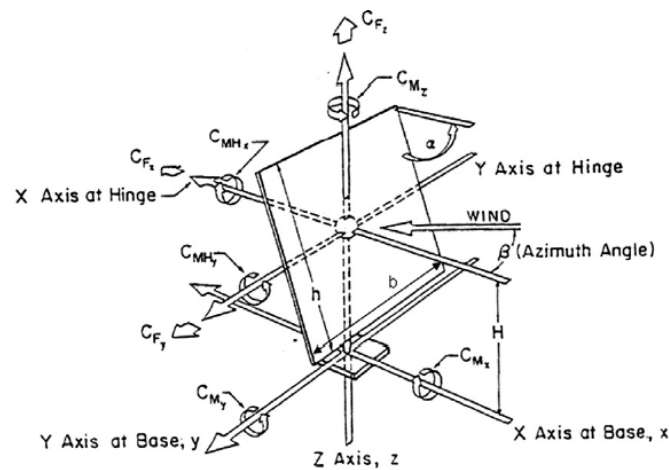


Figure 4.2: Heliostat co-ordinate system and load designations (Peterka & Derickson, 1992)

The Heliopod system was designed to meet accurate tracking requirements up to a windspeed of 20 km/h. The corresponding peak load data is for 20km/h as presented in Table 4.2. Loading corresponds to four alternate elevations (α) and azimuth (β) facet positions with the worst-case condition shaded on the right.

Table 4.2: Peak wind loads for an aspect ratio of 1.5 at 20 km/h

α , [°]	90	30	90	0	Worst-Case Loads
β , [°]	0	0	65	0	
F_x [N]	68.46	34.56		10.05	68.46
F_z [N]		45.37		14.35	45.37
M_{HY} [N.m]		15.77		6.55	15.77
M_Z [N.m]			20.58	0.82	20.58
M_Y [N.m]	86.30			18.61	86.30

The heliostat must be able to move in wind speeds of up to 50km/h. This speed represents the design limit for structure and drives in all possible facet orientations. Accurate tracking performance is not required above 20 km/h.

Table 4.3: Peak wind loads for an Aspect Ratio of 1.5 at 50 km/h

α , [°]	90	30	90	0	Worst-Case Loads
β , [°]	0	0	65	0	
F_x [N]	427.78	215.99		62.83	427.78
F_z [N]		295.22		70.29	295.22
M_{HY} [N.m]		98.58		40.92	98.58
M_z [N.m]			128.63	5.15	128.63
M_Y [N.m]	539.26			116.28	539.26

Survival wind speeds form a design limit for the structure and drives for the stow position only as shown in Table 4.4.

Table 4.4: Peak wind loads for an aspect ratio of 1.5 at 135 km/h

α , [°]	0
β , [°]	0
F_x [N]	445.88
F_z [N]	498.84
M_{HY} [N.m]	290.40
M_z [N.m]	36.52
M_Y [N.m]	825.22

The loads and methods presented are now used as input values to evaluate load bearing components and proportional costs of various heliostat sizes in the proceeding sections.

4.2 Heliopod cost model

In this section, the cost of the Heliopod and its sub-components are modelled. Only the direct costs for the individual parts along with corresponding overhead and labour costs for that particular part are considered. In this instance, installation transportation and assembly costs are excluded.

4.2.1 Invoiced component costs

Since the Heliopod is already in the prototype stages and therefore well-defined, quantitative cost calculations can be made. As indicated by Niazi et al. (2006) this process typically involves the decomposition of the product into elementary units, operations and activities that represent different resources consumed during the

production process. A detailed quantitative cost breakdown for a single Heliopod was established directly from invoices and known production times and labour rates. A more detailed cost breakdown can be seen by Appendix B.

The total invoiced cost of the Heliopod equates to \$544.60 /m², which is high in contrast to current cost benchmarks mentioned in Table 2.1. The majority of the high cost associated with the Heliopod prototype is due to the low production volume. The custom steel parts were built by job-shop steel contractors outside of the university, and the standard drives were ordered in small quantities. As a result, a large portion of the steelwork costs were dedicated to labour, overhead and profit on the part of the contractor. A Pareto chart is used in Figure 4.3 to display the component costs as invoiced to Stellenbosch University.

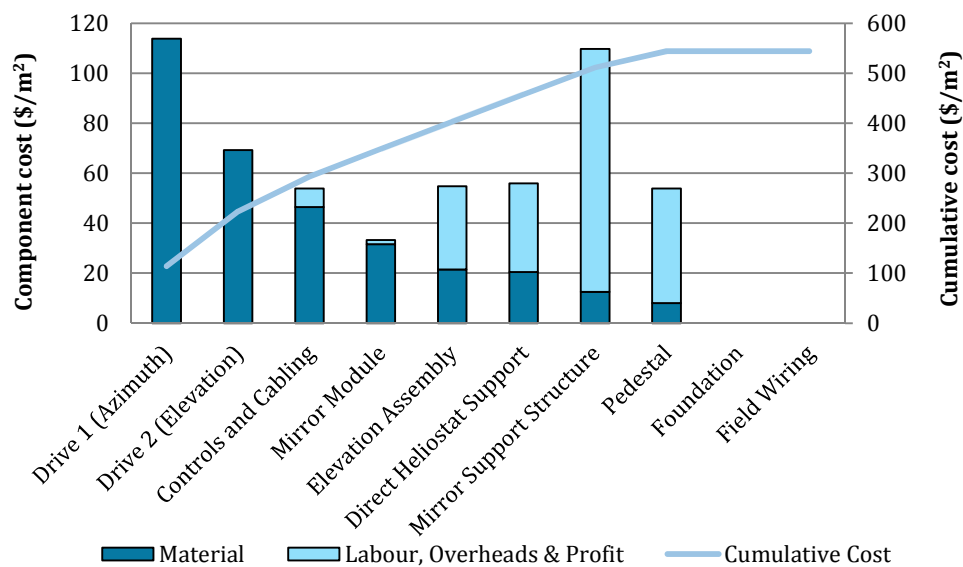


Figure 4.3: Invoiced Heliopod component cost in a Pareto chart– 2013 USD

Only a total cost was obtainable from the respective contractors and suppliers. The component material costs were then estimated separately by acquiring standard raw material and sub-component costs from local suppliers. The subtraction of the estimated material cost from the invoiced component cost resulted in a single value for labour, overhead and profit. Further resolution into the proportions of labour overhead and profit are not known and will differ between contractors. Since the drives, bearings and fasteners were off-the-shelf items, they all were considered to be material costs with a single cost value.

4.2.2 Volume adjusted costs

For products manufactured in high production rates, the products' material mass can be considered a qualitative measure of its cost (Pfhal, et al., 2013) (Kolb, et al., 2007). This is because the reduction of labour costs with an increase in production

rates results in material and commodity costs holding the highest proportion of direct heliostat fabrication cost (Drumheller, et al., 1979).

To estimate an expected production volume for the Heliopod, alternate plant sizes were compared against the number of units required per annum. South Africa is expecting planned CSP growth in the domestic utilities market in the region of 100 MW p.a. between 2016 and 2025 (DOE, 2013). Assuming Heliopod manufacturing meets 10% of this growth, a production volume of 18 685 units would be required per annum. This value was simplified to 20 000 units per annum in order to create a hypothetical production volume for use in this report.

In order to view the Heliopod component costs in a high volume scenario, the cost data shown in Figure 4.4 was adjusted to approximate material costs, which are more relevant in a high volume scenario. The previous Pareto is now adjusted for high volume costs at a production rate of 20 000 units per annum (Figure 4.4). Since detailed estimates of high volume production costs for the Heliopod are out of scope for this study, qualitative assumptions and supplier enquiries were used to estimate the reduced cost resulting from high volume production.

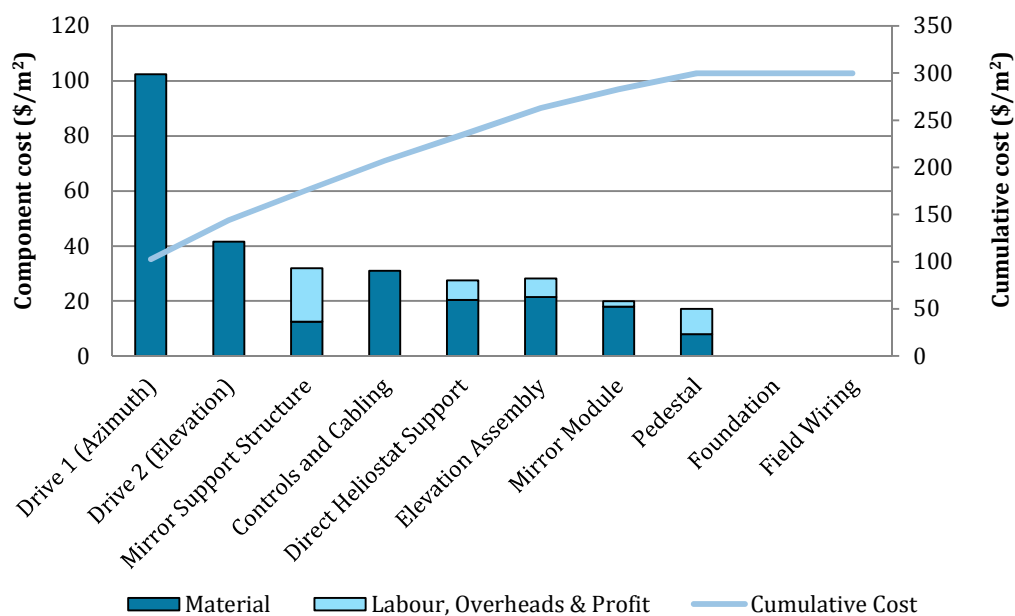


Figure 4.4: Volume adjusted component cost data for 20 000 units – 2013 USD

Since off-the-shelf drives are already higher volume products, lower costs can be assumed at large order quantities. High volume prices were solicited from the Heliopod slew drive and linear actuator suppliers in order to establish volume costs for the current design. The Slew drive supplier indicated that increasing the order volume from 10 units to 10 000 units will only incur a 10% cost reduction at which point a cost ceiling is reached (H-FANG Group, 2013a). The linear actuators showed

a greater cost reduction in the region of 40% (Satcontrol, 2014). These reductions exclude potential cost savings from shipping large quantities as well as the cost savings from product customisation and price negotiation.

As per Britt et al. (1979), an 80% reduction in labour was assumed on all steelwork components to account for higher production volumes. No reductions were made to material cost as the exact design was maintained. Cost reductions from increased order volumes of commodity items such as glass is considered negligible because of the naturally high production rate at which glass is already produced (Kolb, et al., 2007).

The control boards were hand soldered, and electronic components were purchased in low volumes. A 90% reduction in labour was assumed allowing for a conservative estimate as electronics typically experience significant cost reductions at volume. Costing shown above for controls and cabling included that of power electronics and accounted for PV panels wiring and batteries.

The initial design was maintained in all the previous cost assumptions, allowing for the creation of a departure point cost of \$300 /m² at high volume.

4.3 Heliopod error model

The error mode discussed in Section 3.3 was then used to establish the component level error contribution of the Heliopod and its sub-components. The model incorporates a combination of empirical and analytical data modelled in MS Excel. Each component was assessed individually after which the errors were combined to form an error stack and establish a total optical error figure.

4.3.1 Pedestal error

The Pedestal is the triangular base structure and it includes both the pylon and the direct heliostat support structure (Figure 4.1). Deflection measurements were conducted using a laser to simulate the heliostat normal vector. Displacement measurements were recorded from a target at known loads which approximate wind loads (see Appendix C). The pedestal showed better performance in its ability to counter vertical normal vector displacement than its ability to counter horizontal rotation because of the simulated azimuthal wind moments. Worst case operational loads for 20 km/h wind speeds were induced in the pylon showing a vertical error of 0.119 mrad about the pylon base. Azimuthal loading yielded an error of 0.3 mrad about the pylons centre axis. Assuming a normal distribution due to independent load cases, these tests resulted in a total Pedestal error of 0.4 mrad for the Heliopod in operational conditions.

In addition to the experimental data, a simple pylon model was built that assumed a ridged cast-in-place cantilever beam with simulated wind and gravitational loading as shown by Equations 4.1 and 4.2 (Shigley & Mischke, 2003).

$$\theta_x = \frac{F_x l^2}{2EI} \quad (4.1)$$

$$\theta_z = \frac{M_z l}{GJ} \quad (4.2)$$

Torsional deflection values as well as vertical deflections were yielded from the equations above, allowing for subtraction of pylon deflection values from measured values.

4.3.2 Drive error

The slewing drive installed on the Heliopod has a mechanical position error of $< 0.15^\circ$, as per the manufactures datasheet (H-FANG Group, 2013b), corresponding to a NVE of 2.63 mrad. A measured error was found from laboratory tests yielding 0.16° 2.79 mrad as shown by Appendix C. Since the slew drives' mountings embody the primary axis, the backlash error inherent to the slew drive causes an equivalent normal vector error. This error is the same at any azimuth position because of the rotary nature of the drive.

The manufacturers of the linear actuator, which drives the secondary axis, claim a maximum linear backlash of 0.2 mm (Satcontrol, 2013a). Direct linear backlash measurements taken on three identical actuators yields a mean actuator backlash of 0.09 mm.

4.3.3 Elevation assembly error

Unlike a slewing drive with a bolted flange interface, a tracking axes powered by linear actuators requires articulated joints at each actuator connection point as well as the axis of rotation (Larmuth, et al., 2014). These joints can introduce additional, non-deterministic heliostat error due to poor joint or bearing fits as well as shaft deflection.

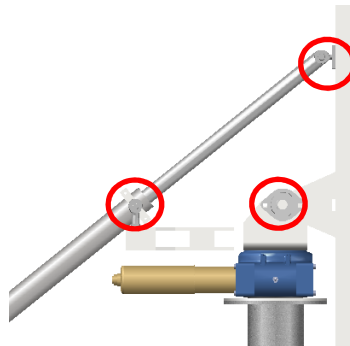


Figure 4.5: Heliopod elevation assembly showing actuator connections

Figure 4.6 shows the linear actuator connection geometry for the Heliopod elevation assembly. The effects of actuator backlash and joint movement on the facet normal vector depends on the position of the actuator connection points (A and B) relative to the secondary axis (O) and therefore differs depending on heliostat design and elevation position.

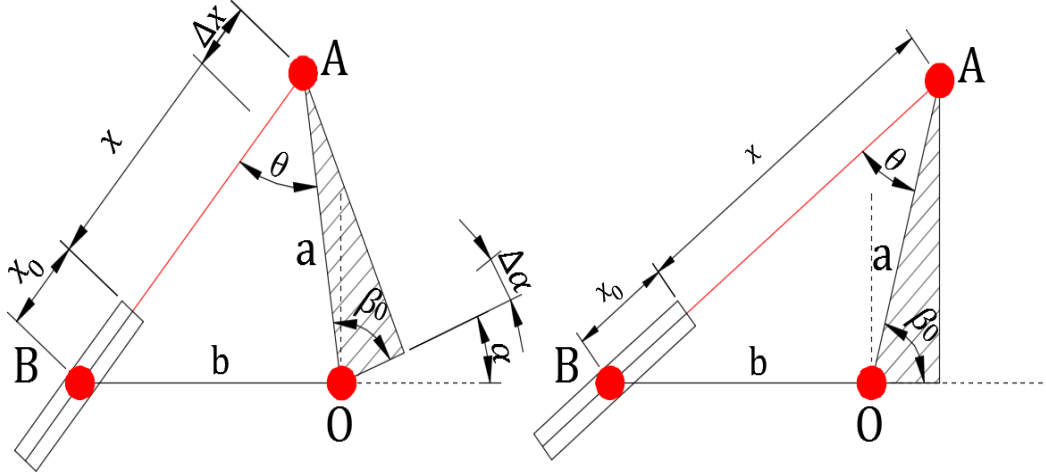


Figure 4.6: Heliopod elevation geometry modified from Guo et al. (2013)

Based on the law of cosines, Guo et al. (2013) develop a generic relationship between elevation angle (α), connection points (A,B,O) and stroke length (x) for a generic elevation assembly. Equation 4.3 shows the variation of the facet normal with a change in stroke length (Guo, et al., 2013).

$$\alpha = \cos^{-1} \left(\frac{(x + x_0)^2 - (a^2 + b^2)}{2ab} \right) - \beta_0 \quad (4.3)$$

Backlash generated in the actuator is treated as an instantaneous change in stroke length (Δx), allowing for the determination of the change in the facet normal vector ($\Delta \alpha$). The effect of backlash on the facet normal vector is a function of angle (θ) and is more prominent at the full actuator extension. The angular deviation of the normal vector induced by backlash is given by Equation 4.4.

$$\Delta \alpha_{\text{backlash}} = \frac{\Delta x}{a \times \sin \theta} \quad (4.4)$$

The actuator connections incorporate a stainless steel pin located by two self-aligning rod-end bearings. To account for the total error induced in the shaft and rod-end fits, a centred normal distribution is assumed as shown by Equation 4.5 (Scholz, 1995; Shigley & Mischke, 2003). T is the total tolerance clearance in mm, while T_1 and T_2 represent the respective shaft and bearing tolerances. The angular deviation of the normal vector induced by backlash is now given by Equation 4.6.

$$T = \sqrt{T_1^2 + T_2^2 + \dots + T_n^2} \quad (4.5)$$

$$\Delta\alpha_{\text{connection}} = \frac{T}{a \times \sin\theta} \quad (4.6)$$

To account for pin deflection, a simple support is assumed between the self-aligning bearings and the actuator pins. This simple support is modelled using Equation 4.7 as shown in Shigley & Mischke (2003). Shaft deflection in line with the actuator is given in mm. F is the force at the corresponding elevation position, l is the centre distance between the rod ends, E is Young's modulus and I is the moment of inertia for the pin. The shaft fit error and the shaft deflection is accounted in both ends of the actuator.

$$\delta_{\text{max}} = \frac{Fl^3}{48EI} \quad (4.7)$$

$$\Delta\alpha_{\text{Pinbend}} = \frac{\delta_{\text{max}}}{a \times \sin\theta} \quad (4.8)$$

The headstock is a laser-cut, welded assembly, which houses the heliostat elevation components and forms the connection interface between the primary and secondary axis. Here the headstock is simplified to embody a uniform beam with the cross-section shown in in Figure 4.7. The beam's length (l) is situated between points OB in Figure 4.6.

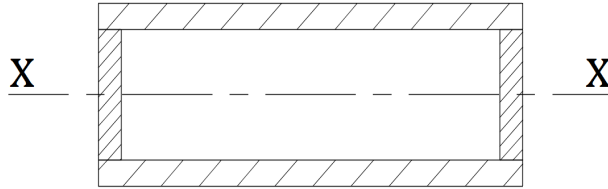


Figure 4.7: Simplified cross-section of the headstock

The bolted connection between the slew drive and headstock is assumed to be rigid with the deflection of its end point equivalent to the deflection of a cantilevered member. Standard beam end deflection was used, shown by Equation 4.9 (Shigley & Mischke, 2003).

$$\Delta\alpha = \frac{Fl^2}{2EI} \quad (4.9)$$

F is the force induced by the facet weight and wind loading, E is the Young's modulus and l is the beam length OB.

4.3.4 Mirror module error

The Heliopod mirror module has a spherical facet profile with a focal length of 47.5m. The resulting image can be seen in Figure 4.8.

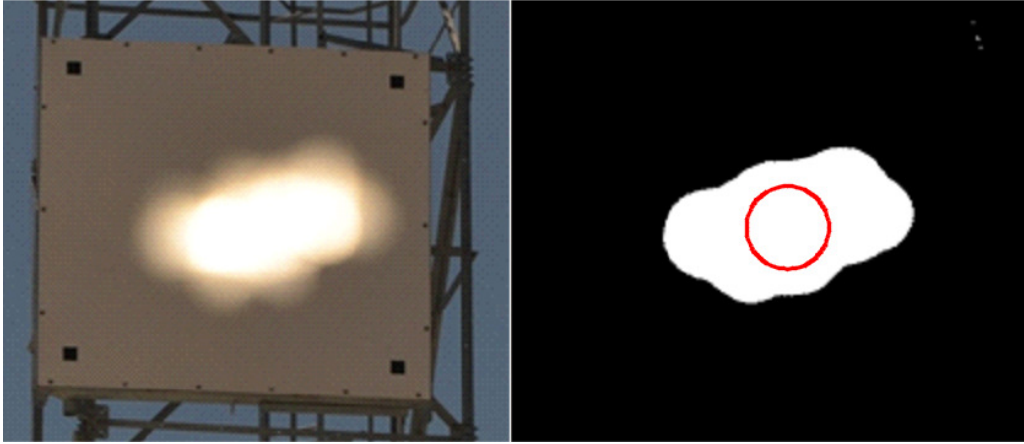


Figure 4.8: Facet image at focal length and time (16h00 at 47.5 m)

A heliostat with an ideal mirror curvature would generate an image at the receiver with a diameter for 9.3×10^{-3} times its focal length (Duffie & Beckman, 2006). In the case of the Heliopod, an ideal image would have a 441 mm diameter at a focal length of 47.5 m. This ideal image size is represented by the red circle in Figure 4.8. It is clear that significant errors are visible which can be attributed to various issues such as backing frame sag, image aberration, inaccurate mandrel manufacture and residual stress from adhesives. An estimation of net facet error is established at 4.65 mrad (normal vector), which encompasses all errors in both the mirror and the backing frame. This figure represents a net value for beam quality; its estimation is based on scale measurements taken from digital photos of the on-target image.

4.3.5 Control system error

The Heliopod incorporates a control system with wireless communication. The control system includes a model based, open loop error correction system, allowing for deterministic errors to be reduced over time due to heliostat calibration (Malan & Gauché, 2013). After the system is calibrated and deterministic errors are accounted for, the residual control system error is 1 mrad (Malan & Gauché, 2013). In the case of this study, the 1 mrad NVE was assumed to be equally divided between the primary and secondary axis.

4.4 Heliopod total error

Modelling the Heliopod error about the two tracking axes as well as the representative beam quality errors yielded the results shown in Figure 4.9. The total

normal vector optical error for the Heliopod was estimated here at 5.58 mrad for operational wind speeds.

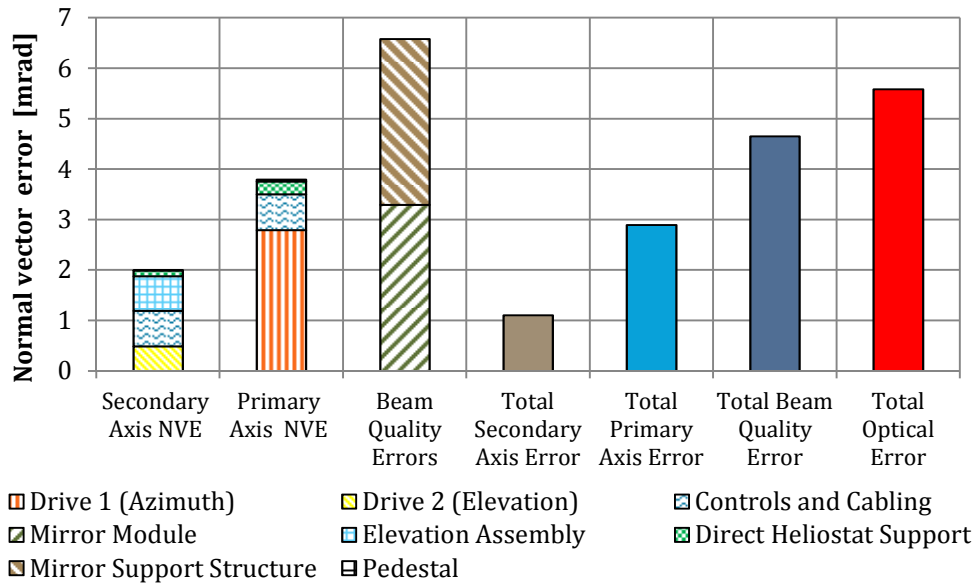


Figure 4.9: Total heliostat optical error (NVE)

The first three columns represent the errors stacked in direct summation; this shows proportion of relative error values but does not indicate a realistic total due to the unrealistic effect of direct summation. The error total for each axis and the beam quality total are shown as a natural distribution in the four right hand side columns. The criteria of this study considered tracking errors as the primary concern. Looking only at tracking errors, the Heliopod has a total error of 3.02 mrad.

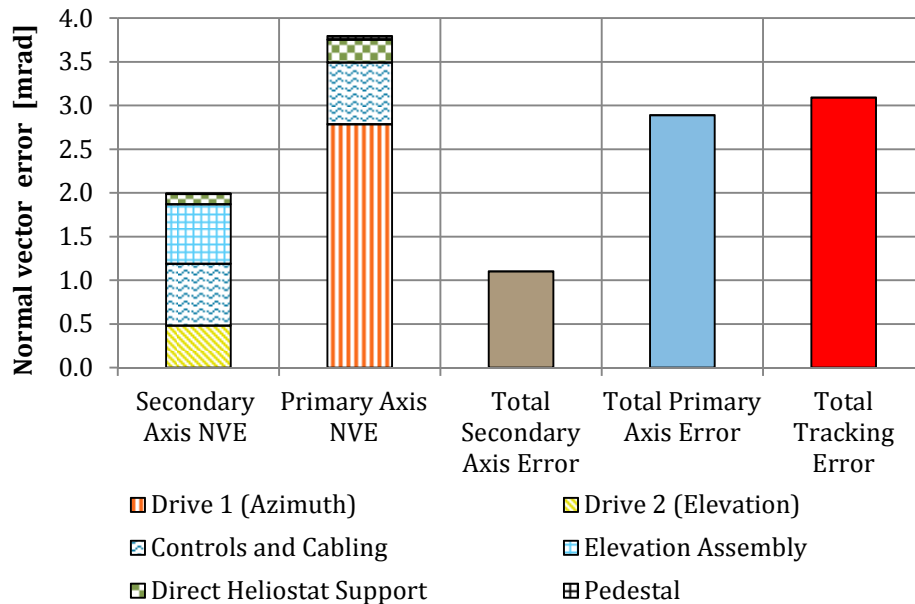


Figure 4.10: Tracking error stack and total (NVE)

4.5 Conclusion

Adaptable cost and error models were proposed that enable a logical search for improvements based on a starting point. Future improvements can be tested against this departure point. In the next chapter, Heliopod cost and performance is evaluated using the above dataset, and a cost improvement is proposed.

5. Analysis

Four different approaches to exploring heliostat cost reduction were applied to the Heliopod system. Each of these approaches provided insight into heliostat cost and performance sensitivities. A final cost reduction proposal was then drawn from the combined outputs of the four approaches. These cost improvement suggestions were then modelled and validated against the original Heliopod data set.

5.1 Heliopod Pareto analysis

Here a Pareto analysis allows for the determination of possible courses of action that are likely to lead to the largest cost reduction. Such a determination is achieved by estimating the potential benefit of the proposed course of action.

Figure 5.1 was used to identify the components responsible for the largest respective cost and tracking error. The chart shows the independent normal vector tracking error associated with each heliostat component as well as the corresponding cost of each component.

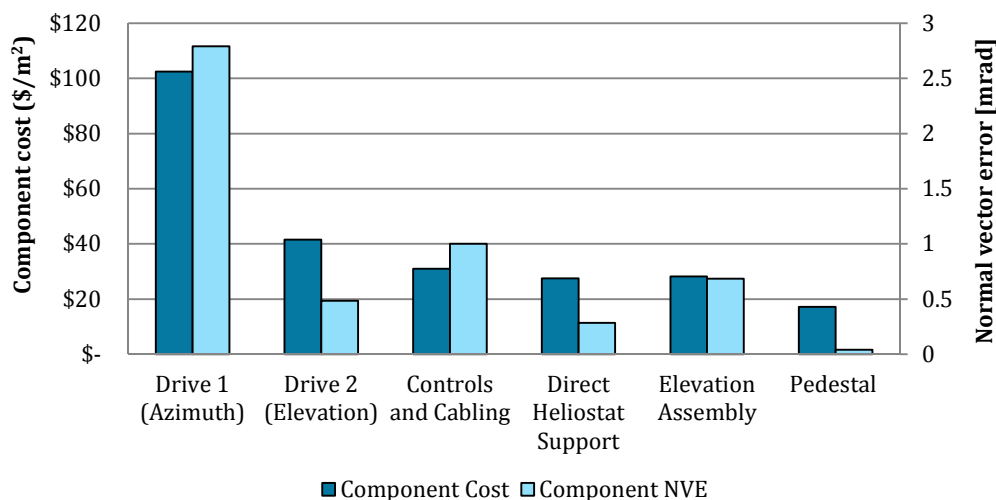


Figure 5.1: Combined cost and error of tracking mechanism components – 2013 USD

The largest contributor to both cost and tracking error is the slow drive used in the azimuth axis. The slow drive contributes 34% of the total heliostat cost (\$102 /m²) and contributes an NVE of 2.79 mrad. Although significantly smaller in cost and error, the linear actuator contributes the second and fourth largest cost and error amount respectively. Figure 5.2 shows that collectively the drives account for 48% of the Heliopod cost.

The elevation assembly, mirror support structure, and direct heliostat support and pedestal are all non-optimised steel components made up of standard steel cross-

sections and plate-work weldments. Together these steelwork items make up 34% of the heliostat's total cost.

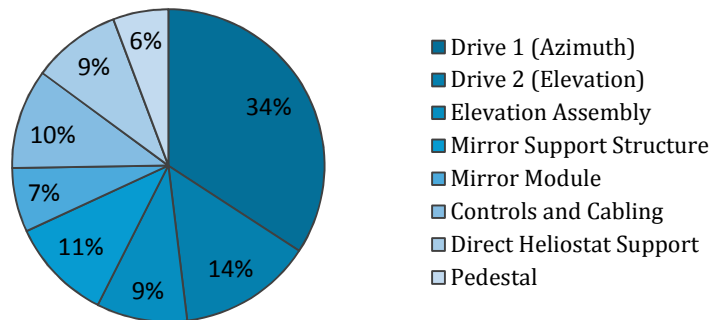


Figure 5.2: Component proportions of total cost (high volume)

The drives, elevation assembly and structure represent the largest cost and error contributors. These are now discussed individually in order to explore future alternate options for cost and performance improvement.

5.1.1 Azimuth drive

The slew drive is an off-the-shelf, generic format drive marketed at applications in a variety of industries such as agriculture, bulk materials handling and solar tracking (H-FANG Group, 2013b). Due to the generic nature of this drive, some features are not ideal for applications in the solar tracking industry. The slew drive has a heavy cast steel housing and robust worm gear stage. This robust design allows for high tilting moments and radial forces that are proportionally higher than the required torque output for a heliostat of this size (H-FANG Group, 2013b). The manufacturer advertises these features for use on cherry pickers, small mobile lifts and other applications where the slew drive is installed at the base of a tall, load bearing pylon (H-FANG Group, 2013b). It is expected that significant cost reduction can be achieved by removing these generic attributes that are not used in heliostat applications.

Other off-the-shelf slew drive manufacturers and product variations were investigated in a techno-economic market review (KMI, 2013) (H-FANG Group, 2013c) (XABC Bearing Company, 2014), (Sunslew, 2014), but no other suppliers were found who readily develop smaller slew drives better suited to the load ratings shown previously in Table 4.3. Each of the manufacturers investigated produce the same increments of standard drive sizes between 3" and 25". However, in all cases the minimum readily available slew drive size is a 3" drive. Although published performance differs somewhat between manufacturer and product range, a 3" drive typically corresponds to an output torque of ≥ 250 N.m., which is 1.95 times the

required azimuthal loading at 50km/h for a 2.23m² heliostat. This loading corresponds to a facet size of 3m² (Peterka & Derickson, 1992).

The inaccuracy on the Heliopod slew drive is due to backlash between the worm gear and the ring gear. Accuracy claims differ between suppliers. One of the manufacturers (KMI, 2013) claims higher precision in the region of 0.175mrad due to the use of a patented enveloping worm gear reduction. Three of the suppliers investigated provided costs for a 3" slew drive in increasing purchase volumes. Figure 5.3 shows the cost of the unit for three increments of order volume plotted against its claimed accuracy.

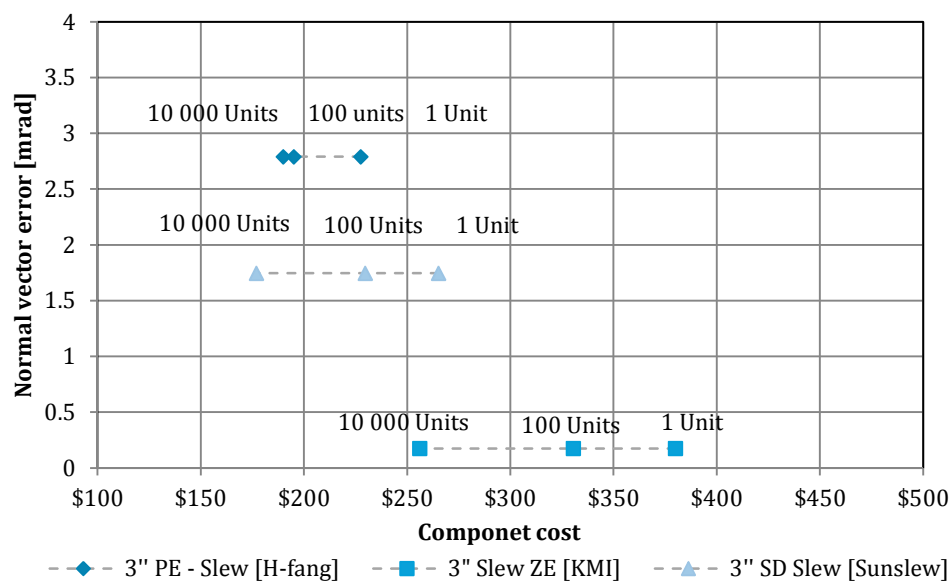


Figure 5.3: Slew drive manufacturer comparison for 3 inch slew drives– 2013 \$USD
(KMI, 2014) (H-FANG Group, 2013a) (Sunslew, 2015)

The slew drives shown above represent off-the-shelf components. A custom slew drive approach is seen by BSE, eSolar and Senner (amongst others) (Franck, et al., 2009) (Ricklin, et al., 2013a) (Vazques, et al., 2006). eSolar claims significant cost and weight reductions from plastic housing and plastic gearing on their custom gear drive (Ricklin, et al., 2013a).

The slew drives that are readily available from the manufacturers investigated here have the same generic design features and load ratings. A single manufacturer offers a more accurate solution, but only in the standard size increments previously discussed. This suggests that the cost reduction for smaller heliostats may lie in either a custom slew drive design or in increasing the heliostat size to correspond to the smallest drive size available. The most significant cost reduction will come from increasing the per unit order quantity.

5.1.2 Elevation drive

The elevation drive contributes 14% of the Heliopod's total cost and has a measured normal vector error of 0.48 mrad. The linear actuator used is an off-the-shelf drive and marketed specifically for use in the solar tracking industry (Satcontrol, 2013b).

A wide variety of actuator manufacturers currently exists in the commercial and industrial spheres. These manufacturers supply actuators to diverse markets for a range of applications. Coventry and Pye (2013) suggest that because of the volume production of existing industries, the use of off-the-shelf linear actuators will result in lower heliostat costs. However, the majority of the linear actuators' products investigated here (Bircraft, 2014) (Duff-Norton, 2014) (Vito Motion, 2014) (SKF, 2014) (Wuxi HongBa, 2014) are marketed for general purpose displacement applications, not accurate positioning. This renders their products inappropriate for use on solar trackers. The need for high mechanical resolution leads to a significantly smaller pool of appropriate off-the-shelf linear actuator products. Moreover, many suppliers who can provide high control resolution typically only supply larger size actuators to the solar tracking industry (NIASA, 2014) (Venture MFG. co., 2014). These suppliers, however, are able to provide custom solutions to larger volume orders. Two manufactures currently supplying smaller drives to the medical industries (Linak, 2014a) (Sito Motor, 2014) were investigated as alternatives to the current Heliopod drive; their cost and accuracy is shown at alternate order volumes in Figure 5.4.

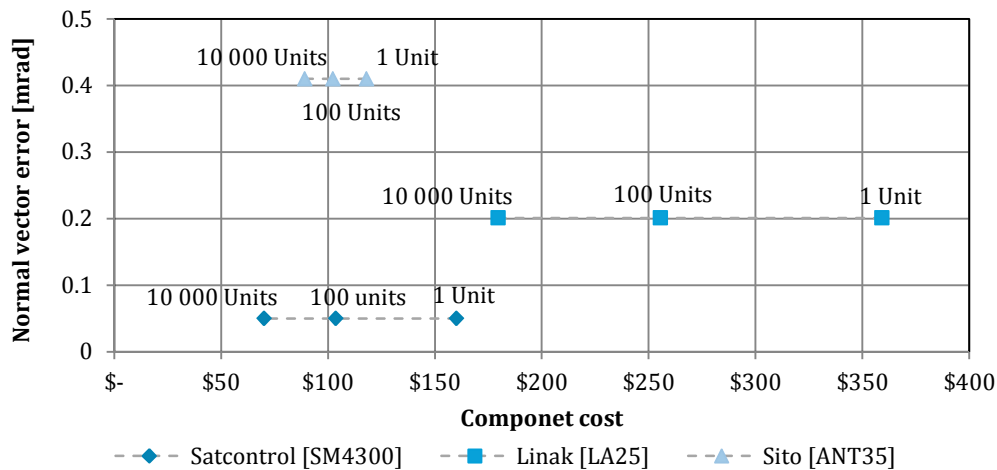


Figure 5.4: Actuator manufacturer comparison; for actuators available at appropriate size

5.1.3 Elevation assembly

The elevation assembly contributes the third largest tracking error to the Heliopod system. As indicated in Figure 4.5, the linear actuator requires three rotational connection points per actuator. The resultant error from these points was modelled

as described in Section 4.3.3 and examined for the worst case. The linear actuator is connected in a triangular configuration, and as a result it experiences a worst case error when the mirror normal is horizontal. This error reduces as the mirror rotates toward the stow position.

A contributor to elevation error is the error induced by the bearing fits and tolerances at the joints. No shafts were machined on the Heliopod; instead, loose running clearance fits were used as obtained from stock diameter steel and standard rod end bearings. These loose fits resulted in movement at the actuator connection points, which induce errors larger than the actuator backlash (Figure 5.5 Left). The deflection in the connection pins and headstock were also calculated (shown in Section 4.3.3), but were found to contribute negligible error within the operational windspeed threshold.

In order to reduce error, accurate alternate connection configurations may be required. The use of alternate fits are now explored. Figure 5.5 shows alternate standard machine fits (Shigley & Mischke, 2003). Each shaft tolerance and deviation limit is increased to reduce error.

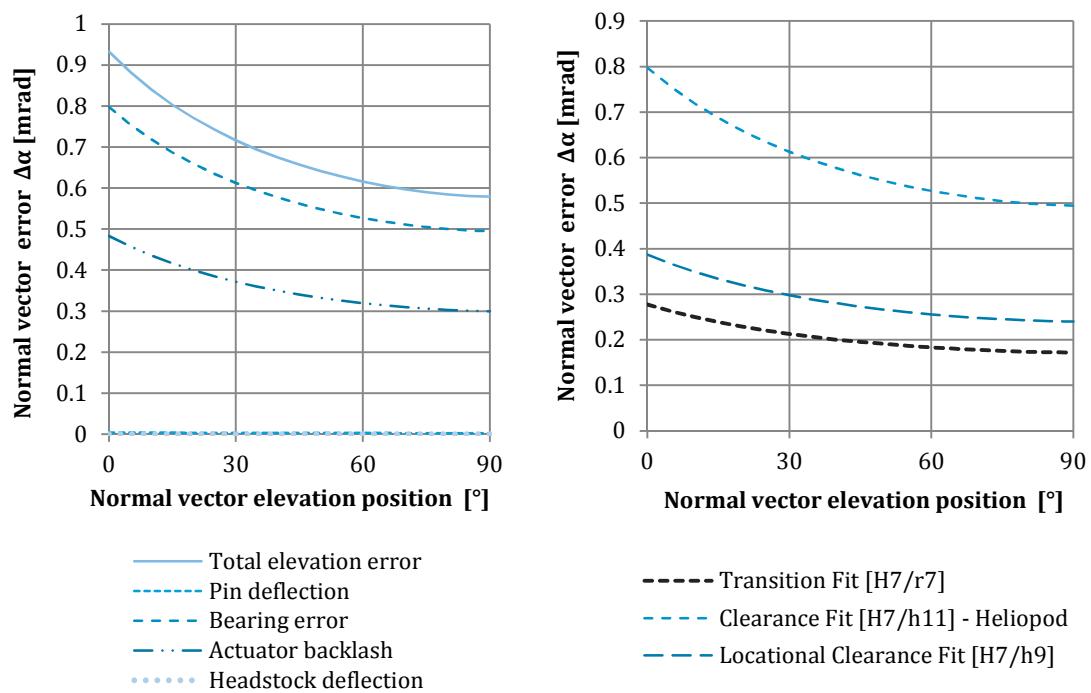


Figure 5.5: Left – Heliopod elevation assembly errors. Right: Errors for alternate bearing fits

The standard steel shafting used on the Heliopod is already a high volume product as it was cut from standard h11 round stock. In order to estimate the cost of higher tolerance fits, quotations were solicited for alternatives and compared to readily available round stock (h11). Several local precision engineering works offered

quotations showing significant cost increases (220%) for r7 tolerances in low volume cases (Bota, 2015) (Comar, 2015) (Metric Engineering, 2014). However, improved costs were achieved in volumes over 10 000 units (Metric Engineering, 2014) (Bota, 2015). Tolerance shafts require material removal to be cost feasible. The setup time for low volumes contributes to the high cost increase, where at high volume these setup costs are aggregated through the total production volume (Bota, 2015) (Chase & Greenwood, 1988).

Based on this comparison, tolerance shaft fits and press fit bearings could be incorporated to improve accuracy, provided high volume production methods are used.

5.1.4 Steel components

The steel components present scope for cost reduction by removing both complex manufacturing processes as well as structural optimisation for material reduction.

By cost proportion, the Heliopod steelwork items hold 35% of the total cost. Delport and Craig (2015) completed an optimization of the Heliopod pedestal structure for the operational windspeed range. This study suggested that by changing some key geometrical parameters in the design, a 27% reduction in steel could be achieved.

The steel prices used in the Heliopod cost model were supplied via an intermediate supplier (MACSTEEL, 2014) and not directly from the steel mill. In addition, quotations were solicited from local suppliers for the specific cost of hot dip galvanising per unit mass. In low volumes, the cost of batch hot dip galvanising added 52% to the pylon cost. The use of pre-galvanised tubing at low volumes added 28% to the pylon cost but would need further corrosion treatment post-processing and may compromise life span (Stephen Leatherbarrow, 2015).

5.2 Uncertainty in component cost reduction

The Pareto chart shown in Figure 5.1 shows the component costs in order of highest to lowest allowing for the strategic identification of the highest cost component contributing to tracking error. In order to further prioritise the cost improvement of these components, a comparative triangular distribution is used. This compares two already established heliostat benchmark costs (shown previously in Table 2.1) against the Heliopod. If any heliostat embodiment with a known corresponding cost has already been achieved or claimed, the probability of realizing lower component costs on the Heliopod can be estimated. A similar study was completed by Kolb, et al. (2007). However Kolb, et al examined the price reduction potential of research proposals in heliostat cost reduction, where this comparison looks at component level comparisons for cost reduction.

The probability density function for the triangular distribution used is shown by Equation 5.2 below (Ward & Dye, 2014). For each component line item, the three heliostats provide a lower limit (a) a peak limit (c) and an upper limit (b).

$$f(x) = \begin{cases} 0, & x < a \\ \frac{2(x-a)}{(b-a)(c-a)}, & a \leq x \leq c \\ \frac{2(b-x)}{(b-a)(b-c)}, & c \leq x \leq b \\ 0, & x > b \end{cases} \quad (5.1)$$

The probability of achieving less than the peak limit was investigated and is shown in the right hand column. Smaller deviations in cost between the three items are likely to show smaller scope for cost improvement or a potential cost ceiling.

Table 5.1: Triangular distribution for component cost reduction probability.

	STERG Heliopod	BSE Heliostat	DLR Novel Heliostat	Probability Percentage
	<i>Estimated High Volume</i>	(Buck, 2014)	(Buck, 2014)	Pr ($x < c$)
Mirror Module (Reflector)	\$19.90	\$16.44	\$13.15	51%
Mirror Support Structure	\$31.95	\$39.73	\$28.77	71%
Elevation Assembly	\$28.16	\$6.85	\$13.70	68%
Drive 1 (Azimuth)	\$68.31	\$28.77	\$2.74	60%
Drive 2 (Elevation)	\$48.53	\$8.22	\$2.74	88%
Controls and Cabling (Fixed Cost Used)	\$69.20	\$132.60	\$153.15	24%
Pedestal	\$17.16	\$15.53	\$12.42	34%
Direct Heliostat Support	\$27.53	\$7.76	\$6.21	93%

A moderate probability of reflector cost reduction is shown, since all three heliostats use glass mirror modules (Franck, et al., 2009) (Pfhal, et al., 2013). The small cost difference shown here may be attributed to the thickness of glass used. The mirror support structure used on the Heliopod and BSE are both steel and glass constructions. The lower cost on the DLR aspirational heliostats suggests a foam facet be pursued instead of steel, allowing for a 71% probability for cost reduction with the use of foam.

The cost of the elevation assembly is the least in the case of the BSE heliostat; this is due to the use of a slew drive in the azimuth axis requiring a less complex drive connection interface. The DLR novel heliostat uses rim drives with locking mechanisms creating a complex elevation assembly for each axis, with the benefit of reduced drive costs. The Heliopod elevation assembly is significantly more expensive since it is an un-optimised plate-work weldment with substantial scope

for material reduction. This probability suggests that the use of a slew drive would reduce the cost of the heliostat connection interfaces as it simplifies the elevation assembly.

The BSE heliostat uses a linear actuator in elevation and a slew drive in azimuth, while the DLR heliostat incorporates cable operated rim drives. A high probability 88% of achieving cost reductions with cable drives is shown here. The high cost of the Heliopod actuators relative to the BSE heliostat also suggests that lower cost actuator alternatives or customisations are available allowing for cost reductions without implementing a cable drive solution.

The control system is the only instance in the Heliopod which is already below benchmark costs. This suggests that only a small decrease in cost is attainable on the current control system. The control system cost data used to model the Heliopod costs, were based on an early wireless design which has no field wiring costs. This system also has undergone no lifetime analysis and included minimal controller redundancy in its design. It is likely that on completion of a second generation testing and particular certification for MTBF values and lifetime analysis would lead to higher costs on a next generation design (Malan, 2014).

A 93% probability for cost reduction is suggested for the direct heliostat support. Here this component line item is compared to traditional foundations used on the benchmark heliostats. These traditional foundations exclude the cost of ground preparation and may account for smaller deviation in cost, although not investigated here.

5.3 Parametric analysis for Heliopod size

The commercial trends discussed in Section 2.5 do not yet show any clear indication of an optimum heliostat size. A parametric cost model for minimum cost per unit area is now discussed. Blackmon (2012) (2013) created a methodology for parametrically determining heliostat minimum cost per unit area for a particular heliostat design. The following section is a summation of the fundamental principals and mathematics included in his works as well as further analysis specific to the Heliopod dataset.

5.3.1 Component cost to size relationships

The basis of Blackmon's parametric model is the creation of three sub-component categories into which heliostat components' costs are divided. Each category has a specific cost estimation relationship which is a function of heliostat area. This relationship is used to extrapolate component costs from an initial design point to alternate heliostat areas. The three cost categories are described as follows:

Category 1: Heliostat costs that are constant irrespective of size.

Category 1 costs are items that already have an inherent cost per unit area. These are components such as the reflector and mirror module purchased on a cost/m² value. For a given field aperture, the total quantity of reflective surface is constant irrespective of heliostat size. Category 1 components do, however, vary with production volume and, therefore, are affected by the field size due to larger order quantities.

Category 2: Heliostat costs that vary with heliostat loading.

Category 2 costs are associated with the load induced moment arms acting on structural and mechanical components. These are components such as drives, pedestals, support structures and foundations. Assuming a uniform wind speed acts on the heliostat, it can be shown that the imposed moment and torque acting on these components is proportional to the heliostat area by the three-halves power ($A_H^{3/2}$). As a result, the wind induced moment per unit area is approximately proportional to the square root of the heliostat area ($A_H^{1/2}$). Blackmon (2012) and Kolb et al (2007) have shown these load bearing component costs to vary linearly with torque and moment arm. This linear relationship causes these component costs/m² to be proportional to the square root of the heliostat area.

Category 3: Heliostat costs that are fixed, i.e. independent of area.

Category 3 costs typically include items that are independent of the heliostat area and, therefore, are sensitive to the number of heliostats in the field. These are items such as controllers, sensors, limit switches and encoders. For example, a heliostat micro controller is generally capable of controlling a 1 m² heliostat as well as a 150 m² without any change in specification.

5.3.2 Parametric cost model

The relationship between the number of heliostats (N), the heliostat field aperture (A_F) and individual heliostat area (A_H) is given by Equation 5.2.

$$N = A_F/A_H \quad (5.2)$$

Once component costs are divided into the respective cost categories, each of the categories' costs per unit area is summed. The total cost per unit area of a heliostat (C_T/A_H) is then given by the sum of each of the three category totals. Each term in Equation 5.3 represents a cost-to-area relationship for a corresponding category. Category 1 items are shown in cost/ m² by C_{Cat-1} and do not fluctuate with area. Category 2 items are represented by the second term, where k is the aggregated cost/m² of load bearing components, and A_H is the heliostat area. The Category 3

fixed costs, which are independent of area, are shown by the third term, where f represents the total cost/m² for Category 3.

$$C_T/A_H = C_{cat-1} + kA_H^{\frac{1}{2}} + f/A_H \quad (5.3)$$

The cost to size curve of each term in Equation 5.3 is plotted in Figure 5.6, each term is summed to show the total heliostat cost variation with size.

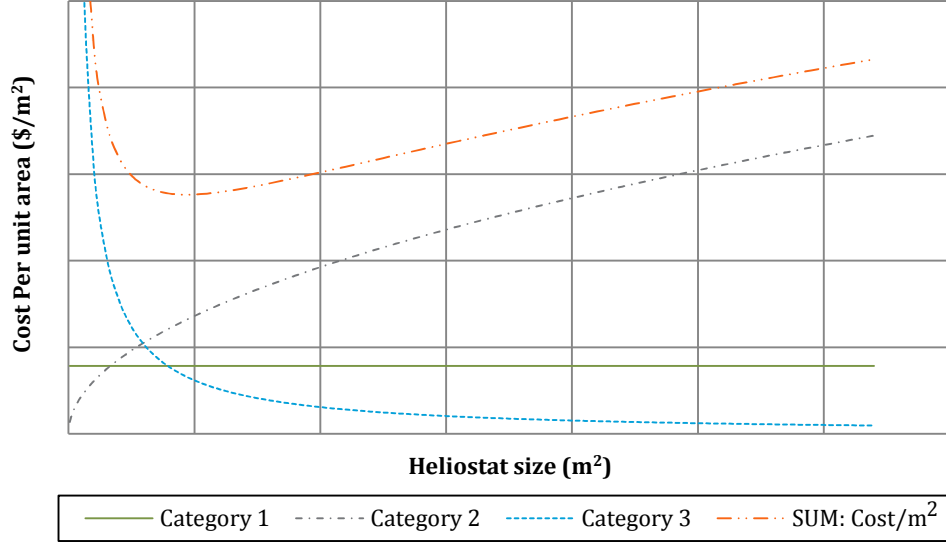


Figure 5.6: Generic component cost to area relationships

Setting the derivative of Equation 5.3 equal to zero and solving returns the corresponding size value on the cost curve where the gradient is zero., It therefore allows for the identification of a theoretical optimum size as shown by Equation 5.4.

$$A_{H\backslash opt} = (2f/k)^{2/3} \quad (5.4)$$

5.3.3 Heliopod analysis

Figure 5.7 shows a parametric analysis of the Heliopod with fixed costs proportions decreasing from 25% to 3%. According to Blackmon (2013), a heliostat's optimum area has more uniformly distributed costs proportions between the three cost categories. In each of the parametric cases explored in Figure 5.7, the optimum size was shown to be less than 2 m². This small optimum size is a result of the low controller costs associated with the Heliopod prototype. Blackmon's generic analysis shows the leveraging effect of the fixed costs on total heliostat cost as the fixed costs approach zero (2013).

Here the cost reduction leverage of low controller costs and their corresponding size can be seen. Additional cost reductions to the Heliopod would be possible by further reducing the fixed costs, resulting in a smaller heliostat. In order to achieve a size

reduction, further cost reductions to the heliostat controller and drive feedback sensors would be required; these hold the largest proportion of the Category 3 costs.

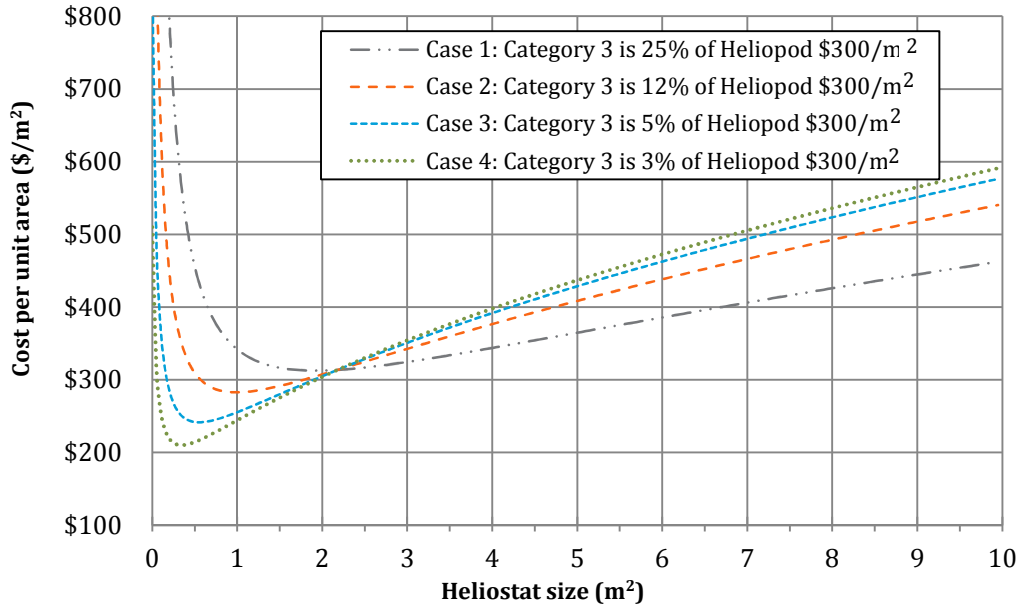


Figure 5.7: Heliostat cost vs. area for the Heliopod system.

Auxiliary cost reductions can come from reducing the cost of load bearing components such as the structure and drives, allowing for a more uniform cost distribution across the three cost categories.

This analysis shows smaller heliostats to be cheaper, provided low fixed costs can be achieved. Increasing the reflective area to a larger size to cater for any load bearing components would result in poor exploitation of the cost reduction potential of low fixed costs.

5.3.4 Cost reduction through size and production volume

Section 0 and 0 discuss the cost reduction potential of increasing heliostat drive production volumes. In the case of the linear actuator a 40% cost reduction could be achieved from a particular supplier by increasing heliostat production volumes without compromising precision (Satcontrol, 2014). Figure 5.8 shows the increase in production volume (Heliostat Units) for alternate size heliostats as shown by Equation 5.2.

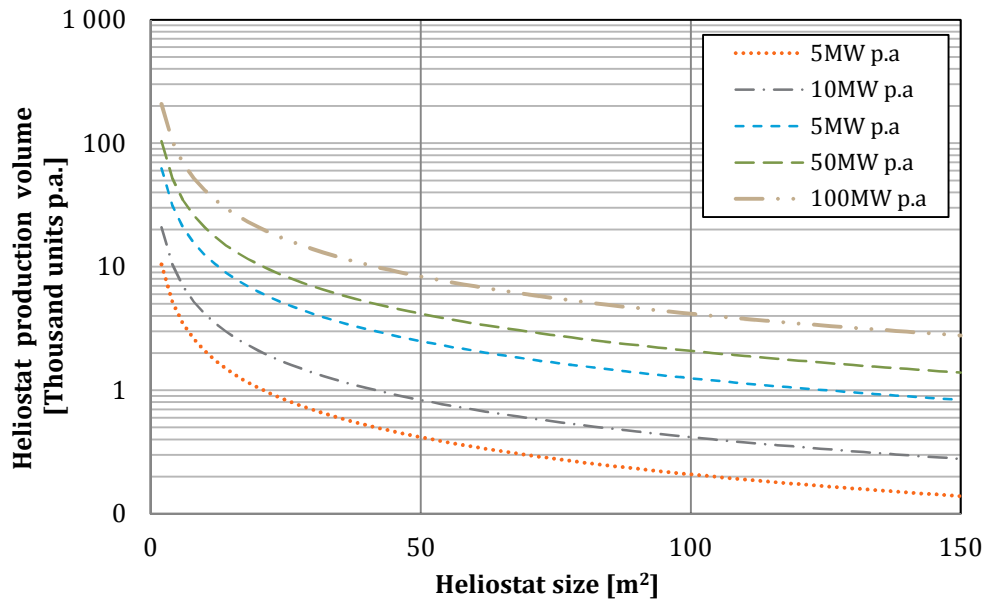


Figure 5.8: HelioStat production volumes for alternate unit sizes. 10MW p.a. indicates 10% of the IRP at which 20 000 2.2m² units are required.

The decrease in size added cost leverage due to its ability to increase the heliostat unit production volumes (see Equation 5.2), thereby reducing costs resulting from higher production rates. Smaller sized heliostats increase production rates on all components with smaller reductions for commodity items such as glass and steel. Further, smaller high volume components lend themselves to low cost automated manufacturing (Bota, 2015) (Coventry & Pye, 2013).

5.4 Heliopod component influence

The influence matrix is a qualitative concept used to rank and identify generic component cost interaction. This analysis was used in conjunction with the previous approaches to further guide cost reduction. A heliostat has to be understood holistically; a single component change for cost improvement may induce a knock-on cost increase or decrease in other parts of the heliostat. Here a qualitative method is used to investigate inter-component cost influences, allowing for the identification of the net cost of a design change.

The influence matrix is presented by Figure 5.9. This tool allows for the true cost effect of a design change to be measured as the reduction or increase in the cost of parts other than the part changed can be identified and pursued for further analysis.

A top-down approach was incorporated in this analysis. As a result, influence was addressed starting with the reflective surface (mirror module) and ending with the foundation (direct heliostat support structure). The primary function of a heliostat is to continuously reflect solar radiation at a target. In this instance, the reflective

surface was assumed to be the single most important heliostat component. Although the other heliostat components are vital, this analysis considered them secondary as they function in an assisting manner.

Consider row 1 in the influence matrix. Mirror support structure, drives, pylon, pedestal and foundation design are all dependent on the surface area, shape and orientation of the mirror module. The mirror module in column A is not dependant on these items except for the connection interface between itself and the backing structure. Now consider row 5. The pedestal cannot be dimensioned before specifying the reflective surface parameters. As a result, it has no bottom-up effect on the mirror module cost, nor does it have the backing structure or drives. Hence, it is ranked with 0 Values in cell 5A, 5B and 5C. The only bottom-up effect is the connection interface between the foundation and pylon. Therefore, if the direct heliostat support is changed and a cost decrease is achieved, the true cost implications incurred must also consider the pylon changes to address the net cost benefit.

			Influences -->						
			A	B	C	D	E	F	G
			Mirror module	Mirror support structure	Drive 2 (Elevation)	Drive 1 (Azimuth)	Pedestal	Direct heliostat support	Control
v - - Heliopod Component	1	Mirror module	Cost/ m ²	3	3	3	3	3	0
	2	Mirror support structure	1	Cost/ m ²	2	2	2	2	0
	3	Drive 2 (Elevation)	0	1	Cost/ m ²	2	2	2	0
	4	Drive 1 (Azimuth)	0	0	1	Cost/ m ²	2	2	0
	5	Pedestal	0	0	0	1	Cost/ m ²	2	0
	6	Direct heliostat support	0	0	0	0	1	Cost/ m ²	0
	7	Control	0	0	0	0	0	0	Cost/ m ²

0	No effect
1	Connection Interface
2	Weight
3	Surface Area, Shape, Orientation, Weight

Figure 5.9: Heliopod influence matrix

Figure 5.9 shows the influence matrix is applied to the Heliopod. The mirror module induces loads through all load bearing components (1B to 1F). These loads result from mass and wind, which correspond to its size and shape. The mirror support structure only has a bottom-up effect on the connection interface between the

reflector and itself. That is, future design changes to the mirror support structure may induce a cost change in bonding materials. Furthermore, if the mirror module was designed in such a way as to reduce wind loads or mass effects, significant cost savings could potentially be achieved on all load bearing components ranked with a three.

The effect of drive selection can also be seen from the influence matrix. The slew drive represents a self-contained azimuth assembly with a single azimuth error and cost. This azimuth error is constant at 2.63mrad through its entire range of motion, where the linear actuator requires a more elaborate elevation assembly for accurate operation. Here the influence matrix suggests that despite the included error and cost, the combination of linear drives and the elevation assembly results in improved error and cost.

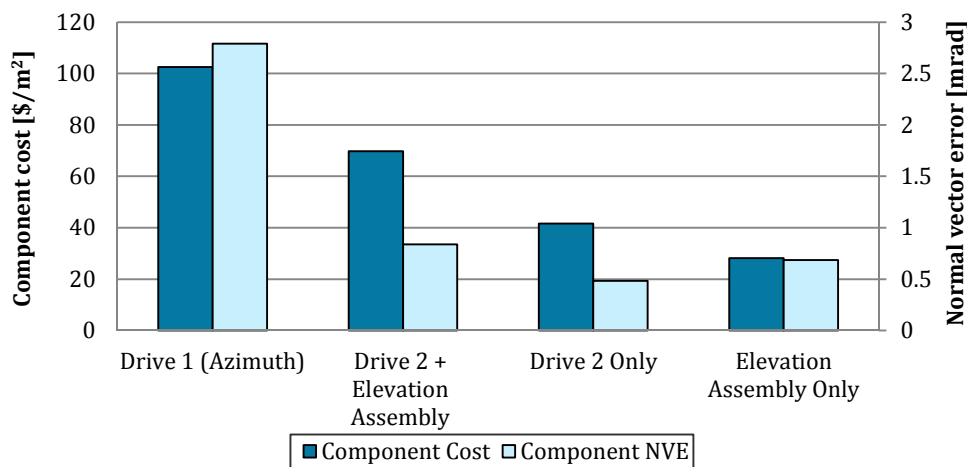


Figure: 5.10 The effect of connection interfaces on heliostat drives

The influence matrix also highlights the separate nature of the control system. As the control system hardware used to control the Heliopod is also capable of controlling alternate heliostat sizes and designs, it has limited effect on component costs. Further delineations can be made to the Matrix to account for the power electronics, which do not obey the $\frac{3}{2}$ power law used to identify costs at alternate sizes.

5.5 Discussion

The Pareto analysis showed drives to hold the largest portion of the Heliopod cost. The slew drive was shown to be the highest contender for replacement/improvement for both cost and error. Linear actuators were shown to be a lower cost alternative capable of providing an added performance increase. Both linear and slew drives experience significant cost reductions at volume. However, the use

of linear drives would result in the need for a suitable tracking mechanism. A mechanism using linear drives is potentially disadvantaged by the increased error associated with its connection points as well as a limited range of motion for tracking. Linear drives present the most appropriate off-the-shelf drive for small heliostats. Alternatively, using an appropriately sized slew drive in combination with a heliostat size increase would also result in a lower cost heliostat.

The size analysis, however, suggested that the heliostat is close to the optimum size, provided the current fixed cost proportion is maintained. The optimum heliostat size is a function of the cost of its subcomponents. Cost sensitivities on fixed costs indicate that smaller heliostats are cheaper. Therefore, increasing the reflective area to cater for an off-the-shelf slew drive or any other load bearing components would result in poor exploitation of the low controller costs. The size analysis also suggested that cost reductions in the facet would further complement the leveraging effect of low fixed costs. Significant cost improvements are seen from increasing production volume by reducing size, as larger component orders significantly reduce costs of value added components. The heliostat size should be maintained since it is already a standard size float glass sheet and can easily be carried by two people, suggesting that cost can be reduced by smaller production facilities and avoiding the need for heavy lifting equipment (Boothroyd, 2010). Although out of scope for this analysis, the facet represents a significant portion for cost reduction and performance improvement, as it has a net effect on heliostat cost irrespective of size.

The influence matrix showed the importance of reducing wind loads as well as the effects of heliostat facet and backing structure mass on reducing component costs. Moreover, it demonstrated the importance of allowing for the comparative cost of alternate drives to be determined. The use of a simpler and cheaper drive results in increased elevation assembly costs and further inaccuracy due to jointed connections. Despite this, the total cost of the linear drive and elevation assembly resulted in net lower costs with greater accuracy than any slew drive available from the manufacturers investigated. The accuracy can be further improved by increasing the connection tolerances.

The highest probability for cost reduction shown in the uncertainty analysis was the use of cable drives and cast-in-place concrete foundations. However, the lower value cost benchmark used in the analysis (Pfhal, et al., 2013) has not yet been tested and only represents aspirational cost values. This re-enforces the use of linear actuators as cost reductions for both benchmarks.

5.6 Analysis adopted

The improvements discussed in Section 5.5 were modelled and measured against the original Heliopod design. This allowed for comparison of the established cost sensitivities as well as the error improvement against the departure point established in Chapter 4.

Many possibilities exist for cost reduction, and only a fraction of these were pursued in this study. However, based on the sensitivities discussed in Section 5.5, the author suggests the use of the following design changes for a cost improvement to the existing Heliopod design.

- Linear actuators for both axes
- A fixed horizontal tracking mechanism
- Improved fits in the elevation assembly pin joints
- Maintain the current single facet aperture of 2.23m^2
- Maintain the current control system
- Cost pedestal structure with pre-galvanised components

5.7 Embodiment

The underlying six heliostat pedestal design remained the same, and the changes above represent a linear improvement on the existing design.

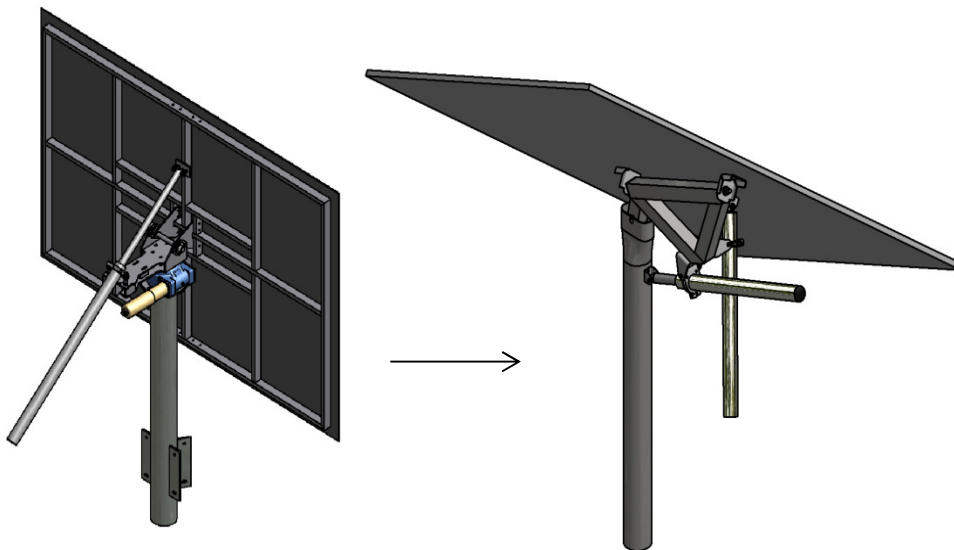


Figure 5.11: Linear changes to the heliostat tracking unit

The cost of these changes was modelled using a combination of regression analyses and analytical cost analyses techniques (discussed in Section 3.2). The results are seen as qualitative and shown in Figure 5.12. The changes induced a 38% cost decrease resulting in a total of $\$185.03/\text{m}^2$.

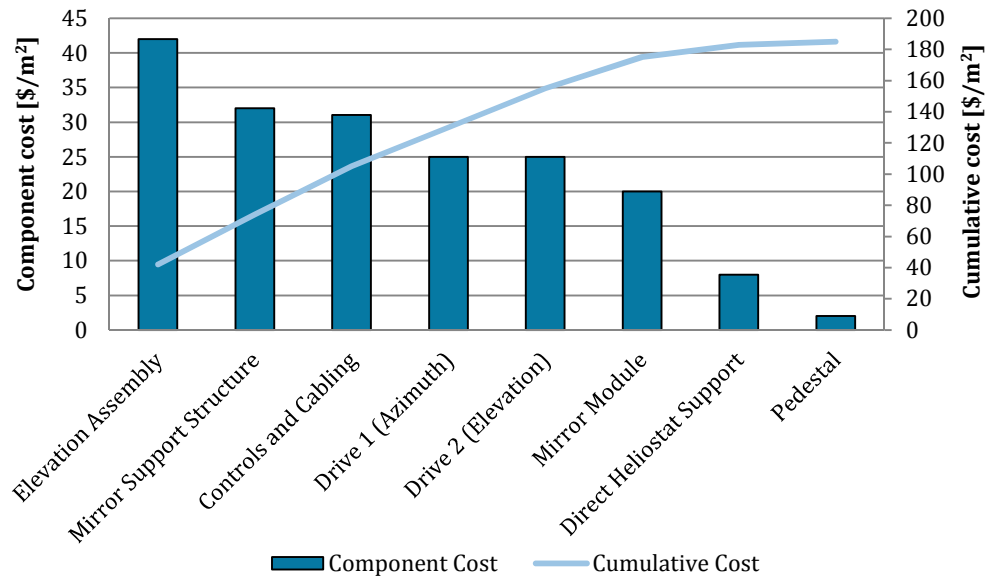


Figure 5.12: Fixed horizontal tracking mechanism

A fixed horizontal tracking axis is proposed to allow for the inclusion of the dual linear actuators. A conservative estimate was used for the elevation assembly because the original cost was doubled to account for both axes. In reality this cost is likely to be less due to a shared structure. No changes were made to the control system, mirror module or mirror support structure. No cost improvements were assumed for structural optimisation, but cost reductions were included for the use of pre-galvanised steel parts.

A revised tracking error stack is now presented to show a total tracking error of 1.3mrad. The majority of which is contributed by the drives and control system. Figure 5.13 shows the Heliopod departure point to have a total tracking error of 3.09mrad.

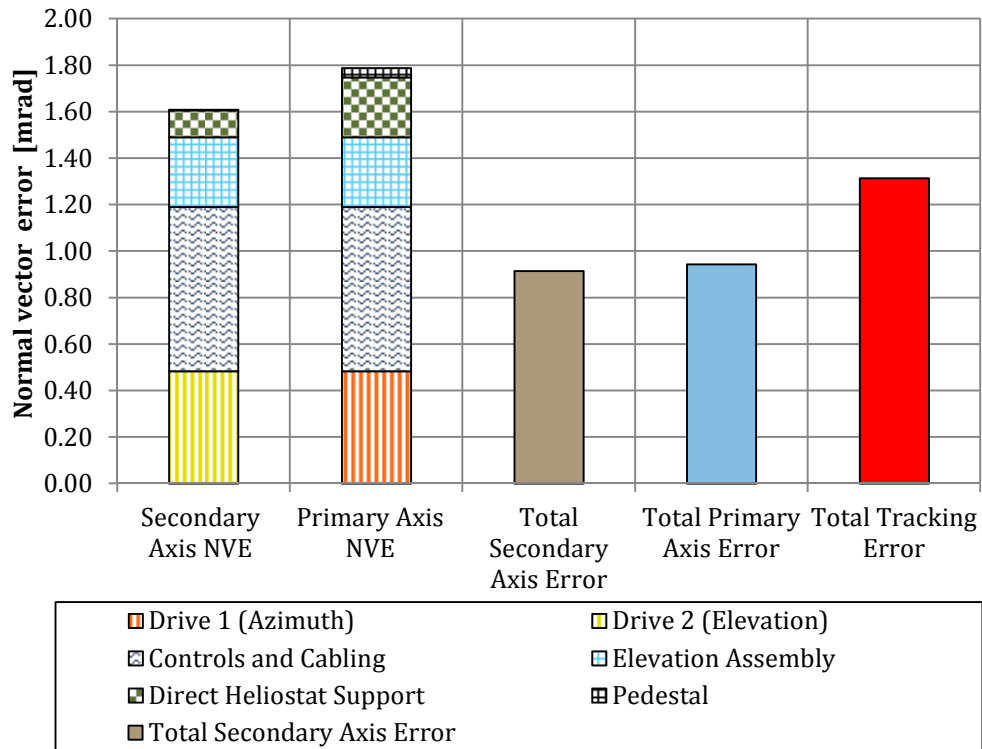


Figure 5.13: Fixed horizontals proposed error stack

5.8 Cost and error comparison

The combined cost and error for the tracking components is shown below in Figure 5.14 along with the Heliopod departure point shown in Figure 5.15.

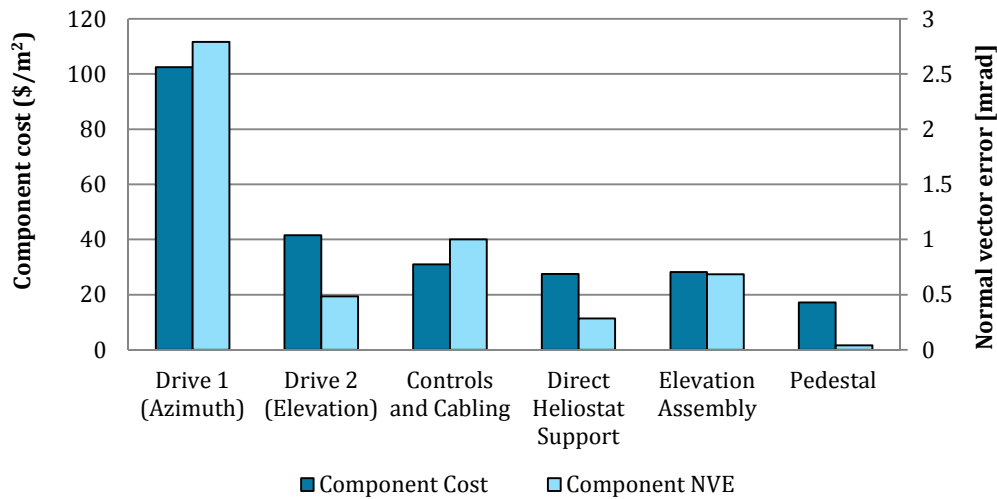


Figure 5.14: Heliopod departure point

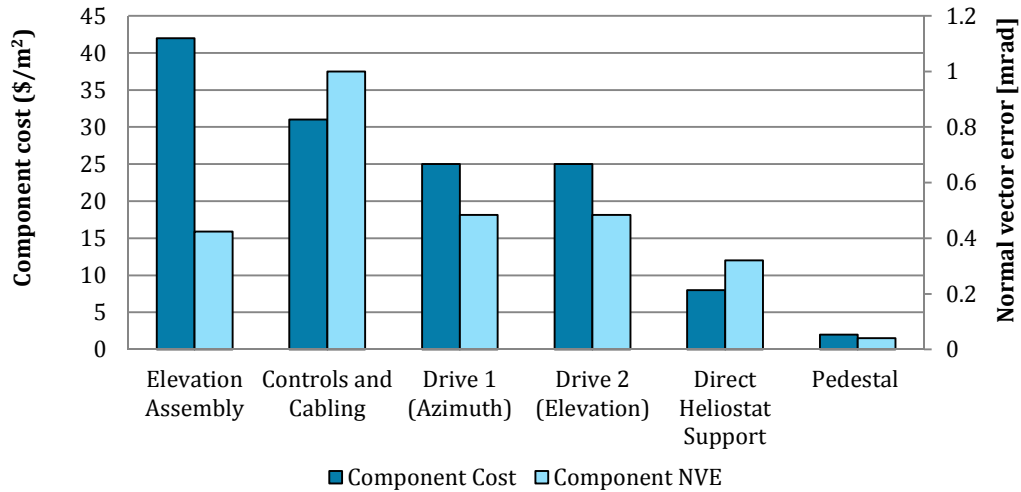


Figure 5.15: Component cost and tracking error for the proposed fixed horizontal solution

The greatest improvement in both cost and error is found to be the replacement of the slew drive. The residual error in the control system is now the largest error contributor, with the drive error following second. The combined error on the pedestal and direct heliostat support is small for a non-optimised structure; this suggests that with structural optimisation, further reduction in cost and stiffness improvements can be achieved. Although smaller drives were used, these drives incorporated the same basic design. Further customisation may result in additional cost reduction.

5.9 Conclusion

Four methods for investigating heliostat cost were pursued. Each provided some tangible insight into heliostat cost reduction. The combined analysis favoured the use of linear drives for both axes, but with the inclusion of improved accuracy in the elevation assembly. Moreover, the heliostat size was considered appropriate for the current controller costs. The following chapter provides synthesis, conclusion and recommends further work.

6. Conclusion

With the aim of understanding heliostat cost at the heliostat component level, a method for comparing heliostat component cost and its corresponding performance has been created. In addition to this, auxiliary methods for exploring heliostat cost were also used to investigate cost sensitivities in the existing Heliopod prototype as a case study. The findings and conclusion are presented hereafter.

6.1 Summary of findings

The use of an error model to quantify cost and error metrics for each subcomponent formed the foundation for the analysis. This model provided qualitative reasoning for measuring cost and performance at the heliostat system level, which allowed for sub-component cost comparisons without the use of a system performance model.

The Heliopod cost model presented an invoiced cost of \$544 /m² in single unit volumes and a high volume cost estimate of \$300 /m² at 20 000 units p.a. The total optical NVE was estimated at 5.58 mrad with pointing error amounting to 3.02 mrad in operational wind speeds.

A Pareto analysis showed drives to constitute more than 40% of the Heliopod system cost and indicated the slew drive to be the largest contributor to both cost and NVE, showing \$102 /m² and 2.63 mrad respectively.

The use of duel actuators reduced the total Heliopod cost by 38%, resulting in an estimated cost of \$185.03 /m², and improved pointing NVE by 56% from 3.02 mrad to 1.31 mrad. The influence matrix showed that the hinges required for interfacing a linear actuator mechanism can induce additional errors into the heliostat. In the case of the Heliopod, these errors exceeded that of the actuator backlash. The use of appropriate standard tolerances was shown to reduce these errors.

A small range of available off-the-shelf options for both linear actuators and slew drives were investigated as a result of the specific positioning precision required by a heliostat. The small availability of suitable off-the-shelf drives, however, indicates that drives built specifically for the solar industry are more appropriate.

The drives investigated experienced a significant cost reduction by increasing order quantities from single unit values to ten thousand unit orders. Results differed

between suppliers, but the average cost was reduced by 39% for linear actuators and 27% for slew drives.

The heliostat size analysis approximated the Heliopod optimum size to be less than 2 m² as a result of the low controller costs associated with the prototype. An additional reduction in fixed costs would result in smaller heliostat sizes and further reduced costs.

Uncertainty analysis is dependent on existing benchmark heliostat costs, which are not readily available and subject to low confidence due to potentially deflated cost claims on the part of the manufacturer. This analysis showed a minimal cost reduction in heliostat reflector. It further indicated linear drives to have scope for cost reduction and specifically showed cable drives to have a high potential for cost reduction. The use of cable drives, however, is seen to be an aspirational improvement since the concept is not yet proven.

6.2 Conclusions

There is currently no consensus within the state of the art as to what constitutes a cost optimum heliostat. As a result, a model was established in this study that incorporates heliostat cost evaluation with a performance parameter and allows for the recommendation of design changes for reduced cost.

The study concludes that improvements in fixed cost components, such as the control system, have a significant leveraging effect on heliostat cost because they allow for the use of smaller heliostats and, therefore, reduced wind loading. The reduced wind loading leads to cost savings in load bearing components. Additionally, heliostat cost is sensitive to production rate, and the ability to increase heliostat volumes as a result of decreasing heliostat size was seen here to be an additional cost lever. This is particularly advantageous to smaller solar field sizes since smaller heliostats allow for higher unit volumes to be achieved without large market demand.

Lastly, the methods used in this study combined with the system complexity yielded multiple results, some of which were congruent with separate methods while others were in contradiction. The multiple results from combined approaches needed to be synthesised using interpretive reasoning on the part of the author. Nevertheless, the combined methods used were able to propose changes for cost reduction and performance improvement and still show scope for further research.

6.3 Summary of contributions

The method developed within this study was formally implemented within the STERG research group, and has contributed to the development of the Stellenbosch University heliostat research project (Helio100).

Contributions from this study were published in peer reviewed proceedings for the 2014 South African Solar Energy Conference in Port Elisabeth (Larmuth, et al., 2013). Further contributions also have been submitted to the 2015 international SolarPACES conference in Cape Town (Larmuth, et al., 2015).

6.4 Recommendation for future work

The work presented herein forms a basis for a heliostat cost analysis. The cost and error models used can now be incorporated into system performance analysis tools in order to better understand the cost and performance effects of heliostat sub-components on a central receiver system LCOE.

A higher level error model was presented in this study that allows for basic error analysis and estimation. More accurate error modelling can be achieved by excluding the assumption of statistical independence and building a detailed heliostat error model.

A qualitative influence matrix was presented in this study. A specific investigation on a quantitative influence matrix can provide more detailed insight into the holistic effects of heliostat design decisions.

Pointing errors are relevant to this study; however, other performance measures not relating to heliostat optics also need to be considered in a holistic cost analysis. These can be factors such as operating windspeed, component life span, logistics costs, required O&M and range of motion, amongst others. Heliostat cost improvements must also consider the effects of design changes on these performance measures.

Data from current off-the-shelf items was used in this study. This study did not address custom drives and the cost reduction potential of customising a drive to suit a heliostat optimised relative to its fixed cost proportion. For additional cost reduction, make or buy strategies can be investigated to explore custom drive solutions.

7. Bibliography

- Abengoa, 2009. *Activity Report: 7.1 Solar*. [Online]
Available at:
http://www.abengoa.com/web/en/accionistas_y_gobierno_corporativo/informes_anuales/2009/
[Accessed 07 November 2014].
- Alpert, D. J. et al., 1990. The development of stretched-membrane heliostats in the United States. *Solar energy materials*, 21(2), pp. 131-150.
- Anderson, J. V., Murphy, L. M., Short, W. & Wendilin, T., 1985. *System performance analysis of stretched membrane heliostats*, Golden, CO (USA): No. SERI/TP-253-2819; CONF-860406-5. Solar Energy Research Inst..
- Balz, M. & von Reeken, F., 2015. Environmental Loading Conditions for CSP Solar Fields.. *Energy Procedia*, Volume 69, pp. 1211-1219.
- Bent, P., Gaul, H. W. & Rabl, A., 1980. *Determining the optical quality of focusing collectors without laser ray tracing*, Colorado: Solar Energy Research Inst..
- Bhargav, K. R., Gross, F. & Schramek, P., 2014. Life Cycle Cost Optimized Heliostat Size for Power Towers. *Energy Procedia*, Volume 49, pp. 40-49.
- Bielecki, B., 2013. *email to James Larmuth*, 17: September.
- Biggs, F. & Vittitoe, C. N., 1979. *Helios model for the optical behavior of reflecting solar concentrators*, Albuquerque, NM (USA): No. SAND-76-0347. Sandia Labs.
- Bircraft, 2014. *Bircraft: Geared Motors - Linear Actuators - Controls*. [Online]
Available at: <http://www.bircraft.co.za/pdf/linear-brochure.pdf>
[Accessed 12 September 2014].
- Blackmon, J. B., 2012. Heliostat size optimisation for central receiver solar power plants. In: K. L. & W. Stien, ed. *Concentrating Solar Power Technology*. Cambridge: Woodhead Publishing, pp. 536-575.
- Blackmon, J. B., 2013. Parametric determination of heliostat minimum cost per unit area.. *Solar Energy*, Volume 97, pp. 342-349.
- Bode, S.-J. & Gauché, P., 2012. *Review of optical software for use in concentrating solar power systems*, Stellenbosch: Southern African Solar Energy Conference.
- Boothroyd, 2010. *Product design for manufacture and assembly*. s.l.:CRC Press.
- Bota, W., 2015. *Conversation with James Larmuth*, February: 05.

- Brandt, L. D. & Chang, R. E., 1981. *Heliostat cost-analysis tool*, Livermore CA (USA): Sandia National Labs.
- Britt, J. F., Shulte, C. W. & Davey, H. L., 1979. *Heliostat production evaluation and cost analysis*, Warren, MI (USA): General Motors Corp.
- BSE, 2014. *BrightSource Limitless Image Gallery*. [Online]
Available at: <http://www.brightsourceenergy.com/image-gallery#.VfGmuBGqqko>
[Accessed 8 November 2014].
- Buck, R., 2014. *Solar Tower Technology - Status and R&D at DLR*. [Online]
Available at: http://sterg.sun.ac.za/wp-content/uploads/2010/12/DLR-PFS_atSTERG2014_v61.pdf
[Accessed 10 June 2014].
- Cavalieri, S., Maccarrone, P. & Pinto, R., 2004. Parametric vs. neural network models for the estimation of production costs: A case study in the automotive industry. *International Journal of Production Economics*, 91(2), pp. 165-177.
- Chase, K. W. & Greenwood, W. H., 1988. Design issues in mechanical tolerance analysis. *Manufacturing Review*, 1(1), pp. 50-59.
- Chen , Y. T. et al., 2004. Comparison of two sun tracking methods in the application of a heliostat field. *Journal of Solar Energy Engineering*, 126(1), pp. 638-644.
- Comar , 2015. *Comar International Pty (LTD) - Precision Engineering Works Quotation*. Stellenbosch: Quotation B01-15-0127.
- Cooper, R. & Slagmulder, R., 1997. The Confrontation Strategy. In: *Target Costing and Value Engineering*. New Jersey: Productivity Press, pp. 3-5.
- Cordes, S., Prosinečki, T. C. & Wieghardt, K., 2012. *An approach to competitive heliostat fields*. Marrakesh Morocco, 18th annual SolarPACES symposium.
- Coventry, J. & Pye, J., 2013. Heliostat Cost Reduction - Where to now ?. *Energy Procedia* , Volume 49, pp. 60-70.
- Delpont, G. & Craig, K. J., 2015. *Optimization of heliostat pod structure for wind loads*. 11-13, 3rd Southern African Solar Energy Conference, South Africa.
- DOE, 2013. *Integrated Resource Plan for Electricity (IRP) Updated Report*, Pretoria: Department of Energy.
- Drumheller, . K. et al., 1980. *Cost of heliostats in low volume production*, Richland, WA (USA): Battelle Pacific Northwest Labs No. SERI/TR-8043-2.

- Drumheller, K., Schulte, S. C., Dilbeck, R. A. & Long, L. W., 1979. *Heliostat manufacturing cost analysis. Volume 1*, Richland, WA (USA), 1979.: Battelle Pacific Northwest Labs.SERI/TR-8043-1.
- Duffie, J. A. & Beckman, W. A., 2006. *Solar Engineering of Thermal Processes*. 3rd ed. New Jersey: John Wiley & Sons, Inc.
- Duff-Norton, 2014. *Duff-norton Linear actuators*. [Online]
Available at: <http://www.duffnorton.com/products.aspx?id=7841>
[Accessed 12 September 2014].
- Falcone, P. K., 1986. *A handbook for solar central receiver design*, Livermore, CA (USA): Sandia National Labs. No. SAND-86-8009. .
- Franck, D., Schwarzbach, J. & Dagan, E., 2009. *Analysis of beam shape and flux distribution of BSE/LUZ II Compact Helisotats*. Las Vegas, NV, SolarPACES.
- Gauche, P. & Wei, W., 2002. Linearized Superposition using CFD for Thermal and Power Characterization of Electronic Equipment with Significant Thermal Radiation and Natural Convection. *Proceedings-spie the International Society for Optical Engineering*, pp. 880-885.
- Google, 2013. *Google RE<C: Heliostat project overview*. [Online]
Available at: http://www.google.org/pdfs/google_heliostat_project.pdf
[Accessed 22 June 2013].
- Guo, M., Sun, F., Wang, Z. & Zhang, J., 2013. Properties of a general azimuth–elevation tracking angle formula for a heliostat with a mirror-pivot offset and other angular errors. *Solar Energy*, Volume 96, pp. 159-167.
- H-FANG Group, 2013a. *Bulk Slew Drive Quotation Q130425-STE*. Stellenbosch: email correspondance with Wenli Fu, 10 April.
- H-FANG Group, 2013b. *H-Fang: Professional Slewing Drive Slewing Ring Manufacturer*. [Online]
Available at: <http://www.h-fang.com.cn/Download.aspx?cateid=22>
[Accessed 2 April 2013].
- H-FANG Group, 2013c. *H-Fang: Professional Slewing Drive Slewing Ring Manufacturer*. [Online]
Available at: <http://www.h-fang.com.cn>
[Accessed 4 April 2013].
- IEA, 2010. *Technology Roadmap Concentrating Solar Power*, Paris: International Energy Agency.
- IEA, 2012. *World Energy Outlook 2012 - Pre realease overview*, s.l.: IEA.

- IRENA, 2012. *Concentrating Solar Power - Volume 1: Power Sector*, Bonn: International Renewable Energy Agency.
- Kishore, V., 2009. *Renewable Energy Engineering and Technology*. 1st ed. London: earthscan.
- KMI, 2013. *KMI: Kinematics Manufacturing Inc.*. [Online]
Available at: <http://www.kinematicsmfg.com>
[Accessed 13 September 2013].
- KMI, 2014. *Bulk Slew Drive Quotation Q082714-STERG*. Stellenbosch: email correspondence with David Pope 29 August.
- Kolb, G. J., Ho, C. K., Mancini, T. R. & Gary, J. A., 2011. *Power Tower Technology Roadmap and Cost Reduction Plan*, Albuquerque: Sandia National Laboratories.
- Kolb, G. J. et al., 2007. *Heliostat Cost Reduction Study*, Albuquerque, NM: Sandia National Laboratories. No. SAND2007-3293. .
- Koretz, B., 2014. *Brightsource Energy: Ivanpah Project*. Solar Thermal Energy Research Group, Stellenbosch : s.n.
- Landman , W., 2013. *Optical Performance of a Reflective Surface of a Heliostat*, *Masters Thesis*, Stellenbosch: Stellenbosch University.
- Larmuth, J. N., Landman, W. A. & Guache, P., 2015. *A top-down approach to heliostat cost reduction*. Cape Town, SolarPACES 2015.
- Larmuth, J. N., Malan, K. & Guache, P., 2013. *Design and Cost Review of 2 m2 Heliostat Prototypes*. Port Elizabeth, 2nd South African Solar Energy Conference.
- Linak, 2014a. *Linak Actuator Technology*. [Online]
Available at: <http://www.linak.com/>
[Accessed 17 September 2014].
- Lovegrove, K. & Pye, J., 2012. Fundamental principles of concentrating solar power (CSP) systems. In: K. Lovegrove, ed. *Concentrating Solar Power Technology*. Cambridge: Woodhead Publishing, pp. 31-33.
- Lovegrove, K. & Pye, J., 2012. Introduction to concentrating solar power (CSP) technology. In: W. S. Keith Lovegrove, ed. *Concentrating Solar Power Technology*. Cambridge: Woodhead Publishing Limited,, pp. 16-67.
- MACSTEEL, 2014. *Macsteel Africas Leading Steel Supplier*. [Online]
Available at: <http://www.macsteel.co.za/documents/download/price-lists>
[Accessed 03 June 2013].
- Malan, K., 2014. *Coversation with James Larmuth*, 8: October.

- Malan, K. & Gauché, P., 2013. *A Heliostat Field Control System, Masters Thesis*, Stellenbosch: Stellebosch University.
- Mancini, T. R., 2000. *Catalog of solar heliostats*, Albuquerque, NM: IEA SolarPACES Report 3.1 .
- Metric Engineering, 2014. *Metric Engineering (PTY) Ltd - Precision Engineering Works*. Stellenbosch: Quotation: 15330 .
- Murphy, L. M., 1984. *Technical and cost potential for lightweight, stretched-membrane heliostat technology*. Golden, CO (USA), Solar Energy Research Inst .
- Murphy, L. M., Anderson, J. V., Short, W. & Wendelin, T., 1985. *System Performance and Cost Sensitivity Comparisons of Stretched Membrane Heliostat Reflectors with Current Generation Glass/Metal Concepts*, Golden, CO (USA): Solar Energy Research Inst.
- NIASA, 2014. *Niasa Products: Linear Actuators*. [Online] Available at: <http://www.niasa.es/en/productos/actuadores-lineales> [Accessed 14 06 2014].
- Niazi, A., Dai, J. S., Balabani, S. & Senevirante, L., 2006. Product cost estimation: Technique classification and methodology review. *Journal of manufacturing science and engineering*, Volume 128, pp. 563-572.
- NREL, 1998. *Heliostat manufacturing for near term markets*. Colorado, National Renewable Energy Laboratory.
- Peterka, J. A. & Derickson, R. G., 1992. *Wind load design methods for ground based heliostats and parabolic dish collectors*, Springfield: Sandia National Laboratories.
- Peterka, J. A. & Derickson, R. G., 1992. *Wind load design methods for ground-based heliostats and parabolic dish collectors*, Albuquerque, NM (United States): Sandia National Labs..
- Pfahl, A., 2014. Survey of Heliostat Concepts for Cost Reduction. *Journal of Solar Energy Engineering*, Volume 136, pp. 1-9.
- Pfahl, A., Buselmeier, M. & Zschke, M., 2011. *Determination of wind loads on heliostats*. Granada , Proceedings SolarPACES.
- Pfahl, A., Buselmeier, M. & Zschke, M., 2011. Wind loads on heliostats and photovoltaic trackers of various aspect ratios. *Journal of Solar Energy*, Volume 85, pp. 2185-2201.
- Pfahl, A. & Uhlemann, H., 2011. Wind loads on heliostats and photovoltaic trackers at various Reynolds numbers. *Journal of Wind Engineering and Industrial Aerodynamics*, Volume 99, pp. 964-968.

- Pfhal, A., Randt, M., Holze, C. & Unterschütz, S., 2013. Autonomous light-weight heliostat with rim drives. *Solar Energy*, Volume 92, pp. 230-240.
- Ricklin, P., Huibregtse, R., Slack, M. & Rogers, D., 2013b. *Presentation Slides: Commercial Readiness of eSolar Next Generation Heliostat*. Las Vegas, eSolar.
- Ricklin, P., Slack, M., Rogers, D. & Huibregtse, R., 2013a. Commercial Readiness of eSolar Next Generation Heliostat. *Energy Procedia*, Volume 49, pp. 201-208.
- Satcontrol, 2013a. *Suntracer Satcontrol Linear Actuators: Technical Datasheet SM4S520M2U8 NC*. [Online]
Available at: <http://www.solar-motors.com/gb/linear-motors-actuators/linear-motors-g70.shtml>
[Accessed 27 October 2014].
- Satcontrol, 2013b. *Solar Tracker & Sun Tracker & Actuator for Solar Tracker*. [Online]
Available at: <http://www.solar-motors.com>
[Accessed 15 09 2013].
- Satcontrol, 2014. *Bulk Actuator Quotation Q130425*. Stellenbosch: email correspondance with Ptricija Hudelja.
- Schell, S., 2009. *Design and Evaluation of eSolar's Helisotat Fields*. Berlin, Proceedings of the SolarPACES Conference.
- Scholz, F. W., 1995. Tolerance stack analysis methods, a critical review. *Research and Technology Boeing Information & Support Services*, pp. 1-44.
- Schramek, P. & Mills, D. R., 2004. Heliostats for maximum ground coverage. *Energy*, 29(5), pp. 701-713.
- Schwarzbözl, P., Schmitz, M. & Pitz-Paal, R., 2009. *Visual HFCAL - A Software Tool for Layout and Optimisation of Heliostat Fields*. Berlin, Proceedings of the SolarPACES Conference.
- Shigley, J. E. & Mischke, C. R., 2003. *Mechanical Engineering Design*. 6th metric edition ed. Boston: McGraw-Hill.
- Silberstein, E. et al., 2009. *Brightsource Solar Tower Pilot In Isreaels NEGEV Operation at 130 bar @ 530°C Superheated Steam*. Berlin, SolarPACES Conference.
- Sito Motor, 2014. *Sito-Motor In line linear actuator*. [Online]
Available at: <http://www.sito-motor.com/>
[Accessed 23 June 2014].
- SKF, 2014. *SKF Linear Actuator Product Range*. [Online]
Available at: <http://www.skf.com/group/products/actuation-systems/linear->

[actuators/index.html](#)

[Accessed 14 September 2014].

Slack, M., Gross, D. A. & Zavodny, M., 2015. Statistical analysis and verification of performance for CSP subsystems. *Energy Procedia* , Volume 69, pp. 1441-1450.

Stephen Leatherbarrow, 2015. *email to James Larmuth*. february: 23.

Stine, W. B. & Geyer, M., 2001. *Power From The Sun*. [Online]

Available at: www.powerfromthesun.net.

[Accessed 13 April 2014].

Sunslew, 2014. *Sunslew*. [Online]

Available at: <http://www.sunslew.com>

[Accessed 15 October 2014].

Sunslew, 2015. *Bulk Slew Drive Quotation Q-150225-1-SAZ*. Stellenbosch: email correspondance with Jason Huang, 25 February.

Terresol Energy, 2011. *Terresol Energy*. [Online]

Available at:

http://www.torresolenergy.com/EPORTAL_DOCS/GENERAL/SENERV2/DOC-cw4e8861b069261/gemasolar-2011-9.jpg

[Accessed 20 June 2012].

Tilley, D., 2013. *Advanced baseload molten salt tower*. In: *Sunshot CSP program review*, Phoenix, Arizona: Abengoa Solar.

Toister, E. & Koretz, B., 2013. *Flexible Assembly Solar Technology*. Phoenix Arizona, In: *Sunshot CSP Program Review* .

Tsai, W.-H., 1998. Quality cost measurement under activity-based costing. *International Journal of Quality & Reliability Management*, 15 (7), pp. 719 - 752.

Ulmer, S., 1998. *Influences of Cost Reduction Measures on the Beam Quality of a Large-Area Heliostat*, IER, University Stuttgart, Stuttgart: Diss. Diploma thesis.

Vant-Hull, L. L., 2012. Central tower concentrating solar power (CSP) systems. In: K. Lovegrove & W. Stein, eds. *Concentrating Solar Power Technology*. Philadelphia: Woodhead Publishing, pp. 240-283.

Vazques, J. et al., 2006. *Sener Heliostat Design and Testing*. Berlin: SolarPACES.

Venture MFG. co., 2014. *Linear Actuator Manufacturers - Venture MFG. co.*. [Online]

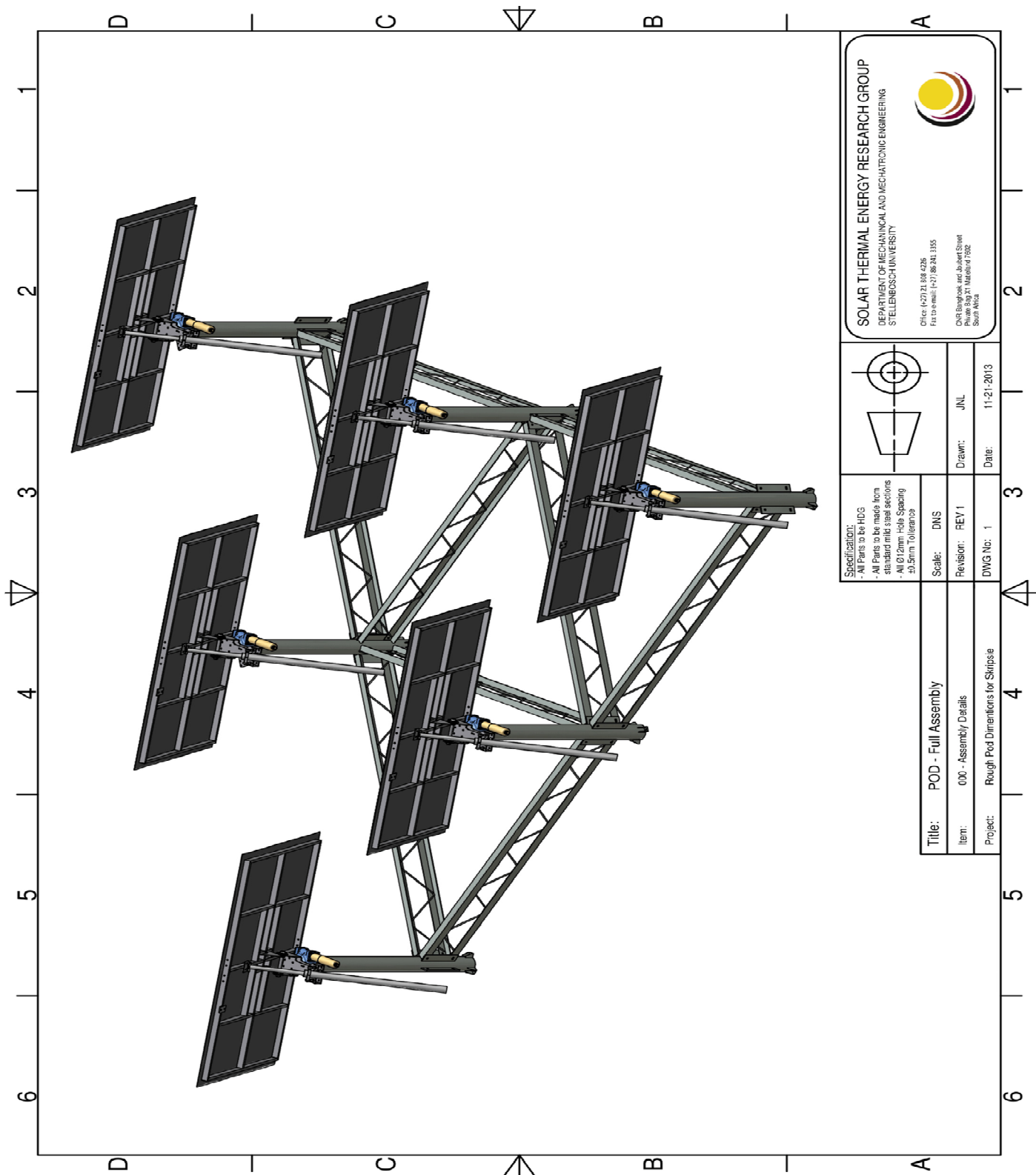
Available at: <http://www.venturemfgco.com>

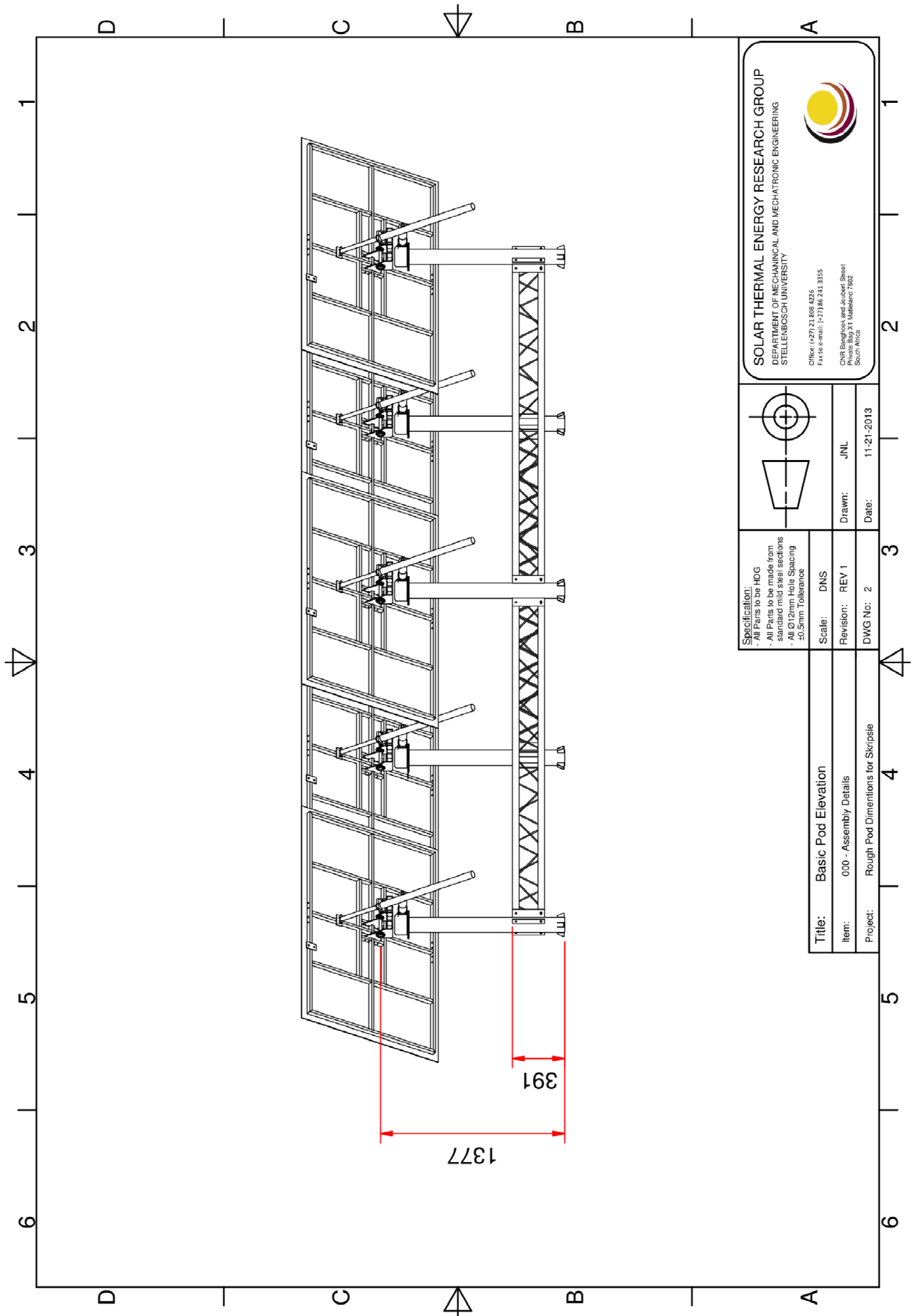
[Accessed 08 September 2014].

- Vito Motion, 2014. *Alibaba Profile: Vito Motion - Linear Actuator Specialist*. [Online]
Available at: <http://cn-vito.en.alibaba.com/>
[Accessed 15 06 2014].
- Ward, N. & Dye, S., 2014. *Statistics Learning Center: Triangular Distribution*. [Online]
Available at: <http://statslc.com/>
[Accessed 01 July 2014].
- Weinrebe, G. et al., 2014 . Towards holistic power tower system optimization.
Energy Procedia , Volume 49 , p. 1573 – 1581.
- Winter, C. J., Sizmann, R. L. & Vant-Hull, L. L., 1991. Status and Trends in Heliostat Development. In: *Solar Power Plants: Fundamentals – Technology – Systems - Economics*. Heidelberg: Springer-Verlag Berlin.
- Wuxi HongBa, 2014. *Wuxi HongBa Mechanical Electrical Equipment*. [Online]
Available at: <http://www.wxhongba.cn/english/>
[Accessed 12 September 2014].
- XABC Bearing Company, 2014. *Xuzou Aosen Slewing Bearing Manufacturer Co.- Enclosed Slewing Drive Products*. [Online]
Available at: <http://www.xabcbearing.com>
[Accessed 12 June 2014].
- Zaibel, R., Dagan, E., Karni, J. & Ries , H., 1995. An astigmatic corrected target-aligned heliostat for high concentration. *Solar Energy Materials and Solar Cells*, Volume 37, pp. 191-202.
- Zavoico, A. B., 2001. *Solar Power Tower Design Basis Document S*, Nexant, San Francisco, 94104 CA,: Sandia National Laboratories, SAND 2001–2100, .

Appendices

A. Heliopod general dimensions

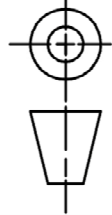




SOLAR THERMAL ENERGY RESEARCH GROUP
 DEPARTMENT OF MECHANICAL AND MECHATRONIC ENGINEERING
 STELLENBOSCH UNIVERSITY



Office: (+27) 21 806 4216
 Fax: (+27) 21 806 4355
 CHB Boshoff and Joubert Street
 Private Bag 21 Matieland 7802
 South Africa

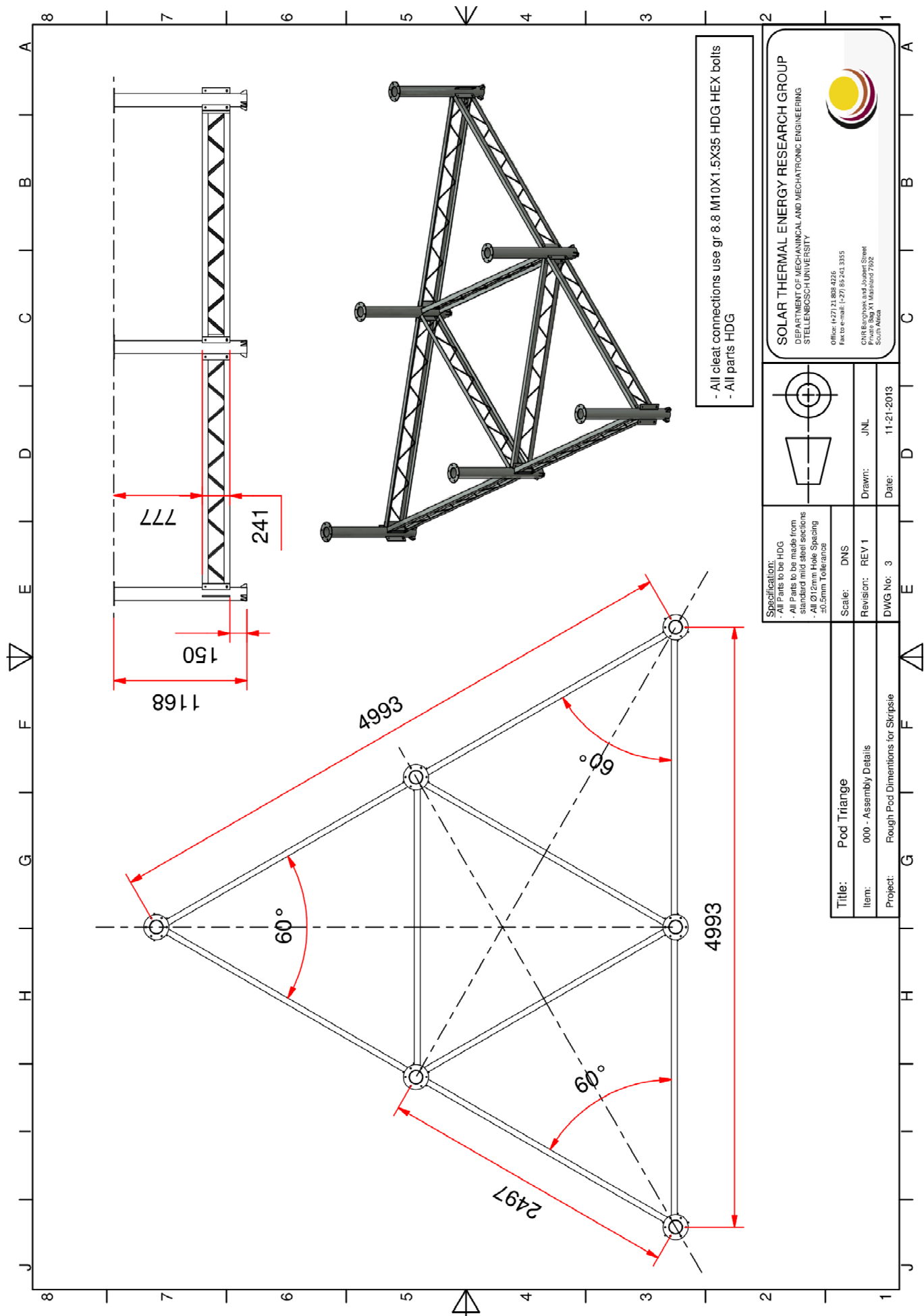


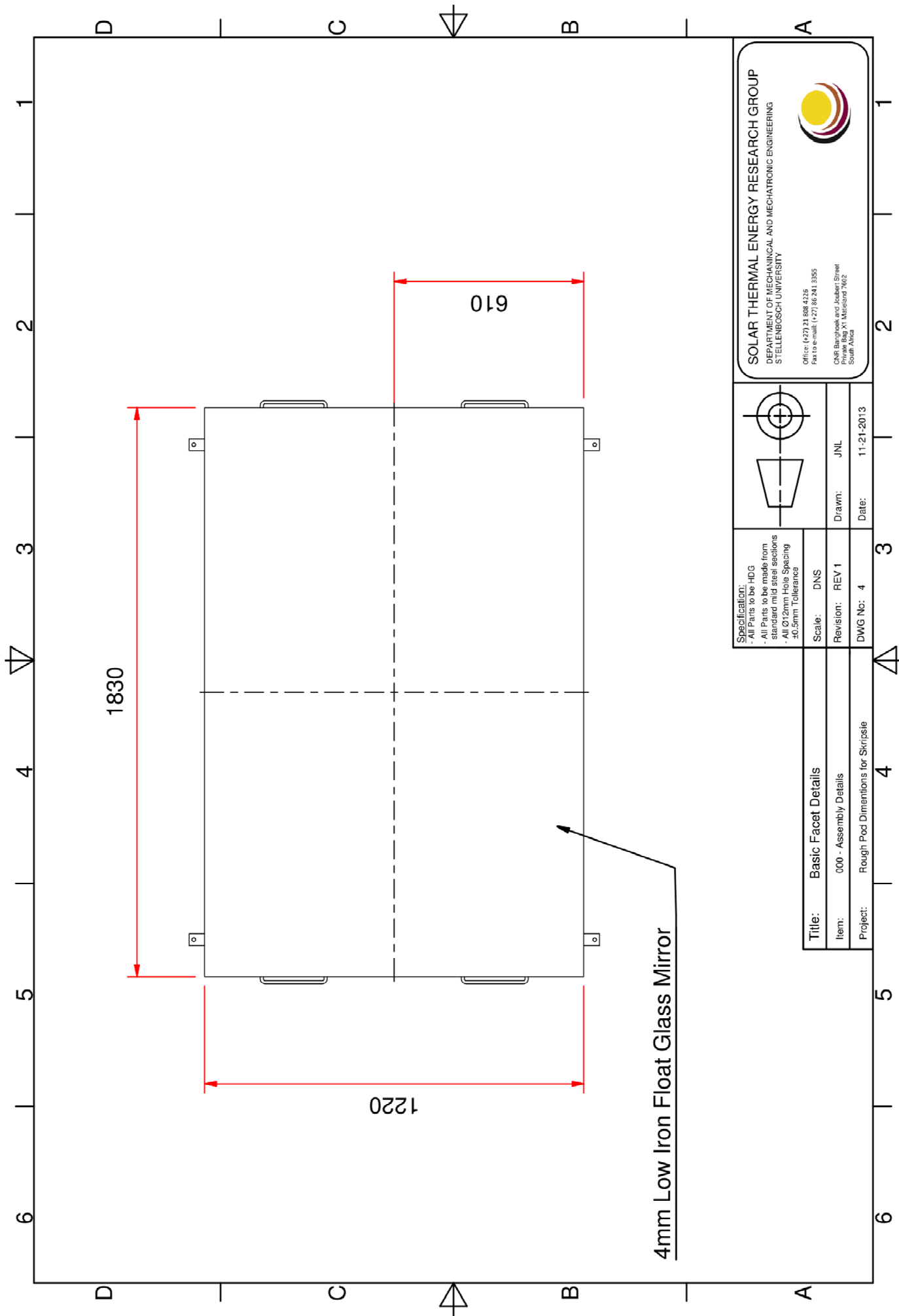
Specification:
 - All Parts to be HDG
 - All Parts to be made from standard mild steel sections
 - All Ø 12mm Hole Spacing
 - 30.5mm Tolerance

Title: Basic Pod Elevation
Item: 000 - Assembly Details
Project: Rough Pod Dimensions for Skripse

Scale: DNS
Revision: REV 1
DWG No: 2

Drawn: JNL
Date: 11-21-2013





4mm Low Iron Float Glass Mirror

SOLAR THERMAL ENERGY RESEARCH GROUP DEPARTMENT OF MECHANICAL AND MECHATRONIC ENGINEERING STELLENBOSCH UNIVERSITY Office (+27) 21 688 4235 Fax (+27) 21 688 4235 CNR Banghoek and Joubert Street Private Bag X1, Maitland 7602 South Africa			
Specification:	- All Parts to be HDG - All Parts to be made from standard mild steel sections - All Ø12mm Hole Spacing 30.5mm Tolerance	 	Drawn: JNL Date: 11-21-2013
Title:	Basic Facet Details	Scale:	DNS
Item:	000 - Assembly Details	Revision:	REV 1
Project:	Rough Pod Dimensions for Skripste	DWG No:	4

B. Heliopod cost breakdown

Detailed cost summary for the Heliopod is provided.

Helio 40: HelioPOD Materials

Single Unit Build - [Single Pod - Six Heliostats]

Total Cost R 32 161.72 R 2 403.72						
Description	Qty Req for System	Qty Req for Assy	Unit Cost Excl VAT	Assy Cost	Sub Total	Cost Basis
<u>Mirror Module</u>	6			R 1 019.94	R 6 119.65	
Float Glass Mirror		2.23	R 295.00	R 658.62		QT: PG Glass -24124
Steel Backing Frame		1	R 289.31	R 289.31		est. Cost Basis 1 - Mass×Cost Rate
Frame Galvanising						
Bonding Agent		1	R 66.03	R 66.03		QT: Max Arcus UNOF107112013001
Neoprene Shims		16	R 0.05	R 0.86		QT: CT Rubr PIR00222@ ave 144/m ²
Fasteners		1	R 5.12	R 5.12		est. Cost Basis 2 - Fasteners
<u>Elevation Assembly</u>	6			R 497.25	R 2 983.50	
Headstock		1	R 68.57	R 68.57		est. Cost Basis 1 - Mass×Cost Rate
Elevation Hinge		1	R 24.04	R 24.04		est. Cost Basis 1 - Mass×Cost Rate
Tie Rod Ends		4	R 43.86	R 175.44		QT: R&V Bearings - QTC455
Elevation Bearing		2	R 86.66	R 173.32		INV: BMG - 0125/00281331
Actuator Clamp		1	R 21.24	R 21.24		est. Cost Basis 1 - Mass×Cost Rate
Fasteners [set]		1	R 34.64	R 34.64		est. Cost Basis 2 - Fasteners
<u>Elevation Drive Unit</u>	6		R 1 603.09	R 4 236.04		
520mm Actuator Unit		1	R 1 602.00	R 1 602.00		est. Cost Basis 1 - Mass×Cost Rate
Actuator Pin		1	R 1.09	R 1.09		See Cost Basis 1 - Mass×Cost Rate
<u>Azimuth Drive Unit</u>	6			R 2 632.95	R 15 797.72	
3" Slew Drive Unit		1	R 2 600.00	R 2 600.00		INV: Hfang -PI130708-SOL
Blank Flange [Adapter PLT]		1	R 32.95	R 32.95		est. Cost Basis 1 - Mass×Cost Rate
<u>POD Pedestal</u>	1			R 3 943.91	R 3 943.91	
Pylon Mid		3	R 256.09	R 768.26		est. Cost Basis 1 - Mass×Cost Rate
Pylon Corner		3	R 184.69	R 554.06		est. Cost Basis 1 - Mass×Cost Rate
Lattice Truss		9	R 256.09	R 2 304.78		est. Cost Basis 1 - Mass×Cost Rate
Fasteners [set]		1	R 316.80	R 316.80		est. Cost Basis 1 - Mass×Cost Rate
<u>Local Control Electronics</u>	6			R 448.29	R 2 689.74	
Plastic Enclosure		1	R 60.00	R 60.00		RS:
PCB		1	R 83.00	R 83.00		INV:WH Circuit CC
Electronic Components		1	R 305.29	R 305.29		Cost Basis Sheet Electronics
Glands		4	R 6.50	R 26.00		
Coms Cable		9.6	R 3.95	R 37.93		
<u>Power Electronics</u>	1			R 627.20	R 627.20	
Power Cable		16.8	R 4.00	R 67.20		est. Karel Malan
PV Panel		8	R 20.00	R 160.00		est. Karel Malan
Battery		2	R 200.00	R 400.00		est. Karel Malan

Helio 40: HelioPOD In house labour

Single Unit Build - [Single Pod - Six Heliostats]

Cost	R	43 124.67
-------------	---	-----------

Assembly/Task	Man-hrs.	Qty Req'd	Total Man-hrs.	Cost	Sub-Total	Basis
<u>In House Fabrication Labour</u>			47.75		R 1 432.38	
Mirror Module				R 228.60		
Prep Mirror	0.25	6	1.5	R 45.00		Actuals - Timed
Prep Backing	0.25	6	1.5	R 45.00		Actuals - Timed
Bond Mirror to Backing	0.6	6	3.6	R 108.00		Actuals - Timed
Catalogue and Index	0.17	6	1.02	R 30.60		Actuals - Timed
Machine Work				R 2 177.28		
Turn 10mm elevation hinge Pin	0.083	12	0.996	R 79.68		est. Frank Hoffman
Turn 20mm Elevation Shaft	0.2	6	1.2	R 96.00		est. Frank Hoffman
Turn 10mm Actuator Facet pin	0.17	6	1.02	R 81.60		est. Frank Hoffman
Mill Actuator Half Clamp	2	12	24	R 1 920.00		est. Frank Hoffman
Controls				R 1 032.80		
Solder Components to PCB	2	6	12	R 960.00		est. Karel Malan
Fit Glands to control Box	0.13	7	0.91	R 72.80		est. Frank Hoffman

Assembly/Task	Qty Req for System	Qty Req Assy	Part labour	Sub Assy Labour	Sub-Total	Basis
<u>Contractors Fabrication Labour</u>					R 40 797.09	
<i>Note: This includes contractors overhead and profit</i>						
Mirror Module	6			R 2 247.69	R 13 486.14	Basis Sheet 2
Cut, weld & galvanise Backing		1	R 2 247.69	R 2 247.69		
Elevation Hinge V3	6			R 376.25	R 2 257.48	Basis Sheet 2
Cut and Weld SS304 Hinge		6	R 62.71	R 376.25		
Headstock	6			R 592.43	R 3 554.56	Basis Sheet 2
Cut, weld & galvanise Headstock		1	R 592.43	R 592.43		
Actuator 1/2 Clamp	12			R 343.11	R 4 117.26	Basis Sheet 2
Laser Cut 16mm SS304		6	R 57.18	R 343.11		
Blank Flange V1	6			R 110.05	R 660.28	Basis Sheet 2
Blank flange complete		1	R 110.05	R 110.05		
POD Pedestal REV1	1			R 11 282.89	R 11 282.89	Basis Sheet 2
Pylon Mid		3	R 1 323.91	R 3 971.74		
Pylon Corner		3	R 1 060.31	R 3 180.94		
Lattice Truss		9	R 458.91	R 4 130.22		

C. Component tests

The methods for empirical performance measurements used in this study are elaborated in the following appendix. These methods allowed for the establishment of initial working values which were later incorporated into the error model.

C1. Heliopod drives

In order to confirm manufacturer claims on the accuracy of drives used in the Heliopod, estimates were obtained from high level bench tests for component performances.

The backlash in both the actuator and the slew drive has minimal friction between the two backlash contact points, as a result, displacement can be easily manipulated between these contact points by hand.

A dial gauge was used to measure the displacement in millimetres. In the case of the linear actuator, measurements were taken in line with the drive direction. A mean error of 0.09 mm was taken from the three actuators.

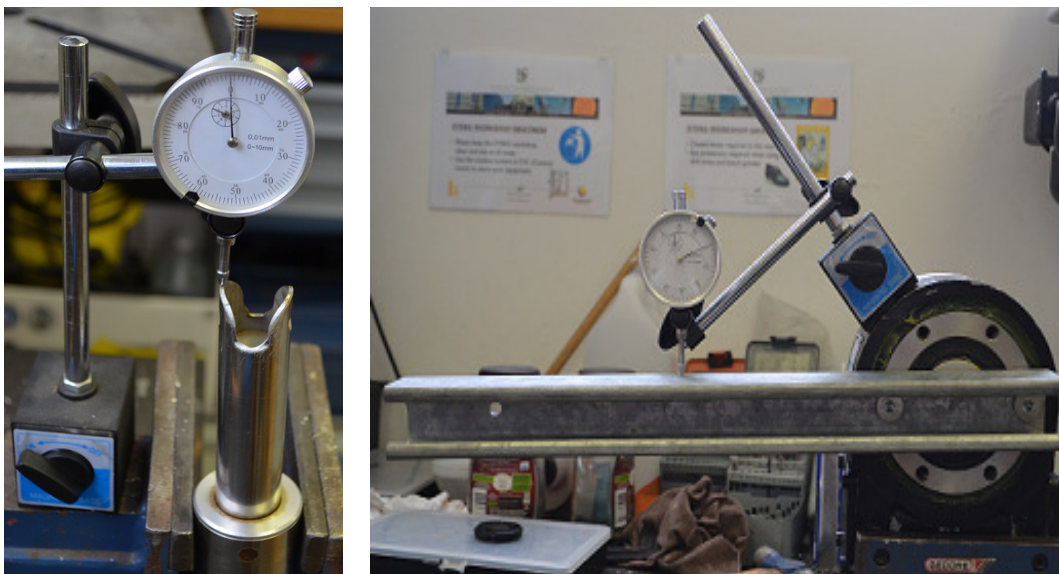


Figure C.1: Heliopod drive backlash measurements

A moment arm was used to measure linear displacement on the slew drive at a known distance from the centre of rotation. The linear displacement was then converted to angular displacement in milliradian. Three identical drives yielded a mean error of 2.76mrad.

C2. Pedestal

Simple deflection measurements were conducted using a laser to simulate the heliostat normal vector. A target was set up in front of the Heliopod onto which the laser was aimed. Displacement measurements were recorded on the target with a digital camera at pre-determined load increments. These load increments correspond to known wind speeds.

A standard off-the-shelf 0.3 mW green laser pointer was used. The laser was fastened to the pedestal flange using a customised steel bracket and housing.

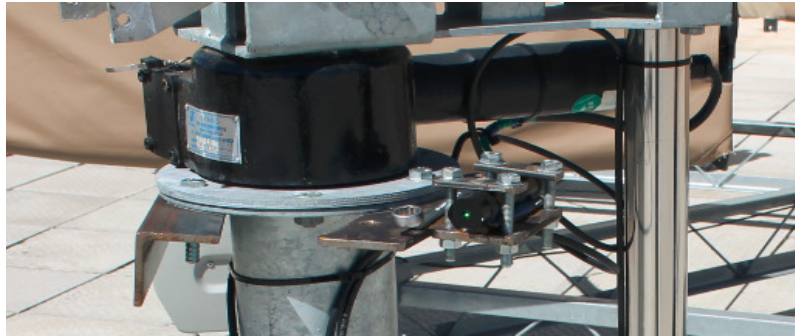


Figure C.2.1: Laser mounted to pedestal below the slew drive

A target was then set up in front of the heliostat which consisted of four grid points placed at known distances apart. Loads were then applied about the azimuthal axis (M_z) as well as at the pedestal base axis (M_y). For each load increment a displacement point was photographed on the target. The photographs were then imported to CAD and scaled using the target grid points and the displacement of the laser centroid was then measured.

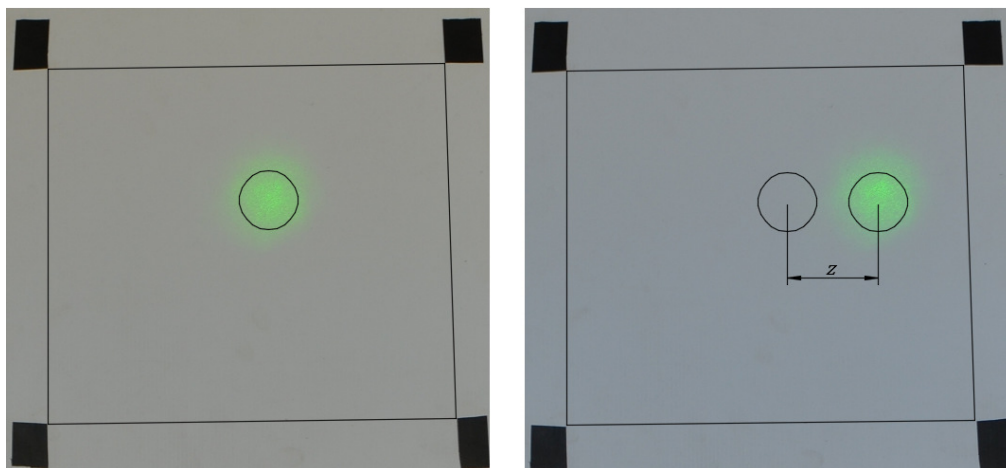


Figure C.2.2: pedestal error measurement showing the zero position on the left and the maximum deflection at on the right.

The milliradian deflection was then calculated from the measured displacement and the distance from the target.

D. Component quotations

A Selection of key component quotations is included here.



Jiangyin Sunslew Machinery Equipment Co.,Ltd
www.sunslew.com
Add: No.309 West RenMin Road ChengJiang Town
JiangYin City,JiangSu Province 214400
China
Tel: +86-510-86608662
Fax: +86-510-86608662
Mob: +86 15851645029

QUOTATION

Q-150225-1-SAZ
 Feb.25th,2015

Contact:Mr.Jason Huang
 Email: jason@sunslew.com

Customer

www.sun.ac.za

Stellenbosch University

Contact: Mr. Larmuth
 Email: larmuth@sun.ac.za

Quantity	Part No.	Description	Unit Price	Amount
1-10	SD3A-62-RC-24H3033-REV.A	3" Precise Enclosed Slewing Drive Ratio:62:1,Right Handed Mounting 24VDC Motor With Hall Sensor Tracking Precision $\leq 0.1^{\circ}$	\$265.18	
100	SD3A-62-RC-24H3033-REV.A	3" Precise Enclosed Slewing Drive Ratio:62:1,Right Handed Mounting 24VDC Motor With Hall Sensor Tracking Precision $\leq 0.1^{\circ}$	\$229.62	
1000	SD3A-62-RC-24H3033-REV.A	3" Precise Enclosed Slewing Drive Ratio:62:1,Right Handed Mounting 24VDC Motor With Hall Sensor Tracking Precision $\leq 0.1^{\circ}$	\$208.56	
10000	SD3A-62-RC-24H3033-REV.A	3" Precise Enclosed Slewing Drive Ratio:62:1,Right Handed Mounting 24VDC Motor With Hall Sensor Tracking Precision $\leq 0.1^{\circ}$	\$176.95	

Production Time As The Quantity
 Price Term Exwork
 Payment Term 100%TT In Advance
 Color Optional
 Shipment TBD
 Packing International Standard Wooden Crate
 HS CODE 8483409000
 Period Of Validity 3 Month



Professional Slewing Drive & Ring Manufacturer

QR09-268

H-FANG Contact: Wenli Fu Email: wenli@h-fang.com.cn Tel: 0086-510-86366117 Fax: 0086-510-86366200 Cell: 0086 13914176590 www.h-fang.com.cn		QUOTATION			
		Number	Date	Page	
		Q130425-STE	25Th, Apr. 2013	1/1	
Vendor Jiangyin Huafang New Energy High-tech Equipment Co., Ltd ADD: No. 20 Yungu Rd. Changshou, Zhouzhuang Town 214400 Jiangyin Jiangsu ATTN: Wenli Fu		Buyer Solar Thermal Energy Research Group ADD: Stellenbosch University Private Bag X1 Matieland 7602 South Africa Contact : Mr. James N. Larmuth Cell: (+27) 21 808 4226 FAX: (+27) 86 241 3355 PH : +44 (0) 1332 697796 Email: larmuth@sun.ac.za Website : www.sun.ac.za/sterg			
No .	Part Number	Product Description	Quantity	Unit price	Amount
1	SE3C-62-R-12H.30.33	3" Slewing drive Ratio :62:1 With 12V motor, With Hall Sensor	10000	US\$193.00	
Note:					
Delivery Time		Freight:	Packaging	TOTAL(Gross)	
About 1000pcs per Month		By Sea	International standard packaging		
Payment		HS Code:			
100 T/T IN ADVANCE		8483409000			
Price Term:		Bank account :			
Door to Door					



Professional Slewing Drive & Ring Manufacturer

QR09-268

H-FANG Contact: Wenli Fu Email: wenli@h-fang.com.cn Tel: 0086-510-86366117 Fax: 0086-510-86366200 Cell: 0086 13914176590 www.h-fang.com.cn		QUOTATION			
		Number	Date	Page	
		Q130411-STE	11Th, Apr. 2013	1/1	
Vendor Jiangyin Huafang New Energy High-tech Equipment Co., Ltd ADD: No. 20 Yungu Rd. Changshou, Zhouzhuang Town 214400 Jiangyin Jiangsu ATTN: Wenli Fu		Buyer Solar Thermal Energy Research Group ADD: Stellenbosch University Private Bag X1 Matieland 7602 South Africa Contact : Mr. James N. Larmuth Cell: (+27) 21 808 4226 FAX: (+27) 86 241 3355 PH : +44 (0) 1332 697796 Email: larmuth@sun.ac.za Website : www.sun.ac.za/sterg			
No .	Part Number	Product Description	Quantity	Unit price	Amount
1	62-R-12H.30.33	3" Slewing drive Ratio :62:1 With 12V motor, With Hall Sensor	1 100	US\$215.00 US\$192.00	
Note:					
Delivery Terms		Freight:	Packaging	TOTAL (Gross)	
2 weeks for produce		By Air	International standard packaging	28Kgs	
Payment			HS Code:		
100 T/T IN ADVANCE			8483409000		
Price Term:			Bank account :		
Door to Door					



Kinematics Manufacturing Incorporated

21410 N. 15th Lane, Suite 104
Phoenix, Arizona, 85027, USA
www.kinematicsmfg.com

QUOTATION

Process Solutions through Excellence in Innovation

Customer: Solar Thermal Energy Research Group
Stellenbosch University
Mechanical Engineering Building
Joubert Street
Stellenbosch
7600
South Africa

Quotation No: Q082714-STERG
Contract No: N/A
Date: August 27, 2014
Payment Terms: TBD
HS Code: 8483409000
Project No: N/A
KMI Sales Contact: David Pope

Shipping:	Shipper	Consignee	Ship To	Notify Party:
	Kinematics Mfg.	Same as customer	Same as customer	TBD

Materials:

Quantity	Model	Description	Unit Price	x1 Unit	Shipping	Amount USD
1	SE3	SE3 Drive geared with geared motor	\$329.27	\$329.27	\$545.00ea Airfreight DAP x1	
1	ZE3	ZE3 Drive geared with geared motor	\$380.31	\$380.31	\$545.00	\$1,254.58
x100 Units						
100	SE3	SE3 Drive geared with geared motor	\$279.48	\$27,948.00	\$1005.95 LCL DAP x1	
100	ZE3	ZE3 Drive geared with geared motor	\$330.51	\$33,051.00	\$1,005.95	\$62,004.95
x100,000 Units						
100,000	SE3	SE3 Drive geared with geared motor	\$196.80	\$19,680,000.00	\$3520/Container X 83 + \$1905.17 x1 LCL DAP	
100,000	ZE3	ZE3 Drive geared with geared motor	\$218.48	\$21,848,000.00	\$294,065.17	\$41,822,065.17

1. Pricing is based on receipt of blanket order(s) and/or contractual obligation to be agreed upon at a later date
2. Due to the varying costs of commodities including but not limited to materials, fuel, and services, this quote is valid for 30 days.
3. Pricing is EXW China

Total Order **\$41,885,324.70**

Kinematics Manufacturing Group

Ph: +1 623 780 8944
Fax: +1 623 780 8945

www.kinematicsmfg.com
bbielecki@kinematicsmfg.com

Want to get more?

QUOTATION:

Stellenbosch University

Banhoek Street

**ZA-7600 Stellenbosch
SOUTH AFRICA**

karelmalan@gmail.com

Tel.: +27 (0)74 900 2118

No.: 14 / 9689

Page: 1/1

Date: 11. september 2014

Validity: 26. september 2014

Terms of Delivery: EXW

Payment Conditions: 50% deposit 50% bef. delivery

Value: EUR

Ser.	Product Code/Description	EAN	Quantity	UM	Price	VAT	Amount
1	SM4S300M2NC Solar linear actuator-motor SM4S300M2NC w/o clamp	383106390070	400,00	PCS	87,00		34.800,00
2	SM4S300M2NC Solar linear actuator-motor SM4S300M2NC w/o clamp	383106390070	10.000,00	PCS	70,00		700.000,00

Amount: 734.800,00

VAT: 0,00

Denote payment with code: **00-9689-502443498-99**

Total: EUR 734.800,00

Thanks for your inquiry. If there are some changes about the product, quality, delivery destination or delivery time, please ask for new quotation with changed conditions.

for SAT CONTROL d.o.o., BOGDAN BOLKA




SHANGHAI SITO MOTOR CO.,LTD

Add: Room 708, No.389, Jinwan Road,
Shanghai, China, 201206
Tel: 0086-21-58999803 Fax: 0086-21-58992839

**QUOTATION SHEET**

Customer:		Supplier:			
Company name:	Stellenbosch University	Company name:	SHANGHAI SITO MOTOR CO.,LTD		
Email address:	larmut@sun.ac.za	Email address:	jhsales24@sito-motor.com		
Tel:		Tel:			
Attn:	James	Submitted by:	Jason Guan		

Model:	Product Picture	Specifications	Quantity(pcs)	Unit Price(US\$)	Remark
ANT35		Voltage: 24v Stroke: 400mm Load capacity: 600N Hall sensor	Samples	\$118.00/pc	
			400pcs	\$95.00/pc	
			10000pcs	\$89.00/pc	
Shipping and Delivery info:		FOBSHANGHAI			
		Delivery time within 30days			

Note:
1).Payment terms:T/T or L/C with official PO
2).Price valid for 30 days